Reconstructing Past Climate Signals of northern Mozambique using Giant Corals

July 2012

Gila Merschel

Vrije Universiteit Amsterdam
Faculty of Earth and Life Sciences
Applied Environmental Geosciences
Master Thesis Project (450268)

Royal NIOZ
Department of Marine Geology

Supervisors: Dr. C. A. Grove
Dr. K. Beets

Abstract

Little is known about what drives climate in eastern Africa, links to large scale climate oscillations like ENSO or the PDO have only been suggested. Tropical corals have been shown to record past rainfall variability as they grow and coral based rainfall reconstructions extend up to a few hundred years. Here we examine four coral cores spanning up to 100 years from northern Mozambique. The annual averages of their luminescence G/B records were all significantly correlated with the exception of one relationship. A coral composite record was constructed which shows a correlation with rainfall data once the 1-year moving median was removed. The coral composite record shows a positive relationship with the IOD. At multi-decadal timescales, the coral composite record shows a strong positive relationship with the AMO and a negative relationship with the PDO when filtered with a 10 year low band bass filter. Without removing the 1 year moving median, the coral composite shows a strong relationship with SST, meaning it is likely that rising SST associated with global warming has caused runoff to increase. The composite G/B record shows a significant correlation to maximum wind speed as well as historical cyclone tracks over the Indian Ocean and extreme events, identified in the luminescence and geochemistry data, can be linked to individual cyclones. We conclude that rainfall in northern Mozambique is not only controlled by local factors as well as cyclone activity in the Indian Ocean, but also forced remotely from the Pacific and Atlantic Ocean. These teleconnections will likely modulate future rainfall variability in eastern Africa and should be considered when mitigating agricultural development and water management.

Preface

This report presents the results of my Master Thesis Project (450268) as part of the Earth Sciences, specializing in Applied Environmental Geoscience program at the Vrije Universiteit Amsterdam. This research project was carried out at the Royal Netherlands Institute of Sea Research (Royal NIOZ).

My Master Thesis Project focuses on the climate signals that are recorded in giant corals from northern Mozambique. Its focus is directed towards the interpretation of luminescence signals of the four coral cores, but additional geochemical profiles are used to provide additional data and to confirm potential hypothesis. This thesis examines past variability in rainfall and its connection to large scale climate oscillation, as recorded in the luminescence records of the four corals. Samples were collected covering a North-South profile in the bay Baia de Tunge in northern Mozambique, which is believed to be under the influence of the river plume of the Rovuma River that disembogues into the Indian Ocean approximately 40 km north of the bay.

Coral samples were collected in Baia de Tunge, northern Mozambique in October 2011 by Craig Grove, Andrew Rodgers and I. Core cutting was performed at the Geotechnical Laboratory at the VU University Amsterdam. Luminescence scanning, geochemical and isotope analysis were performed at the Royal NIOZ, Texel.

Table of Contents

1. Introduction

Reconstructing paleo-climatic conditions from giant corals such as *Porites* spp. has become increasingly more in recent years (e.g. McCulloch et al., 2003; Fleitmann et al., 2007; Grove et al., 2010; Prouty et al., 2010; Lough 2011a). Such long lived annually banded massive corals grow approximately 1-2 cm/year (Grove et al., 2012b) and have been shown to incorporate a range of tracers that help understanding past climate variability, allowing for the reconstruction of past local environmental conditions (Lough, 2011a). *Porites* spp. are particularly suitable for these studies due to their fast and regular growth, which allows for precise dating by band counting as well as easy and continuous sampling (Lough, 2011b). This study examines four cores from Baia de Tunge, Mozambique focusing on the drivers of past climate variability as recorded in the corals' skeleton.

1.1 Reconstructing environmental conditions

As corals grow, they take up the building blocks of their skeleton from the water column. Trace elements incorporated into the crystal lattice have been shown to be influenced by the geochemical composition of the water column and can thus be used as a proxy for past marine environmental conditions (e.g.: Fallon et al., 2002; McCulloch et al., 2003; Corrège, 2006; Fleitmann et al., 2007; Prouty et al., 2010; Grove et al., 2012b). There are several mechanisms how trace elements can be incorporated into the coral skeleton. They can be taken up as a substitute for calcium ions by the coral from the water column when it is collecting the building blocks for crystallization. The trace element is then incorporated into the crystal lattice as a substitute for Calcium (Fallon et al., 2002). Alternatively, they can be taken up through feeding or by the passive uptake of organic matter through coral tissue (Taylor et al., 1995; Fallon et al., 2002). Another incorporation mechanism is the trapping of particulate matter in skeletal cavities (Fallon et al., 2002). Relationships relating a certain environmental parameter, e.g. SST, with a proxy in the coral skeleton, e.g. Sr/Ca, have been previously demonstrated (Correge, 2006). The established relationships allow to reconstruct past environmental conditions from proxies recorded in the coral skeleton during its time of growth.

1.1.1 Density banding

Coral skeletons consist of alternating low and high density bands. Generally, every year the coral secrets one couplet consisting of one low and one high density growth band. These density bands can be visualized through X-radiography of coral core slabs (Fig. 1). Visualizing the growth laminae allows to define the sclerochronology by constructing an age model where one year consist of a high and a low density band. Additionally, optimal sampling tracks and sampling resolution can be defined according to X-radiograph images.

Figure 1: X-radiograph of four coral cores from Baia de Tunge, Mozambique. Density banding is visible in all cores.

1.1.2 Reconstructing SST and SSS

During the growth of the coral skeleton, some ions such as Sr^{2+} are incorporated into the crystal lattice by replacing Ca^{2+} (Corrège, 2006; Fallon et al., 2002). The concentration of Sr^{2+} relative to the one of Ca^{2+} in the crystal lattice has been shown to be dependent on the temperature of the surrounding water (Corrège, 2006). As SST warms, Sr/Ca ratios in the coral skeleton decrease at an average rate of -0.06 mmol/mol/°C (Corrège, 2006). Nevertheless, variability between sites and individual species is still high, which is why there is still no uniform equation to relate Sr/Ca to SST. However, theoretically Sr is an ideal element to examine past SST. It is a widely accepted that Sr-concentrations in the surface waters are relatively constant throughout the annual cycle, while other proxies such as $\delta^{18}O$ are strongly affected by the seasonal cycle of the changing balance in evaporation and transpiration (Corrège, 2006).

Another widely used proxy to reconstruct SST is the isotopic composition of the coral's carbonate skeleton. However, stable isotopes are more sensitive to changing environmental conditions and strongly susceptible to variations in evaporation and transpiration (Ren et al., 2002; Corrège, 2006). The transport of oxygen from the water column to the calcification site is very complex and includes different chemical forms, making it difficult to adequately estimate the fractionation of oxygen isotopes during transport. Additionally, it has been proposed that $\delta^{18}O$ can also be affected by the coral's growth rate, feeding habits, light availability or metabolic activity (McConnaghey, 1989). Estimates suggest that $\delta^{18}O$ increases with 0.18-0.22‰ per °C warming (Corrège, 2006). Since $\delta^{18}O$ is very susceptible to evaporation and transpiration, it can be used to track salinity changes in surface waters (Ren et al., 2002). Thus by removing the temperature signal from the $\delta^{18}O$ record using the relationship of Sr/Ca and SST, Sea Surface Salinity (SSS) can be estimated. Next to Sr/Ca and $\delta^{18}O$, U/Ca, Mg/Ca and B/Ca have been suggested to carry a signal of SST (Corrège, 2006). Nevertheless, the reliability of these proxies as a tracer of SST is still questionable.

1.1.3 Reconstructing rainfall variability

Ba/Ca ratios in the coral skeleton are not significantly affected by temperature, however, have been shown to reconstruct terrestrial sediment input (Fleitmann et al., 2007; McCulloch et al., 2003; Prouty et al., 2010;, Grove et al., 2012b). In the river catchment, Barium is adsorbed to suspended sediment particles, mostly clay particles. Once transported to the estuarine mixing zone, Barium desorbs from the clay particles in the low salinity zone due to the higher ionic strength of seawater (McCulloch et al., 2003). After desorption, Barium behaves as a conservative dissolved tracer following a conservative mixing pattern (Sinclair and McCulloch, 2004; McCulloch et al., 2003) and is incorporated into the coral skeleton in proportion to its concentration in the ambient water column (McCulloch et al., 2003; Prouty et al., 2010). Thus the relative amounts of Ba in the coral skeleton offer insight into past sediment discharge into the bay where the coral was sampled (Grove et al., 2012b; McCulloch et al., 2003; Prouty et al., 2010).

In addition to geochemical proxies, coral luminescence has been utilized to reconstruct past river discharge (Lough, 2011b; Grove et al., 2010). When placed under ultraviolet (UV) light, corals display luminescent bands of varying intensities. Faint changes in luminescent banding can be explained by changing aragonite densities due to the annual density cycle (Grove et al., 2010). Bright luminescent bands, however, can be linked to terrestrial runoff (Lough et al., 2002). They are likely caused by the incorporation of soil derived humic acids which are transported to the ocean via rivers (Grove et al., 2010). Thus bright luminescent bands can therefore be related to the seasonal cycle of river runoff. The brightness of the luminescent bands has been related to the amount humic acid carried by rivers and thereby to river runoff and rainfall intensity (Lough et al., 2002). The most intense bands correspond to flood events (Lough et al., 2002). As luminescence intensity is controlled by the amount of humic acids incorporated into the skeleton as well as skeletal density, it is important to reliably deconvolve the two signals in order to accurately reconstruct past changes in rainfall. Grove et al. (2010) developed a new method that allows differentiation between the two components. They used spectral luminescence scanning whereby a Dichroic RGB beam filter splits the luminescence intensities into Red, Green and Blue spectral domains. Intensities of green and blue were found to be of a similar magnitude, while red intensities were significantly lower. Spectral emissions of both, humic acids and aragonite, are of similar wavelengths in the green/blue spectrum. However, wavelengths associated with humic acids are slightly longer and cluster at the green end of the spectrum, while the blue is more representative for aragonite. Thus the Green/Blue spectral ratio is a measure of the humic acid concentration relative to the aragonite density of the coral. Removing the density effect from the luminescence record by applying spectral luminescence scanning allowed the authors to reconstruct a clearer record of past river runoff.

Past studies on coral luminescence have identified declining trends in luminescence records with time, common to a significant proportion of records (Grove et al., 2010; Lough, 2011b). These declining trends can be linked to a decline in skeletal density (Grove et al., 2010; Lough, 2011b). However, the cause of this trend is still unclear. While Grove et al. (2010) propose that the observed changes are caused by recent changes in the marine environment, Lough (2011b) suggests that the declining density trend is the result of an age artifact.

1.2 Corals in a changing climate

As anthropogenic climate change proceeds, environmental conditions in which corals thrive are likely to change: i.e. SST are modeled to increase approximately by 0.8 – 1.0 °C along the east African coast within the next 100 years (Deser et al., 2010); rainfall is expected to decrease by 0 - 0.6 mm/day over eastern Africa due to Walker-cell-like disruptions of atmospheric circulations causing more moisture to be released over the open ocean while less moisture reaches eastern Africa (Funk et al., 2008; Deser et al., 2010); tropical cyclones reaching the coast of eastern Africa are expected to increase in strength and frequency (Elsner et al., 2008) and the recurrence of El Niño events is predicted to increase (Spencer et al., 2000). In addition to climate change, land use change of the hinterland due to increasing population and demand for resources will enhance erosion and thereby alter the amount of sediment transported to the Ocean by East African Rivers (Funk et al., 2008; Grove et al., 2012a).

1.3 Accuracy of climate reconstruction based on coral cores

Coral proxies are used to reconstruct past river flow (McCulloch et al., 2003), SST (Corrège, 2006), SSS (Corrège, 2006) and sediment input into coastal areas (McCulloch et al., 2003). Many show correlations with climate phenomena such as El Niño Southern Oscillation (ENSO) (Lough, 2011a) or the Pacific Decadal Oscillation (PDO) (Grove et al., 2012a). Long-term reconstructions of past hydro-climatic conditions based on coral cores are currently being incorporated into multi-proxy, large scale climate reconstructions (Lough, 2011b; Lough, 2004). Next to reconstructing local climatic conditions, coral cores are also used to constrain the recurrence of inter-decadal and multi-decadal climate oscillations, such as ENSO or the PDO (Lough, 2011b; Lough, 2004). Despite good correlations between coral records and climate indices, little is known about the reproducibility of the data (Lough, 2004). Lough (2004) compared twenty annually or sub-annually resolved coral records from the Pacific and Indian Ocean to assess the reliability of coral records to reproduce large-scale relationships with climate. She concluded that the relationship between corals and climate varies between different corals and in some corals even with time. Thus, climate reconstructions should be verified with independent proxy climate reconstructions and replications should be performed to ensure the presence of a common environmental signal.

This study looks at four corals originating from a small bay in the Quirimbas Archipelago, northern Mozambique. The corals were sampled at the same time and occurred within the close vicinity of each other. The records spans the time periods 1910-2011, 1941-2011, 1967-2011 and 1975-2011. By comparing the four corals' luminescence records as well as their Ba/Ca and Sr/Ca records, this study aims at quantifying the reproducibility of environmental signals recorded in different corals located in the same climatic and environmental setting.

1.4 Climate oscillations

Climatic variability can have a crucial influence on the delicate balance of environmental parameters corals need to thrive in (Spencer et al., 2000; Obura, 2009). The climate of Eastern Africa is influenced by several climate oscillations including the El Niño Southern Oscillation (ENSO), the Indian Ocean Dipole (IOD) as well as the Pacific Decadal Oscillation (PDO). Consequently, such signals may be recorded by the coral as they grow, relating to SST and rainfall variability.

1.4.1 ENSO

The El Niño Southern Oscillation is the most prominent climate variation on Earth and recurs within a period ranging from two to seven years (McPhaden et al., 2006). Typically the trade winds cause the transport of warm water masses from the eastern Pacific to the western Pacific, thus creating a warm pool in the west, while upwelling of cold water masses is dominant in the east, along the coast of South America. The cold, upwelled waters typically form a cold tongue along the equatorial Pacific (McPhaden et al., 2006). The SST gradient between the eastern and western Pacific reinforces the air pressure difference between the eastern and western Pacific in turn strengthening the trade winds. During an El Niño event, the trade winds weaken and the transport of warm water masses from the east to the west is reduced, resulting in anomalously cold (warm) temperatures in the west (east) and reduced upwelling along the west coast of South America (McPhaden et al., 2006). The reduced SST gradient causes a weakened air pressure gradient between the east and west and thus a further weakening of the trade winds. Internal ocean dynamics favoring upwelling and delayed negative feedback mechanisms eventually break the cycle and bring about the end of an El Niño (McPhaden et al., 2006). A La Niña event occurs, if the trade winds are exceptionally strong and in turn the SST gradient as well as the air pressure gradient between the eastern and western Pacific are higher than usual. ENSO typically peaks around the end of the calendar year. The months November – January are considered the mature ENSO phase (Tzipermann et al., 1998).

ENSO is shown to have teleconnections all over the globe, including Eastern Africa. It is responsible for variations in regional weather patterns causing droughts, floods, heat waves and extreme events (McPhaden et al., 2006). During an El Niño event, SST are anomalously warm in the western Indian Ocean (Spencer et al., 2000). Typically an increase of approximately 0.5°C is observed in the western Indian Ocean. Nevertheless, during extreme El Niño events, such as the one that occurred in 1997/1998, positive SST anomalies of up to 2° have been observed in the western Indian Ocean (Ramana et al., 2004). ENSO is responsible for approximately 50% of the variability in East African rainfall (Indeje et al., 2000). During the onset of ENSO, rainfall over southern Tanzania and northern Mozambique significantly increases from October – May. Contrastingly, in the year following an El Niño event, the months March, April and May are significantly dryer than average (Indeje et al., 2000).

The variability of the El Niño Southern Oscillation can be correlated with several distinct features in SST anomalies almost all over the globe (Fig 2). SST can be negatively correlated with ENSO indices in the southern Pacific Ocean, where a tongue extends from the west coast of South America towards Australia. This correlation exists all year round but is strongest from August – March. SST close to eastern Indonesia and north of Australia also negatively correlate with ENSO all year. This correlation is strongest from July – February. Positive correlations of SST with ENSO can be found in the equatorial

Pacific all year, just north of the typical El-Niño tongue in the southern Pacific. Additionally, positive correlations occur in the central Indian Ocean from September – June. From December – April, ENSO can be positively correlated with SST over the study area, while the months of February and March display the strongest correlations.
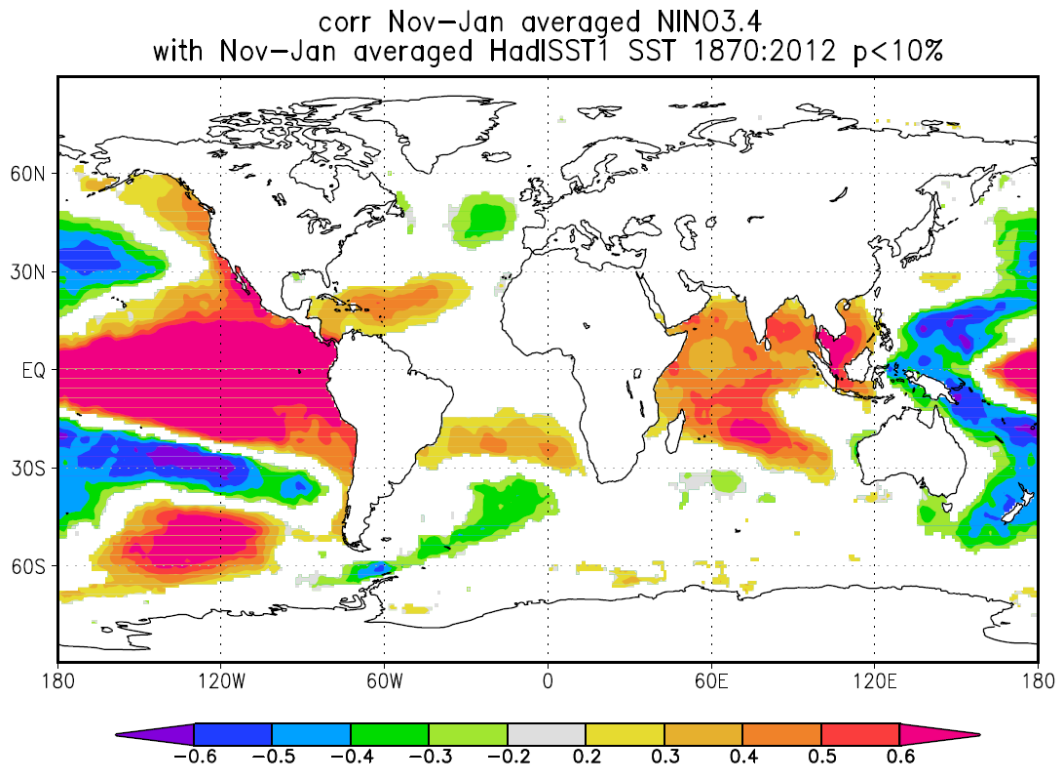
Figure 2: The effects of ENSO on Sea Surface Temperature during its mature phase November – January.

1.4.2 IOD

Another climate oscillation with worldwide teleconnections is the Indian Ocean Dipole (IOD) (Meyers et al, 2006). During an IOD event, an east-west dipole of SST anomalies evolves in the Indian Ocean. The peak phase of the IOD is September – November (Yamagata et al., 2004). During the peak phase of a positive IOD event, the equatorial winds reverse from westerlies to easterlies (Yamagata et al., 2004). Changes in SST are closely linked to changes in wind patterns. During a positive IOD event, anomalously cool SSTs occur in the eastern Indian Ocean while temperatures in the west are warmer than usual. Also, rainfall over eastern Africa is increased and characteristically occurs as active short rains during a positive IOD event (Yamagata et al., 2004). During the negative phase of the IOD, conditions are exactly opposite to those of a positive IOD event with colder SST and decreased rainfall in the western Indian Ocean (Yamagata et al., 2004). The strongest SST anomalies occur when a positive (negative) IOD event coincides with the occurrence of El Niño (La Niña) (Meyers et al., 2006).

The IOD also has effects on SST that go beyond the Indian Ocean (Fig 3). In the period July – December, a positive correlation occurs in the equatorial Pacific. In the western Indian Ocean, SST positively correlates with the IOD index from May – December. This correlation is most pronounced in October and November. In the eastern Indian Ocean a negative correlation occurs for the period February – December, which is strongest from July – October.
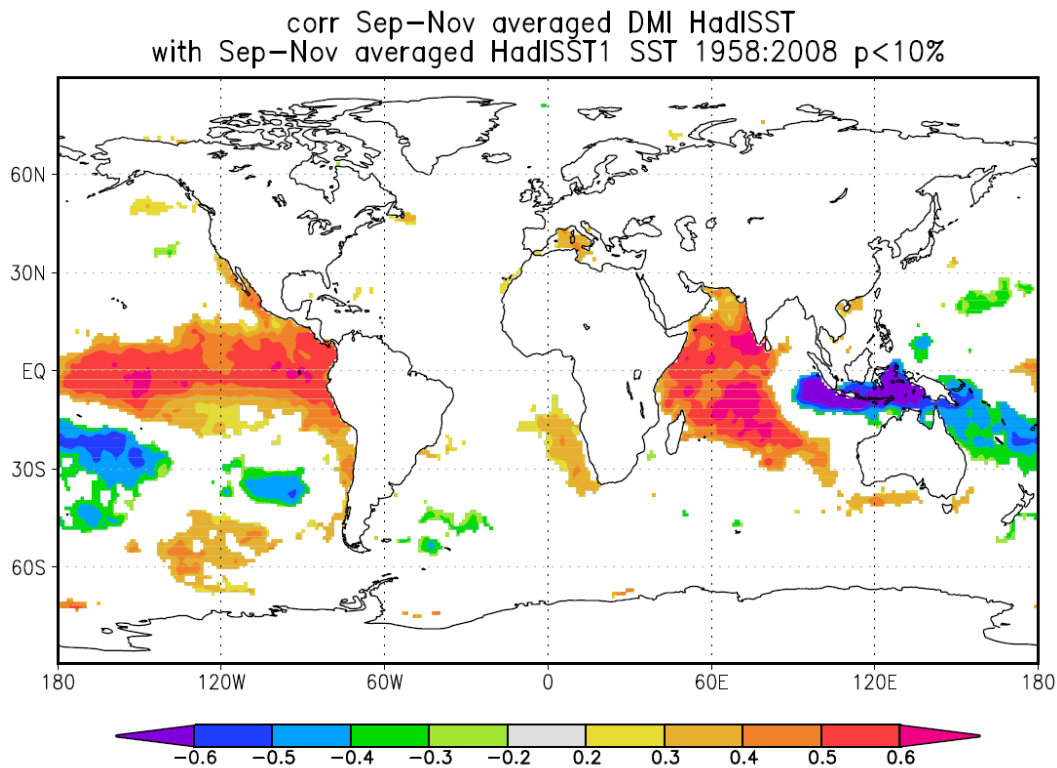
Figure 3: The effects of IOD on SST during its peak phase.

1.4.3 PDO

The Pacific Decadal Oscillation (PDO) is a major climate oscillation with multi-decadal (50-70 years) and inter-decadal (15-25 years) periods originating in the north Pacific, but with teleconnections extending all over the globe, including the Indian Ocean (Mantua and Hare, 2002). It has been shown, that the PDO is modulated by ENSO at inter-annual and multi-decadal timescales (Newman et al., 2003). During a positive PDO phase, Indian Ocean SST anomalies are warm while during a negative PDO phase SSTs are anomalously cool (Deser et al., 2010). During phases of positive (negative) PDO, rainfall over northern Madagascar has been shown to increase (decrease) (Grove et al., 2012a). Deser et al. (2004) estimate that during the positive PDO phase ranging from 1979 to 1997, rainfall over southeastern Africa was increased by 4 – 8 mm/day from December till March.

The PDO has also been shown to affect SST (Fig 4). There is a negative correlation between the PDO index and SST in the north Pacific all year. This correlation is strongest in the period October – July. A positive correlation can be identified over the equatorial and north-east Pacific all year, which is most pronounced in the period February – June. A positive correlation also occurs over the central Indian Ocean for the months February – May and August.
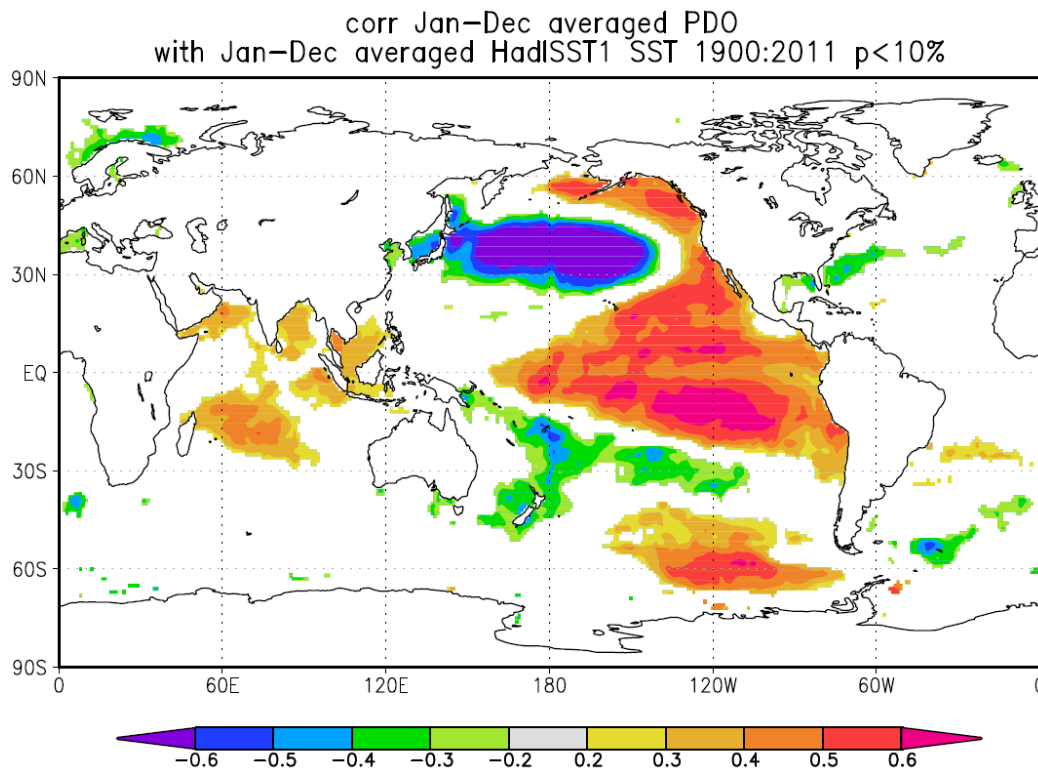
Figure 4: The effects of the PDO on SST averaged over one year (January-December)

1.4.4 AMO

There is another climate oscillation that operates on similar timescales as the PDO. The Atlantic Multidecadal Oscillation (AMO) is a climate oscillation that recurs with a periodicity of 65-70 years (Schlesinger and Ramankutty, 1994). The AMO is an alternation of warm and cold SST in the North Atlantic that switches every few decades (Guan and Nigam, 2008). The SST anomalies originate in the Davis Straits and the Labrador Sea, from where they move eastward in the mid-latitudes (Guan and Nigam, 2008). Subsequently they move equator-ward at the eastern edge of the basin along the Canary current track. Finally, the SST anomalies propagate westward in the subtropics. During the mature phase of the AMO, SST anomalies can be as large as 0.4°C and are centered at approximately 50°N (Guan and Nigam, 2008). Cool AMO phases occurred in the 1900s – 1920s and 1960s – 1980s, while warm phases occurred the 1930s – 1950s and since the 1990s (Knight et al., 2006).
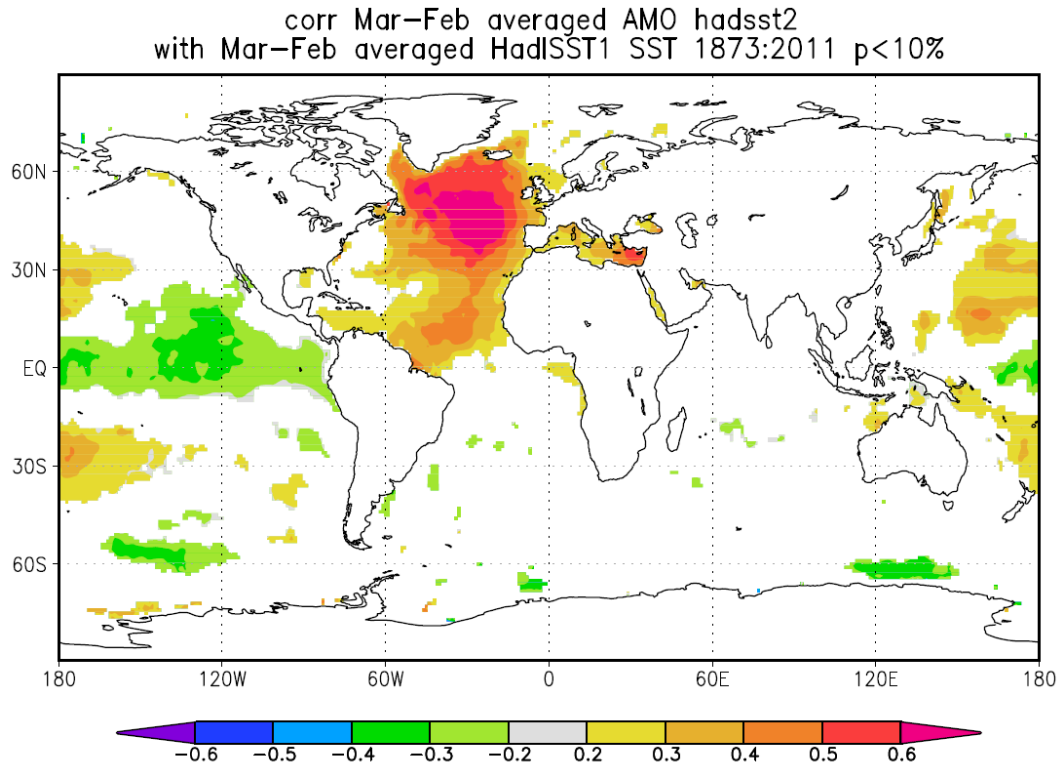
Figure 5: Effects of the AMO on SST averaged over one year (March – February)

The AMO has been shown to impact climate on the continents surrounding the Atlantic Ocean basin. A warm (cold) phase of the AMO has been shown to reduce (increase) rainfall over Northeastern Brazil and increase (reduce) rainfall over the Sahel region (Knight et al., 2006). This is due to a northward displacement of the ITCZ relative to its climatological MAM position, which is caused by elevated SST in the North Atlantic during a positive AMO phase. It has also been suggested that the AMO (partly) controls the amount and strength of hurricanes that develop over the tropical Atlantic Ocean (Knight et al., 2006). Additionally, it has been shown that the AMO has an impact on rainfall in the United States of America and Northern Europe (Knight et al., 2006). So far, it has been shown that the AMO has an impact on climate systems that are bordering the Atlantic Ocean.

1.5 Study Site: The north of the Quirimbas Archipelago

The corals investigated in this study were sampled close to the Quirimbas Archipelago off the coast of northeastern Mozambique in the Indian Ocean. The coral cores were drilled in the bay 'Baia de Tunge', close to the northernmost island of the Quirimbas Archipelago – Tecomaji (Fig.6). The Quirimbas Archipelago is part of the province of Cabo Delgado. It consists of 28 islands, which are located close to the coast. The sizes of the islands vary from 24 km^2 to less than 1 km^2. The maximum distance between two islands is not more than 10 km and the archipelago is spread out over 340 km of coastline (WIOMSA, 2011). The southernmost island is located just north of Pemba, while the northernmost island – Tecomaji - is located approximately 40 km south of the Mozambique-Tanzania border.
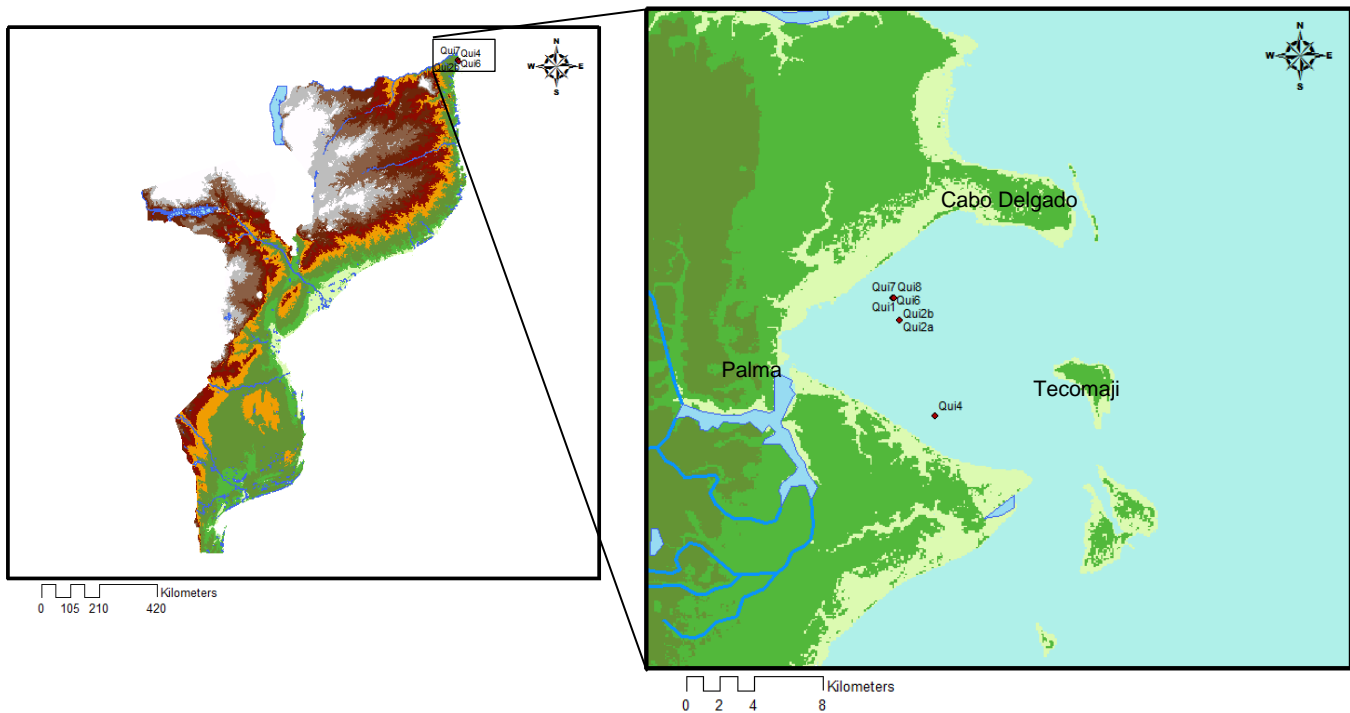
Figure 6: The location of research area is shown on the left. The sampling location of the Quirimbas coral cores is indicated on the right.

Parts of the Quirimbas Archipelago are protected as they are part of the Quirimbas National Park (Bunce et al., 2010). Additionally, the coast just north of the Quirimbas is also protected area (Bunce et al., 2010). The Mozambican government plans to establish the Rovuma-Palma National Park, which would protect areas adjacent to both already existing National Parks (Guerreiro, 2011). Baia de Tunge would be included in the protected areas, which could have huge influences on future land use changes of the hinterland, fishing practices within the bay, mining practices and/or oil and gas exploration.

Coral reefs occur abundantly in the region (Cuoto et al., 2008, p. 155). They are found on the shallow shelf (water depth <50 m) located between the coast and the islands as well as on the seaward side of the islands up to the continental slope. 152 species in 42 genera and 15 families have been

identified close to the study site in the Vamizi island area, among which *Porites* spp. were identified as one of the most commonly occurring corals (Cuoto et al., 2008, p. 155).

Coral reefs in the Quirimbas are thought to be the most pristine of the country, with only 20% damaged and 10% mortality (Rodrigues et al., 1999 as referred to in Cuoto et al., 2008, p. 155). During a Representative Marine Habitat Survey, conducted in 2007 by Impacto Lda, no bleaching or diseases were identified in the northern Quirimbas. Further, limited damage of natural or anthropogenic origin to the corals were observed (Cuoto et al., 2008, p. 155). The good state of the coral reefs is attributed to low pressure from people, despite some artisanal fisheries in the area (Cuoto et al., 2008, p. 155). In contrast to the observations described by Rodrigues et al. (1999), Motta et al. (2002) suggested that the reefs in the Quirimbas are in very bad shape due to intense bleaching that occurred during the 1997-1998 El Niño. They looked at coral reefs in the southern Quirimbas and estimated that approximately 74% of the reefs were dead and covered by algae or consisted of rocky debris. They estimated the fishing pressure on the Quirimbas reefs to be very high.

People in the Cabo Delgado province mostly live in rural areas (83%) and depend on agriculture, fishery and forestry (Guerreiro, 2010). In the few last years, illegal logging increased in the area due to increasing economic pressure and weak law enforcement (Guerreiro, 2010). The strategic plan of the government to support the economic development of the region includes the development of natural gas mining as well as increasing tourism and artisanal fishery (Guerreiro, 2010).

The natural gas reservoirs in the Rovuma basin are the largest ones in Mozambique (Anadarko Petroleum Corporation, 2012b). In 2006, the company Anadarko obtained the rights to extract natural gas from the Rovuma Offshore Area 1, which includes the northern Quirimbas Archipelago (Anadarko Petroleum Corporation, 2012b).

As of January 2012, Anadarko has discovered five natural gas fields, drilled three successful wells and has plans to drill at least six more wells in the close vicinity of the study area (Anadarko Petroleum Corporation, 2012a). The estimated volume of recoverable natural gas from the Rovuma Offshore Area amounts to 17 - 30+ trillion cubic feet (Anadarko Petroleum Corporation, 2012b). Due to the large amounts of recoverable natural gas, Anadarko plans to establish a commercial liquefied natural gas development. The commercial liquefied natural gas development is planned to initially process 10 million tons per year with the option to extend the production to 30 million tons per year (Anadarko Petroleum Corporation, 2012b). The production plant will be located onshore, on the southern side of Baia de Tunge, while the liquefied natural gas will be transported via pipelines (Boman, 2012). The distance between the production site and the production plant that has to be covered with pipelines is 56 km (Anadarko Petroleum Corporation, 2012b). The production plant will be the largest LNG plant in Africa and could make Mozambique the third largest LNG exporter in the world (Boman, 2012). The construction of this large LNG production plant will have huge impacts on the coastal communities close to and within the bay, as well as the hinterland. Infrastructure on land will be extended, land use changes to accommodate the facilities and its workers will occur, pipelines will be built within the bay to transport the gas as well as dredging will occur to build channels that can accommodate the large

vessels that will finally transport the processed liquefied natural gas. This will have a huge impact on the coral communities living close to and within the bay.

1.5.1. Rivers influencing the corals

The rivers that drain directly into Palma bay have a relatively small watershed and drain an area of approximately 450 km^2 (Fig. 7). Approximately 40 km north of the sampling site the Rovuma River disembogues into the Indian Ocean (Fig. 7). The riverhead is located in the Mantogaro Mountains, southern Tanzania, from where it continues towards the Indian Ocean (Rovuma Consultancy, 2012). It has a length of 800 km, 650 km of which form the border of Tanzania and Mozambique. Its catchment area has the size of 155,000 km^2, 64 % of which are in Mozambican territory, while 34% belong to Tanzania and 2% to Malawi (Rovuma consultancy, 2012). The two largest tributaries feeding the Rovuma River from the Mozambican side are the Lucheringo and Lugenda rivers, while the Likonde, Muhuwesi and Lumesule rivers are the most important tributaries joining the Rovuma River in Tanzania. In general, the Rovuma River Basin is very scarcely populated and no major dams or hydroelectric infrastructure have been installed in the river basin. The geology of the basin consists of manly volcanic and metamorphic rocks, few sedimentary rocks can be found (Rovuma Consultancy, 2012). The vegetation in the Rovuma basin includes lowland coastal forests, diverse types of woodlands, wetlands and mangrove forests. The river's mean annual runoff is estimated to be 27.5 x 10^9 m^3 at the river mouth (Rovuma Consultancy, 2012).
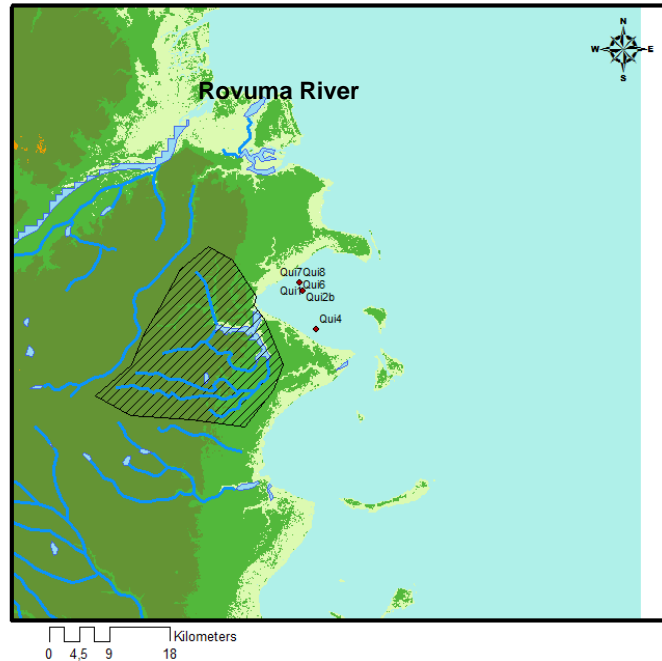
Figure 7: The rivers draining into the sampling bay next to the city of Palma drain an area of approximately 450 km^2
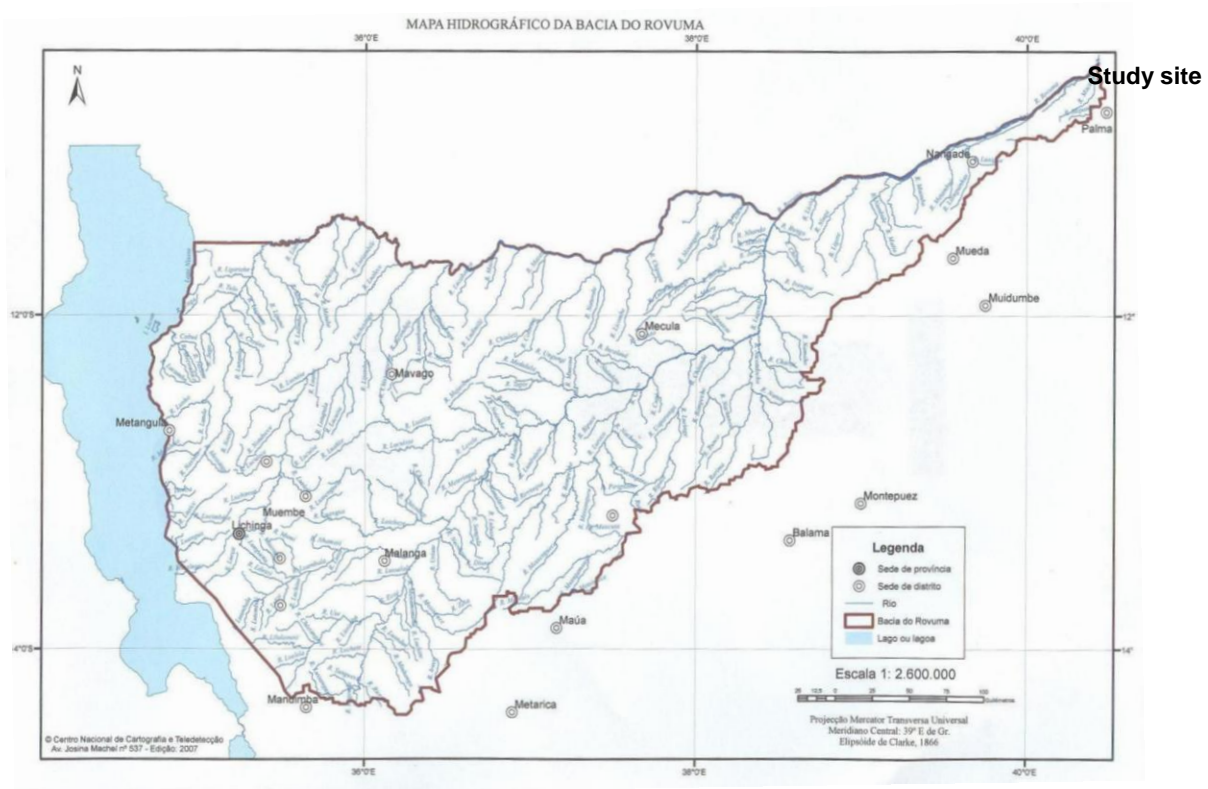
Figure 8: Watershed of the Rovuma River. Adapted from Centro National de Cartografia et Teledetecção, Av. Josina Machel n° 537 – Edição 2007.

1.5.2 Climate of the study site

The Quirimbas Archipelago is strongly influenced by the Intertropical Convergence Zone (ITCZ). The climate is characterized by typical wet and dry seasons (Cuoto et al., 2008, p. 98). The wet season lasts from November till May and the dry season occurs during the months ranging from June till October (Fig. 19). In the dry season, average rainfall is below 20 mm/month, with a minimum of 11 mm/month in September (Fig. 10). In the wet season, average rainfall is generally above 50 mm/month, increasing up to 200 mm/month in January (Fig. 10). At the study site, rainfall approximates to 1070 mm/year, 92% (990 mm) of which fall in the wet season (Fig. 10). No significant change in total annual precipitation could be observed over the study area in the period 1901-2009 (Fig. 9). The data presented here is a composite of the two datasets CRU TS3.1 and GPCC V5. The two datasets are significantly correlated. Both datasets are reanalysis fields based on station data. Daily measurements spanning the entire globe are integrated in order to create one reanalysis field reconstructing global climate since January 1901 (Schneider et al., 2011, University of East Anglia Climate Research Unit, 2008). When interpreting the data, it is important to check how many stations were measuring data close to the area of interest at the time of interest. There are fewer stations available when going back in time, making the early data more unreliable than the recent data. The GPCC currently integrates climate stations that are spread as evenly as possible worldwide. The amount of stations available has increased with time, there are only ca. 1.500 stations available covering the period 1901-1910, increasing to approx. 21.000 in 1961 and currently 40.000 climate stations are used to assess today's climate (Schneider et al., 2011). The error of the reconstruction has been estimated to be 7-40% if five stations are used for the reconstruction, while this value declines to 5-20% if 10 stations are included (Schneider et al., 2011).
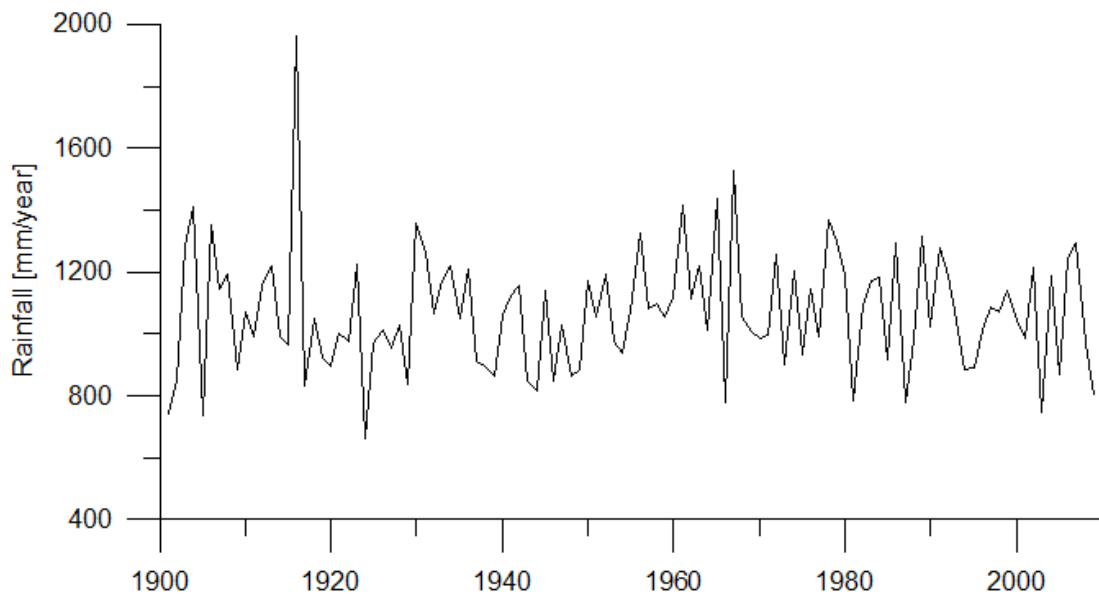
Figure 9: Total annual precipitation (composite of CRU TS3.1 and GPCC V5) from 1901-2009. Annual precipitation was calculated by summing up the precipitation of the individual months. Calculations are based on the annual cycle of precipitation, thus one year represents the period September-August.
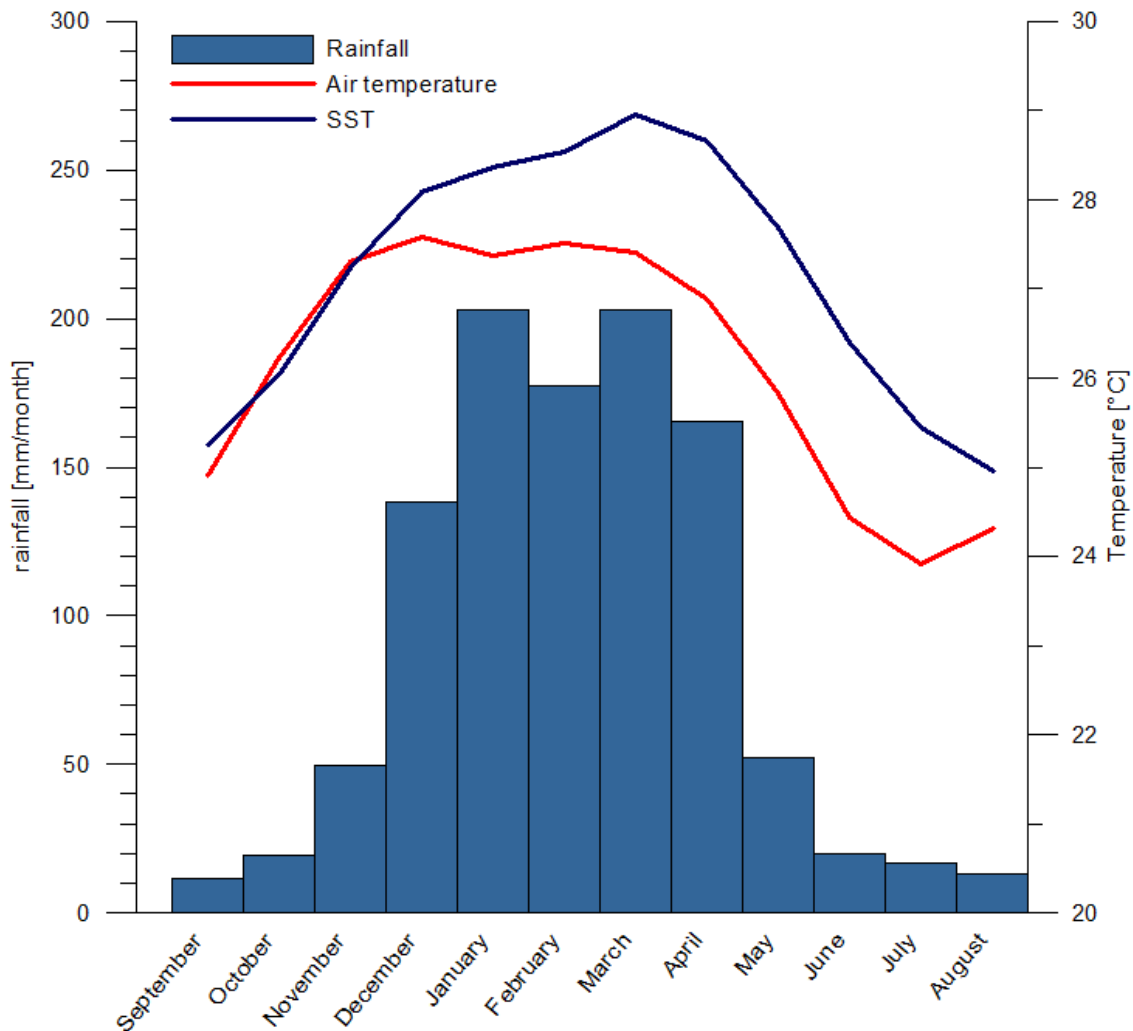
Figure 10: Climate diagram of the study area. Data presented is averaged for the time period 1901-2009. The presented rainfall data is a composite of the modeled data of CRU TS 3.1 and GPCC V5; temperature data is an average of the maximum and minimum temperature of CRU TS 3.1 and SST is a composite of the model results of HadISST and ERSST (data obtained from the KNMI climate explorer http://climexp.knmi.nl).

The data presented here is an average of the period 1901-2009. The presented rainfall data is a composite of the modeled data of CRU TS 3.1 and GPCC V5; temperature data is an average of the maximum and minimum temperature of CRU TS 3.1 and SST is a composite of the model results of HadISST and ERSST. In the wet season, temperatures range from 25.8°C to 27.6°C while in the dry season temperatures are lower, ranging from 23.9°C to 26.2°C (Fig. 10). The coldest month of the year is July with an average temperature of 23.9°C; while the hottest month is December with an average temperature of 27.6°C. The yearly temperature averages at 26.1°C.

The seasonal cycle of sea surface temperatures (SST) close to the study site lags the seasonal cycle of air temperatures by approximately one month (Fig. 10). The coldest average sea surface

temperatures are observed in August (25.0°C) while the warmest average temperatures occur in March (29.0°C) (Fig. 10). Yearly average sea surface temperatures in the region are 27.1°C.

Winds in the study area are influenced by the monsoonal system and are therefore closely linked to the position of the ITCZ (Cuoto et al., 2008, p 98). Winds generally come from the northeast during southern hemisphere summer while during southern hemisphere winter the wind mostly comes from the southeast. Wind speeds are generally low, except when a tropical cyclone passes through. In January, when the ITCZ is located south of the study area, the winds come from a north/northwest direction while wind speeds averaging 5-10 km/h are most common (Cuoto et al., 2008, p 99). In April, winds mostly come from the south/southwest and have average wind speeds of 10-15 km/h (Cuoto et al., 2008, p 100). In July the wind blows stronger (Cuoto et al., 2008, p 101). Here, average wind speeds are between 15-20 km/h, yet wind speeds above 20 km/h are commonly observed. The general wind direction in July is from the south/southeast. In September, the wind direction is still from the south/southeast while the most common wind speed declines to 10-15 km/h during this period (Cuoto et al., 2008, p 102).
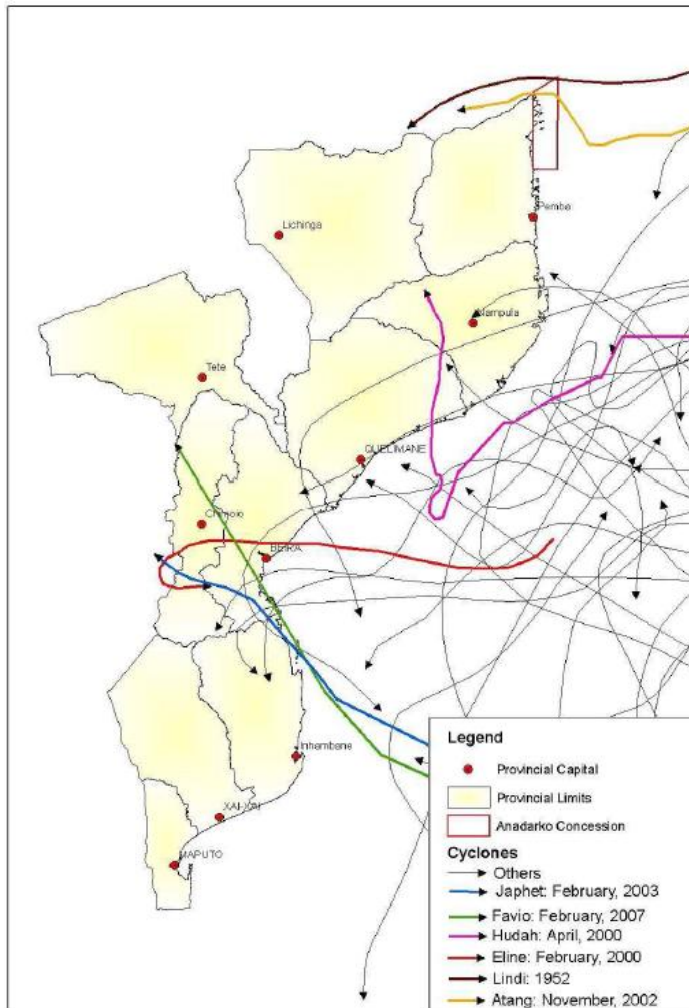
Figure 11: Tracks of cyclones reaching the Mozambican coast, including the cyclones Lindi and Atang that hit in the North of Mozambique. Adapted from Cuoto et al. (2008, p 105).

Mozambique is prone to tropical storms and tropical cyclones (Cuoto et al., 2008, p 103). They are typically generated in the middle of the Indian Ocean from where they move west/southwest towards the coasts of Madagascar and Mozambique. Cyclones typically impact the coast of Mozambique at the province Namupla or Cabo Delgado, where the study site is located. They move at speeds of approximately 10 km/h. After impacting the coast they usually turn south and reduce their speed while passing over the Mozambique Channel, where they are finally downgraded. There are approximately 15-20 cyclones generated every year, but most of them do not reach the Mozambican coast, as they lose energy before reaching the coast and/or hit the Madagascan coastline (Cuoto et al., 2008, p. 104).

The coastline of central Mozambique is prone to cyclone activity. In the past years, significant damage caused by heavy rains and strong winds has been observed (Cuoto et al., 2008, p 104). Contrastingly, the northern coastline of Mozambique, where the Quirimbas Archipelago is located, is not frequently subjected to the effects of tropical cyclones. In 1952, when Cyclone Lindi passed over the area, notable damage occurred in the District of Palma and southern Tanzania (Cuoto et al., 2008, p 104). More recently, Cyclone Atang reached the coast of Northern Mozambique in November 2002. It caused heavy rains and strong winds with velocities of up to 70 km/h (Cuoto et al., 2008, p 104).

1.5.3 Oceanographic conditions of the study area

The general ocean circulation in the Mozambique Channel is controlled by the large scale circulation of the Indian Ocean (Cuoto et al., 2008, p 108). Water masses in the southern Indian Ocean circulate anticlockwise in a huge gyre, which is driven by winds. The current defining the northern edge of this gyre is the South Equatorial Current, which flows westward in the Indian Ocean, just south of the Equator. When this current reaches Madagascar it splits into two branches, the Eastern Madagascar Current and the continuation of the South Equatorial Current (Fig. 12) (Cuoto et al., 2008, p 108). While the Eastern Madagascar Current flows southward along the eastern coast of Madagascar, the South Equatorial Current continues westwards to the east coast of Africa (Fig. 12). Close to the coast it splits into a northward flowing branch, which continues as the East African Coastal Current along the coast of Tanzania and Kenya, and a southward flowing branch – the Mozambique Current, which flows southward along the coast of Mozambique (Fig. 12) (Cuoto et al., 2008, p 108). The general direction of flow along the Mozambican coast is southward. Nevertheless, it has been shown that secondary currents can occur in smaller basins and bays, which can even exhibit a flow direction opposite to the general one (Fig. 12) (Cuoto et al., 2008, p 108). There is no detailed information available on the regional circulation patterns in the Quirimbas Archipelago. Hammer et al. (2012) investigated the tidal currents at a bay inlet and a coral based channel in the Quirimbas close to Pemba, but could not identify any strong currents, which they attributed to difficulties with their site-screening and vague information.

Little is known about the bathymetry of the study area. In general, the northern coast of Mozambique is characterized by a narrow continental shelf and a steep continental slope (Cuoto et al., 2008, p 112). The continental shelf along the province of Cabo Delgado is characterized by alternating sandy flats with coral reefs and rough volcanic rock structures. Beyond the fringing coral reefs of the

Quirimbas Archipelago, the continental slope begins and is typically quite steep with slopes of up to 45° (Cuoto et al., 2008, p 114).
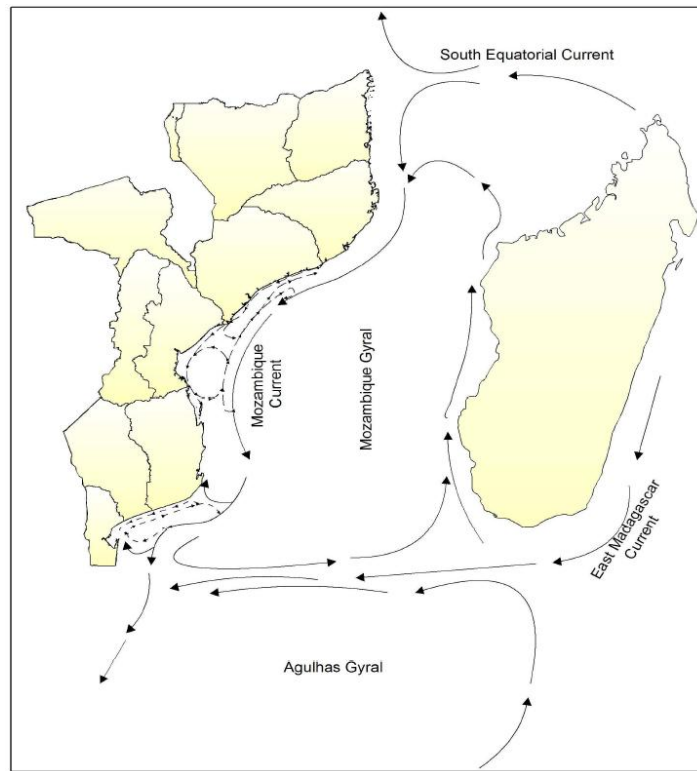
Figure 12: Surface currents in the Mozambique channel. Adapted from Cuoto et al. (2008, p. 109). Solid arrows indicate general surface currents while the broken arrows represent secondary currents.

Tides in the Quirimbas are diurnal and the tidal waves turn anticlockwise due to the influence of the Coriolis force. In Pemba, just south of the Quirimbas Archipelago, the amplitude of the tides ranges from 2.8 m (mean neap tide) to 4.0 m (mean spring tide) (Cuoto et al., 2008, p 107).

Salinities on the continental shelf of northern Mozambique have been shown to be approximately 35 psu. Slight variations occur due to the varying evaporation - precipitation balance throughout the year (Cuoto et al., 2008, p 116). The surface waters in the Quirimbas Archipelago are well oxygenated throughout the entire year (Cuoto et al., 2008, p 117).

2. Methods

2.1 Fieldwork in Mozambique (02.10.2011 – 22.10.2011)

Fieldwork was carried out in Mozambique in October 2011. Coral samples were collected in three locations: near the island of Inhaca, just outside Pemba Bay and in the bay 'Baia de Tunge' in the Quirimbas Archipelago. While Inhaca is situated near the city of Maputo in the South of Mozambique, the other two sampling locations are located in the North of the country. This study focuses on the cores from the Quirimbas archipelago. In the period of the 15th to 20th October 2011 samples were collected in the Quirimbas archipelago in the north of Mozambique. The corals in this area of the Quirimbas were generally not in a good shape. Many *Porites* spp. had died on top and in the reefs, a lot of damaged or dead coral could be found. Close to the mainland at the northeastern edge of the bay, an entire reef community was found dead and overgrown with algae. Water temperature was estimated at approximately 30°C.

The corals selected for drilling originated from three sites. Site 1 was located towards the northern shoreline of the bay, while Site 3 was close to the southern shoreline (Fig. 6). Site 2 was located in between the two sites towards the center of the bay (Fig. 6). The distance between Site 1 and Site 2 was approximately 1.35 km, while the distance between Site 2 and Site 3 was approximately 6 km. Seven coral cores originating from six different corals were collected (Table 1). Four corals were sampled at Site 1 and one coral each at sites 2 and 3. The cores were between 35 and 186 cm long and the maximum age was determined to 102 years.

Core Name	Locality	GPS Position	Species	length	Estimated growth	Age	Tissue thickness	depth
Qui1	Quirimbas, Site 1	S10º44.134' E040º32.649'	P. lutea	125 cm	1.75 cm/yr	1970 - 2011	5 mm	1-2 m
Qui6	Quirimbas, Site 1	S10º44.112' E040º32.646'	P. lobata	112 cm	1.5 cm/yr	1967 - 2011	10 mm	2-3 m
Qui7	Quirimbas, Site 1	S10º44.119' E040º32.650'	P. lutea	130 cm	2 cm/yr	1957 - 2011	8 mm	2-3 m
Qui8	Quirimbas, Site 1	S10º44.123' E040º32.651'	P. lutea	50 cm	1.2 cm/yr	1990 - 2011	7 mm	2-3 m
Qui2a	Quirimbas, Site 2	S10º44.815' E040º32.837'	P. lutea	35 cm	1.5 cm/yr	1997 - 2011	6 mm	2-3 m
Qui2b	Quirimbas, Site 2	S10º44.815' E040º32.837'	P. lutea	165 cm	1.5 cm/yr	1941 - 2011	5 mm	2-3 m
Qui4	Quirimbas, Site 3	S10º47.854' E040º33.959'	P. lutea	186 cm	1.5 cm/yr	1910 - 2011	3 mm	2-3 m

Table 1: Details of the sampled cores. Cores Qui4, Qui6, Qui7 and Qui2b were selected for further analysis. Growth rates were estimated in the field. The given age was later determined by applying an age model (see section 2.7)

A tissue sample to determine the Porites species and zooxanthelleae genetic types was collected from every coral from which a core was obtained. Additionally, six HOBO U22 temperature loggers were installed, two at every location. The temperature loggers are set to record the water temperatures every hour and will be collected approximately one year after their deployment. In the Quirimbas, temperature loggers were attached to the corals Qui 2 and Qui 4 at sites 2 and 3.

2.1.1 Procedures in the field
Coral drilling

In order to drill a coral core, a commercially available hand-held pneumatic air tool (CRAFTOMAT) with a working pressure of 6 bar was used. A first stage was connected to the pneumatic air tool and the dive cylinder to regulate the working pressure from 220 bar to 6 bar. The air tool was driven by compressed air from dive tanks. The diamond drill was manufactured in Germany by DIA-G Kiel. It was 30cm long and had a diameter of 4cm. Metal extensions were used to extend the drill length. A maximum core length of 5 m can be achieved. Approximately one dive cylinder of 220 bar was needed to drill 30 cm of coral core section. Each 30 cm core section was broken at the base to remove the single pieces.

Tissue sampling

All corals sampled were also sampled for DNA. A piece of coral was taken with a chisel and transferred into a plastic bag. In the lab, the tissue was scraped off with a knife blade, transferred into an epi-vial and stored in ethanol. During the entire procedure, gloves were worn to ensure no DNA interference from the sampler's skin.

Seawater sampling

Seawater sampling was performed at the sites where the corals were drilled, and continuous water sampling was implemented in Inhaca and Tecomaji. A clean, 500 ml PE bottle was taken to the field and the sample was taken against the current, upstream of the boat. The bottle was rinsed three times with seawater before filling it to the top and closing the lid under water. The water sample was labeled with the location name and the date. Processing of the water sample was performed immediately after returning to the laboratory in the field. Seawater sampling was done for nutrients, carbon isotopes and dissolved inorganic carbon (DIC) and oxygen isotopes. For all samples, the water was filtered with a syringe and an attachable filter. The syringe and the filter were cleaned three times with the sample seawater prior to collecting the individual samples. The vials for oxygen isotope samples and nutrients were also rinsed with sample seawater three times before storing the sample. The nutrient samples were stored in the freezer. Therefore, the vials were not filled up completely to give the sample room to expand. The oxygen isotope samples were stored in 30 ml glass bottles, which were filled completely and stored on their side in the fridge until further analysis. Two vials were filled with seawater for carbon isotope and DIC analysis. Prior to adding the sample, a drop of concentrated mercury chloride had been added to the vial in order to poison the sample, so that the original composition could be preserved. The vials were filled with filtered seawater sample to the top and stored in the fridge until further analysis. In addition, trace metal samples were also taken. Previously

cleaned 50 ml PE-bottles were taken to the field in a plastic bag. Water samples were taken against the current upstream of the boat by opening the bottle underwater, collecting the sample and restoring the cap under water. The sample was labeled and taken back to the lab in a plastic bag. At the lab, approximately 2 ml of sample were discarded and 1 ml of 1M HNO_3 was added to acidify the sample and prevent trace metals from sticking to the walls of the container. The sample was stored in a plastic bag in the fridge.

In addition, conductivity measurements of the water samples were performed at the lab with an Eco Sense EC 300 conductivity meter.

On Inhaca and Tecomaji, water sampling was set up to be continued for one year by local scientists. Nutrients, carbon isotopes, DIC and oxygen isotopes will be sampled bi-weekly, while trace metal samples will be taken every four weeks.

2.2 Handling of the corals

After collecting the corals, an initial examination of the cores was performed in order to estimate their quality and age. Subsequently, the cores were rinsed with freshwater and left in a freshwater bath over night before putting them out to dry in the sun. The dried cores were shipped to the NIOZ for further analysis. During transport some of the cores that had not dried properly got infected with a fungus. Further analysis revealed that the fungus had not spread to the centre of the cores, but only affected the outer rim.

At the NIOZ, the coral cores were laid out and marked for cutting. The cutting axis was aligned at the optimal angle to the growth axis. All core pieces were marked to ensure optimal alignment of the slabs after cutting. Cutting of the cores was performed at in the geo-technical laboratory of the Vrije Universiteit Amsterdam, Amsterdam, the Netherlands. A diamond coated saw blade with a diameter of 40 cm was used. The cores were cut into four slabs. The two central slabs were set to have a thickness of 7 mm. Subsequently the cores were washed with freshwater to remove any carbonate residue from the cutting.

The following cleaning steps were performed at the NIOZ. All coral pieces were placed in an ultrasound bath filled with RO-water and ultrasonified for 10 minutes. The coral pieces were then blown with compressed air to loosen and remove carbonate residue and particles stuck in the skeleton. This procedure was repeated two times. Subsequently the corals were dried in a laminar flow.

The central slab most suitable for analysis was selected for further analysis. The selection was based on avoiding skeletal imperfections, such as boreholes, diagenetic parts and/or slabs that had been significantly affected by the fungus. The selected central slabs, as well as the outer slab from the opposite side of the core, were cleaned with bleach. The slabs were fully submerged sodium hypochlorite solution for 24 hours. The sodium hypochlorite solution employed was half reagent grade sodium hypochlorite solution, 10-15% available chlorine (Sigma-Aldrich) and half RO-water (Nagtegaal et al., 2012). After the treatment, the slabs were thoroughly rinsed with RO-water, before being placed in the ultrasonic bath for 10 minutes. Next, the slabs were blown with compressed air and put to dry in the laminar flow.

2.3 Scanning of the cores

UV luminescence and visual scanning was performed with an Avaatech XRF core scanner (Grove et al., 2010). The scanner is equipped with a Jai CV-L107CL 3CCD RGB line scan camera and a Dichroic RGB beam splitter, enabling it to differentiate between the different intensities of the reflected colors. Additionally, a visual or UV light source can be mounted to the scanner. For the UV luminescence analysis, the UV lights were mounted and a 450 nm cut-off filter was attached to the receiver to ensure that only UV waves reach the receiver. Prior to analysis, the lights have to warm up for 30 min to ensure optimal results. The image resolution is better than 0.1 mm, with one pixel imaging an area of 80 x 80 µm.

Visual images were made of both central slabs, bleached and not bleached, while UV scans were only taken for the bleached slabs. The visual scans were only performed for the inner side of the slab. UV scans were performed for both the central side and the flipped side.

2.4 Age Model

Age models for the corals were based on the seasonal changes in density of the coral skeleton which were visible by X-radiography and UV-luminescence. Using the program LineScanV1.9, a track along the coral's growth axis was defined. The program allows the splitting of colour intensities along the defined track into green, blue and red spectral domains. The G/B ratio has been shown to be a robust record of past humic acid variability, which can be linked to rainfall (Grove et al., 2010). As rainfall varies on a seasonal scale, an age model can be constructed based on the oscillations in the G/B record. The troughs in the G/B record that signify low humic acid concentrations and thereby little rain can be linked to September, which is the driest month in northern Mozambique. The peaks in the G/B record signify periods with maximum humic acid runoff. The age model was based on how the seasonal oscillation of rainfall is recorded in the coral. However, this age model was confirmed by band counting and visual correlation of the G/B record with the actual luminescent image of the cores. After assigning dates to certain points in the luminescence record, the data was integrated into a time series with a monthly resolution using the program DataAnalys2.0. In subsequent analysis, annual G/B averages were compared. These averages were calculated by averaging the data over one growth year, which was defined to range from the driest month to the driest month, in this case from September to August, e.g. the annual average of 1991/1992 is the average of the monthly G/B data for the period of September 1991 to August 1992.

2.5 Sub-sampling with the drill

In addition to UV luminescence, geochemical sub-sampling of the corals was performed to determine their elemental and isotopic profile. Sub-sampling was carried out with a hand held drill that had been attached to a holding device in order to ensure precise sampling. The sample was placed on a stage, that could be adjusted manually in the x and y plane in order to follow the growth axis. The growth axis was determined by interpreting X-radiography and UV-luminescence scans. Samples were taken along the growth axis of the coral using a diamond coated ball point dentist drill with a diameter of 0.9 mm. Sampling intervals were set at 1 mm and sampling depth was typically 3-4 mm. This ensured

a bi-weekly to monthly resolution. After sampling, the sample was transferred into small analyzer cups and stored until further analysis.

2.6 ICP-MS

The geochemical composition of the coral profile was determined with inductively coupled mass spectrometry (ICP-MS). Approximately 1 mg of sample was dissolved in 0.1M supra-pure HNO3. 1ml acid was used to dissolve 1 mg of sample and the amount was adjusted accordingly if the sample weight differed from 1 mg. Subsequently the sample was shaken to ensure the complete dissolution of the carbonate. A 0.25 ml aliquot of the sample was transferred into test tubes. Prior to transfer, the pipette tip was cleaned with Milli-Q water, supra-pure 0.1M HNO3 and with the sample. 9.75 ml of supra-pure 0.1M HNO3 were added to the selected aliquot, so that the final volume of the sample was 10 ml. The final solution had a concentration of approximately 10 ppm of calcium. Every 30 samples, two blanks and one standard were measured to monitor the performance of the machine. Thus 22 blanks and 11 standards were measured throughout the analysis of one core. The selected standard was JCP-1. In addition to blanks and standards, replica of the same samples were included into the measuring series every 15 samples. The Sr/Ca ratio of the standards averaged at 8.835 and its standard deviation was 0.031. The official Sr/Ca ratio of the JCP-1 is 8.82. The internal precision (during one measurement) was 0.4% while the external precision (averaged over all measurements) was 0.25%. Ba/Ca was determined to average 6.53 and its standard deviation was 0.328, while the target value of the JCP-1 was 7.39. The internal precision was 0.78% and the external precision was 2.27%.

2.7 Stable Isotopes

Next to ICP-MS analysis, the samples were also scheduled for stable isotope analysis. 200 samples of the core Qui2b were analyzed with a Kiel IV Carbonate device. Approximately 0.08 mg of sample were used for analysis. The selected standard was NBS 19. Due to a significant offset of the measured standard values relative to its target as well as a high variability within the measurements of the standard, the data obtained could not be considered reliable. Therefore, the stable isotope analysis of the samples was postponed until the machine was properly calibrated.

3. Results

3.1 Selection of cores to analyze

Seven cores from six different corals were sampled during field work in the Quirimbas Archipelago in October, 2011. After an initial examination by employing UV luminescence, four cores were selected for further analysis. The selection of the cores was based on the quality of the records, time period covered and inter-colony correlations ofG/B. The cores Qui2b, Qui4, Qui6 and Qui7 were selected for further analysis.

3.1.1 Excluded cores

Qui2a
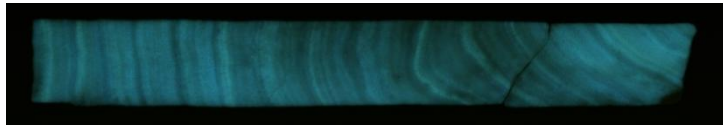
Figure 13: Luminescence scan of core Qui2a

When drilling coral Qui2, the first attempt was unsuccessful. A hole was discovered after 35 cm, which is why a second attempt was made at drilling this coral. The core obtained in the first attempt, core Qui2a, spans the time period of 1997-2011. UV luminescence scans revealed dark discolorations in the coral piece covering the period 1997-2003 (Fig 13). The annual averages of the remaining G/B record showed significant correlations with those Qui6 and Qui4. No other significant correlations were obtained. Thus due to the shortness of the good record (8 years) and the lack of correlations with other coral records this core was excluded from further analysis.

Qui8
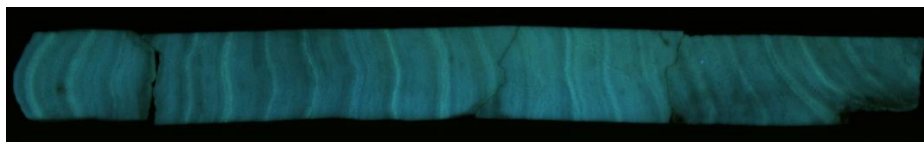
Figure 14: Luminescence scan of Qui8

Qui8 was the shortest core obtained from Site 1. It covers the time period of 1991-2011, but the lower part revealed green and dark discolorations under UV light suggesting that the lower part has also been subject to diagenisis (Fig 14). The unaffected top part covers the period from 2001-2011. Correlations of these 10 years with the other coral records from the Quirimbas only revealed significant results when correlated to the core Qui6. Consequently, this core was also excluded from further analysis.

Qui1
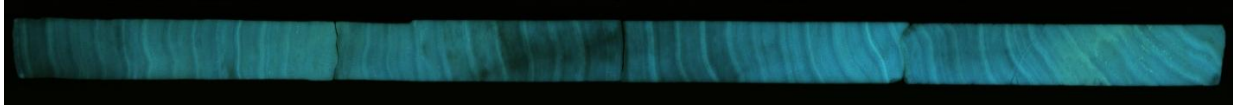
Figure 15: Luminescence scan of Qui1

The core Qui1 covers the time period of 1970-2011. Throughout the core green and dark discolorations as well as bright green dots, were visible under UV light, indicating that the core has been subject to diagenisis (Fig 15). Although the G/B record is significantly correlated with the G/B records of Qui6, Qui7, Qui 2b and Qui4, the diagenisis makes it unsuitable for reconstructing climatic conditions of the region. This is why core Qui1 was not used for further analysis.

3.1.2 Selected cores
Qui6
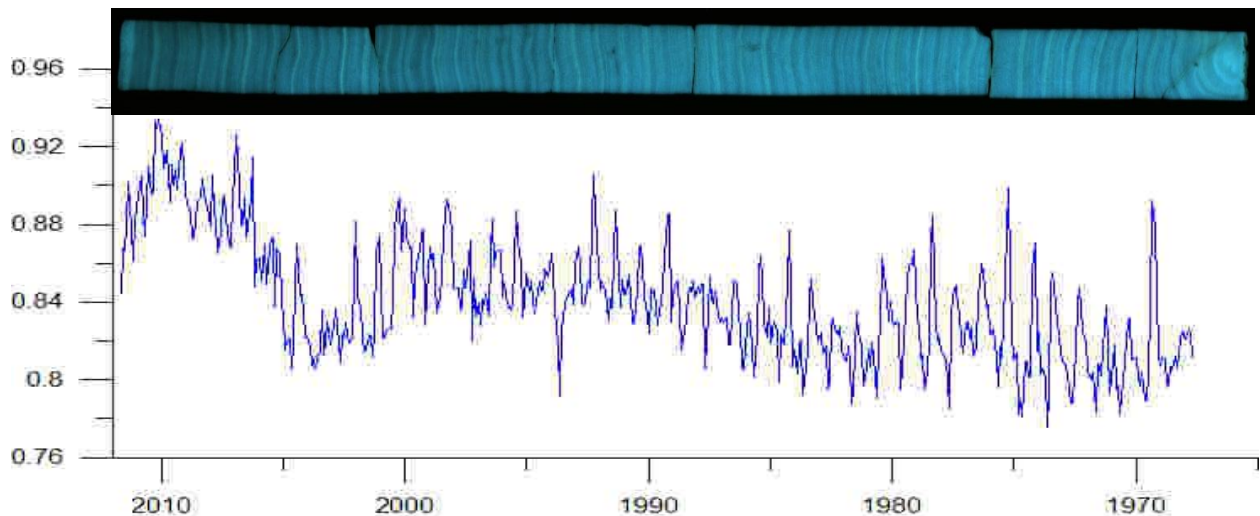
Figure 16: Luminescence scan and G/B profile of Qui6

Core Qui6 spans the time period 1967-2011. No diagensis could be observed and only minor imperfections could be found in the coral skeleton (Fig 16), which were avoided when defining the luminescence transect. The growth lines are relatively straight and the bands are spaced relatively equally. The variation between high and low G/B can be recognized clearly in the luminescence record, while the amplitude varies from year to year. The annual averages of the G/B record of this core significantly correlated with the ones of the cores Qui7 and Qui2b (Table 2). The correlation between Qui6 and Qui4 was just outside the significance window.

Qui4

Qui4 is the longest record of all cores obtained from the Quirmbas and spans the time period 1910-2011. There are some minor dark discolorations in the top 40 cm of the core and the last 50 cm have been subject to diagenisis, indicated by bright green spots as well as dark and green discolorations (Fig 17). Banding is not always as clear as in core Qui6, but annual cyclicity in the luminescence record is still distinguishable. The correlation of the G/B record of the core Qui4 was highly significant with the the cores Qui2b and Qui7, while it was just outside the significance window with the G/B record of Qui6 (Table 2).
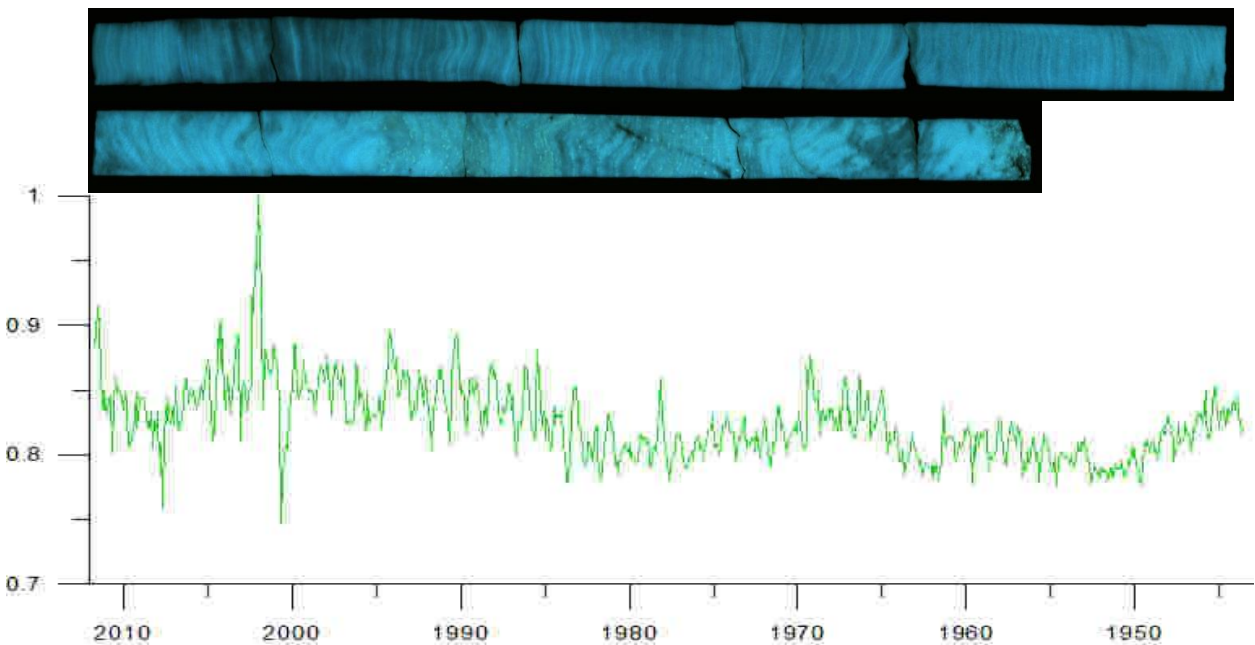
Figure 17: Luminescence scan and G/B profile of Qui4

Qui2b

Core Qui2b is the second longest record sampled in the Quirimbas, spanning the time period 1941-2011. Except for some minor dark discolorations in the top 20 cm of the core, the quality of the luminescence data obtained from the core is good (Fig 18). Similar to Qui6, banding is very distinct and the growth lines are relatively straight and equally spaced throughout the record. The G/B record of this coral was significantly correlated with all other corals selected for this study (Table 2).
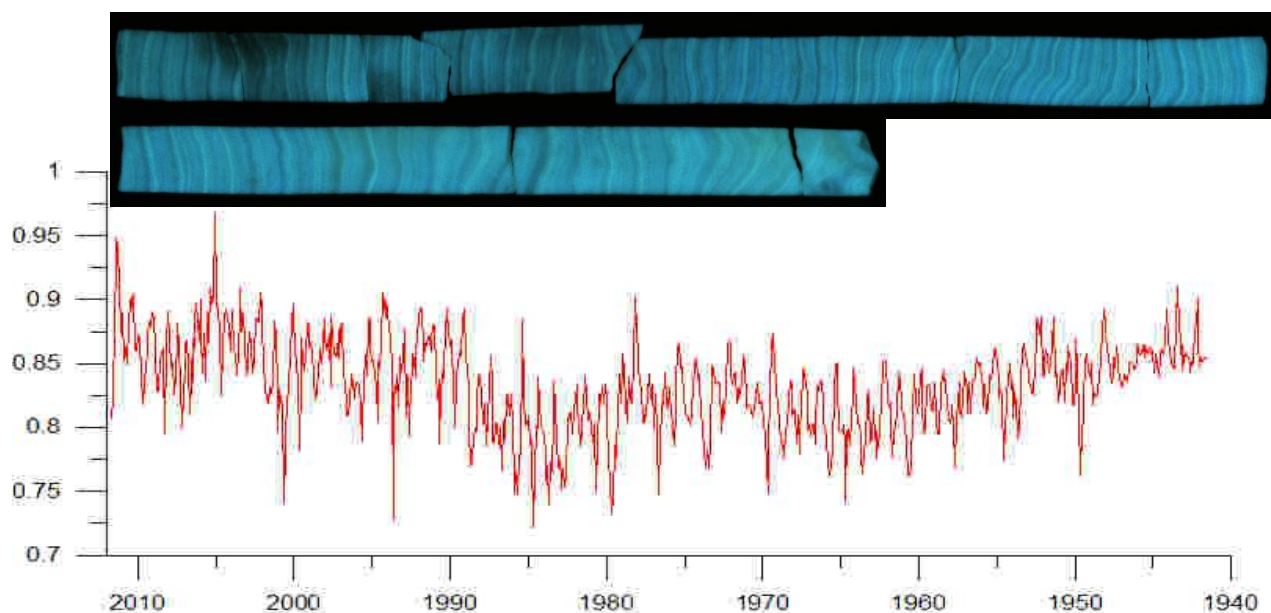
Figure 18: Luminescence scan and G/B profile of Qui2b

Qui7
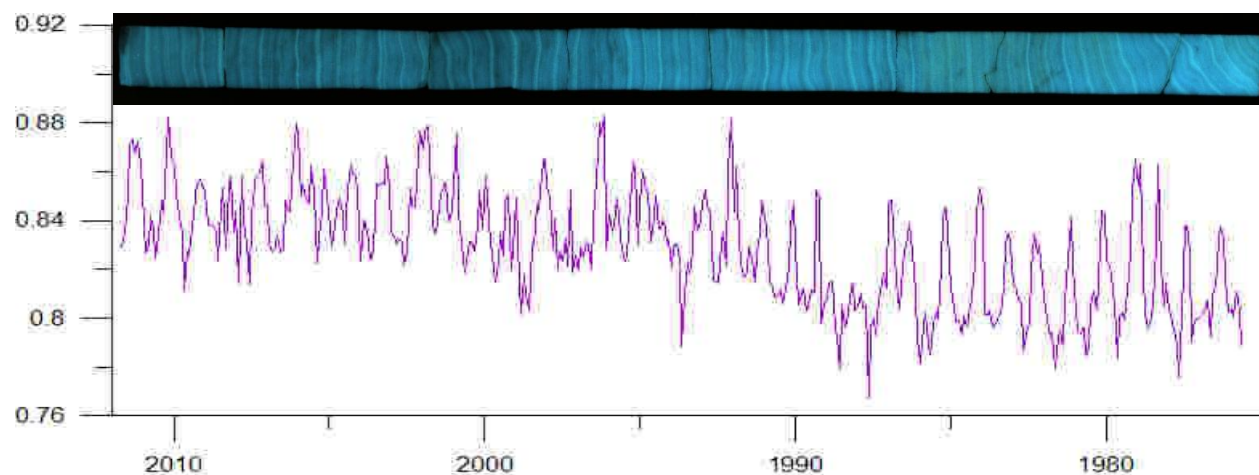
Figure 19: Luminescence scan and G/B profile of Qui7

The core Qui 7 covers the time period 1957-2011. It has some significant green discolorations in its lower 40 cm (Fig 19). Therefore, the record is only reliable for the period 1975-2011 (Fig 19). The top of the core is of good quality with distinct banding and relatively constant growth pattern and direction. Its G/B record spanning the period 1975-2011 significantly correlated with all other luminescence records of corals selected for this study (Table 2).

Correlation	Time period	n	P	R	R^2	Distance
Qui6 – Qui7	1975-2011	36	<0.001	0.602	0.362	13.5 m
Qui6 – Qui2b	1967-2011	44	<0.001	0.583	0.340	1347 m
Qui6 – Qui4	1967-2011	44	0.061	0.284	0.0809	7339 m
Qui7 – Qui2b	1975-2011	36	<0.001	0.745	0.555	1334 m
Qui7 – Qui4	1975-2011	36	<0.001	0.556	0.309	7326 m
Qui2b – Qui4	1941-2011	70	<0.001	0.459	0.210	5996 m

Table 2: Correlation of the four selected cores. For the correlation, annual averages of their G/B records were compared. Additionally, the distance between the two cores correlated is given.

3.1.3 Inter-colony luminescence relationships

The G/B annual averages (September – August) of all cores were significantly correlated, with the exception of Qui6 and Qui4. The correlation of these two cores was just outside the significance window. To investigate whether these significant relationships were influenced by inter-annual variability and/or long-term trends, the one year running median and the two year running median were subtracted from the original time series. Thereby, long-term trends were removed from the records and inter-annual variability could be assessed for all cores without the interference of long-term trends. After removing long-term trends, the corresponding G/B records were labeled by adding '1m' or '2m' to the original name. '1m' indicates that the 1 year running median has been subtracted, while '2m' was added when the 2 year running median was removed, e.g. core Qui4 after removing long term trends was labeled 'Qui4.1m' and 'Qui4.2m' respectively. Normalizing gives positive and negative anomalies. In addition to the de-trended records that consider both, negative and positive anomalies, de-trended records that only considered the positive monthly anomalies were constructed. These records labeled by adding an additional '(pos)', e.g. Qui4.1m (pos) is core Qui4 with the 1 year running median removed where only the positive anomalies were considered.

Correlation	time span	n	p	r	r2
Qui6.1m - Qui7.1m	1968 - 2010	42	0.01	0.394	0.156
Qui6.1m-Qui2b.1m	1968 - 2010	42	0.187	0.208	0.0423
Qui6.1m - Qui4.1m	1968 - 2010	42	0.287	0.168	0.0283
Qui7.1m - Qui2b.1m	1958 - 2010	52	0.332	0.137	0.0189
Qui7.1m - Qui4.1m	1958 - 2010	52	0.857	0.0256	0.000658
Qui2b.1m - Qui4.1m	1942 - 2010	68	0.02	0.282	0.0794

Table 3: Significant correlations of the G/B records, which have been de-trended by removing the one year running median

Correlation	time span	n	p	r	r2
Qui6.2m - Qui7.2m	1968 - 2010	42	0.001	0.634	0.401
Qui6.2m -Qui2b.2m	1968 - 2010	42	0.843	0.0315	0.000994
Qui6.2m - Qui4.2m	1968 - 2010	42	0.289	0.167	0.028
Qui7.2m - Qui2b.2m	1958 - 2010	52	0.834	0.0298	0.000886
Qui7.2m - Qui4.2m	1958 - 2010	52	0.991	0.00166	0.00000276
Qui2b.2m - Qui4.2m	1942 - 2010	68	0.014	0.297	0.0881

Table 4: Significant correlations of the G/B records, which have been de-trended by removing the two year running median

After de-trending the time series of the four records, their annual averages (September – August) were correlated with each other in order to check for significant correlations. By de-trending the G/B records, only cores Qui2b and Qui4 as well as cores Qui6 and Qui7 are significantly correlated (Table 3 and 4). If only the positive values were considered, the same result was evident (Table 5 and 6).

Correlation	time span	n	p	r	r2
Qui6.1m (pos) - Qui7.1m (pos)	1968 - 2010	42	0.001	0.477	0.227
Qui6.1m (pos) -Qui2b.1m (pos)	1968 - 2010	42	0.623	0.0782	0.00612
Qui6.1m (pos) - Qui4.1m (pos)	1968 - 2010	42	0.965	0.007	0.0000489
Qui7.1m (pos) - Qui2b.1m (pos)	1958 - 2010	52	0.904	0.0172	0.000295
Qui7.1m (pos) - Qui4.1m (pos)	1958 - 2010	52	0.99	0.00173	0.000003
Qui2b.1m (pos) - Qui4.1m (pos)	1942 - 2010	68	0.007	0.322	0.104

Table 5: Significant correlations of the G/B records, which have been de-trended by removing the one year running median only considering the positive anomalies

Correlation	time span	n	p	r	r2
Qui6.2m (pos) - Qui7. 2m (pos)	1968 - 2010	42	0.007	0.408	0.167
Qui6. 2m (pos) -Qui2b. 2m (pos)	1968 - 2010	42	0.348	0.149	0.0221
Qui6. 2m (pos) - Qui4. 21m (pos)	1968 - 2010	42	0.925	0.015	0.000225
Qui7. 2m (pos) - Qui2b. 2m (pos)	1958 - 2010	52	0.981	0.00345	0.0000119
Qui7. 2m (pos) - Qui4. 2m (pos)	1958 - 2010	52	0.956	0.00779	0.0000607
Qui2b. 2m (pos) - Qui4. 2m (pos)	1942 - 2010	68	0.001	0.47	0.221

Table 6: Significant correlations of the G/B records, which have been de-trended by removing the two year running median only considering the positive anomalies

In order to create a more robust record and reduce the influence of local variability, a composite G/B record based on the individual coral records was constructed. For the time period 1975-2011 all corals were included into the calculations, for the period 1967-1975 cores Qui6, Qui4 and Qui2b were used and for the period 1941-1967 the composite record was based only the cores Qui4 and Qui2b. The composite record was calculated in two ways. The first method averaged the four G/B records over the time period they had in common. The second method required a normalization of the data first. This was done by subtracting the mean from the time series first and then dividing the resulting time series by the standard deviation. Subsequently, the average of the records was calculated for the time period they had in common.

Monthly correlations:
p=<0.001, r=0.809, n=816

Annual averages (Sep-Aug):
p=<0.001, r=0.908, n=68
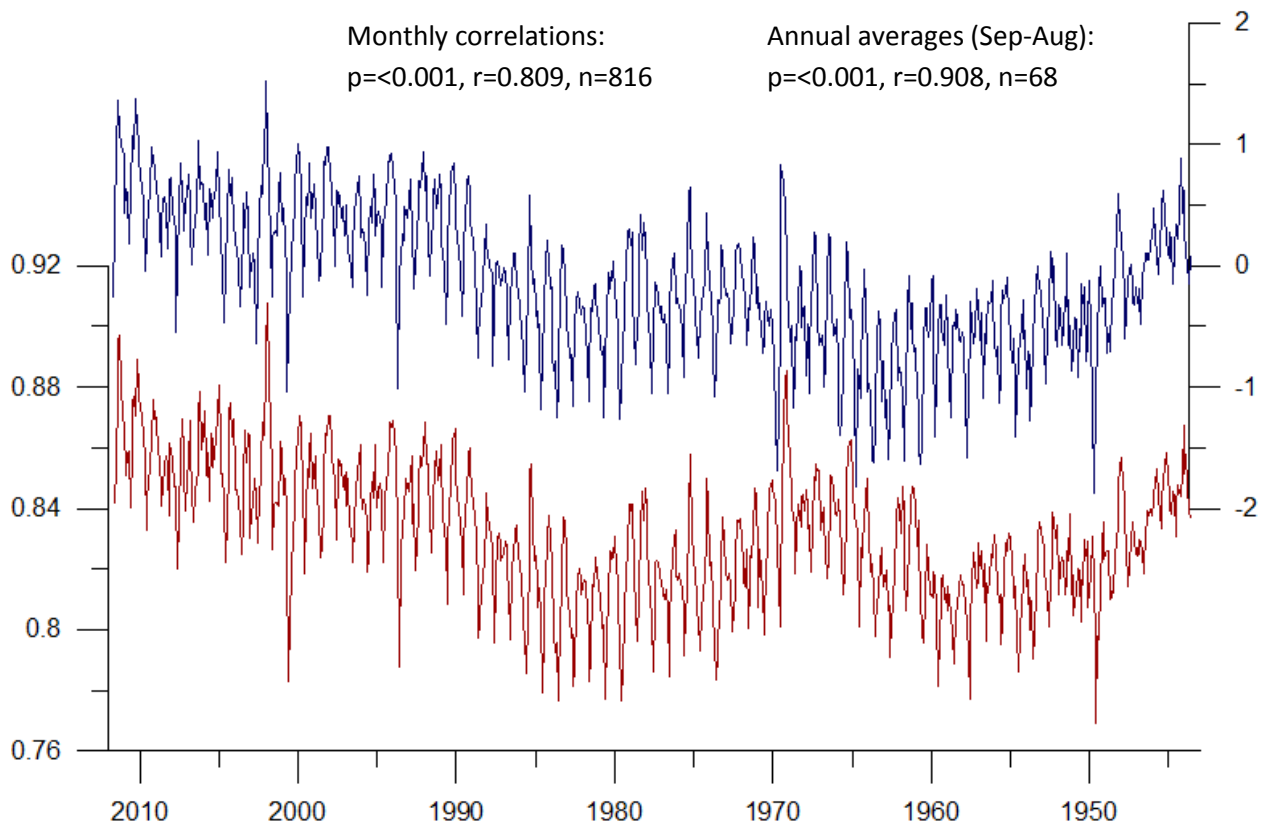
Figure 20: Composite records of the four coral cores Qui2b, Qui4, Qui6 and Qui7. The record indicated in dark red was calculated by averaging the individual G/B over the time period they have in common. The variability of this record is indicated on the left Y-axis. The record shown in dark blue was determined by normalizing the data first and then averaging the four records over the time period they have in common. The Y-axis on the right shows this record's variability.

3.2 Correlation with rainfall

To test whether the G/B records were linked to rainfall in northern Mozambique, the annual averages of the G/B records were compared to the annual averages of rainfall records from close to the study area. Four rainfall records were available for correlation with the coral G/B records. Two datasets were station data from Mtwara (Tanzania) and Mocimba da Praia (Mozambique). The distance of the stations to the sampling site was 66 and 71 km, respectively. The record from Mtwara covers the time period 1961-2009, while data from Mocimba da Praia is available for 1933-1996. The data series were interpolated using DataAnalys2.0 to fill in missing data points. In addition to station data, the G/B records were compared to the reanalyzed rainfall data CRU TS3.1 and GPCC V5. Both datasets provide rainfall data for the period 1910-2008. Annual averages of all datasets were significantly correlated with each other (Table 7).

Correlation	Time period	n	P	R	R^2
Mtwara – Mocimba da Praia	1961-1996	36	0.015	0.404	0.163
CRU – Mocimba da Praia	1933-1996	64	<0.001	0.702	0.493
CRU – Mtwara	1961-2008	48	0.003	0.423	0.179
GPCC – Mocimba da Praia	1933-1996	64	<0.001	0.539	0.291
GPCC – Mtwara	1961-2008	38	<0.001	0.555	0.308
CRU – GPCC	1910-2008	98	<0.001	0.702	0.493

Table 7: Correlations of the annual averages of the four selected rainfall datasets.

When correlating the annual averages of the four individual cores with rainfall, only Qui4 shows a positive correlation with GPCC V5 rainfall (n=98, p=0.049, r=0.2, r^2=0.0399). Therefore, both composite records did not show any significant correlation with rainfall. However, when the running median was subtracted from the averaged G/B record to remove the long-term trend, it significantly correlated with rainfall data from Mtwara station. The correlation was stronger when only the one year running median (n=49, p=0.003, r=0.411, r^2=0.169) was subtracted, instead of the two year running median (n=49, p=0.03, r=0.31, r^2=0.0961).

Individually, the annual averages of the de-trended records also revealed several correlations with rainfall. Qui6 and Qui2b showed positive correlations with rainfall when the one year and the two year running median was removed, while Qui4 only showed significant correlations with rainfall when the one year running median was removed (Table 8 and 9). No significant relationships between the de-trended Qui7 records and rainfall could be identified. From now on, only the composite records are considered for analysis to reduce the influence of local variability.

Correlation	n	P	R	R^2
Qui6.1m – Mtwara	42	0.012	0.383	0.147
Qui6.1m – GPCC V5	40	0.009	0.407	0.165
Qui2b.1m – Mtwara	49	0.019	0.334	0.111
Qui4.1m – GPCC V5	97	0.024	0.228	0.0522
Qui6.1m (pos) - Mtwara	42	0.027	0.342	0.117
Qui6.1m (pos) – CRU TS 3.1	41	0.014	0.383	0.146
Qui6.1m (pos) – GPCC V5	40	0.003	0.452	0.205
Qui4.1m (pos) – GPCC V5	97	0.013	0.251	0.0632

Table 8: Significant correlations of G/B records de-trended by subtracting a one year running median and rainfall.

Correlation	n	P	R	R^2
Qui6.2m - Mtwara	42	0.004	0.423	0.186
Qui6.2m – CRU TS 3.1	41	0.017	0.370	0.137
Qui6.2m – GPCC V5	40	0.003	0.456	0.208
Qui2b.2m - Mtwara	49	0.016	0.343	0.118
Qui2b.2m – GPCC V5	50	0.009	0.368	0.136
Qui6.2m (pos) – GPCC V5	40	0.004	0.442	0.196

Table 9: Significant correlations of G/B records de-trended by subtracting a two year running median and rainfall.

3.3 Spatial correlation of G/B with SST

To investigate the influence of SST as a driver of climate conditions in northern Mozambique, spatial correlations of the G/B records with SST were performed using the KNMI climate explorer (http://climexp.knmi.nl/). The HadISST dataset spanning the time period 1870-2011 was selected for the spatial correlation.

When both composite records were compared to SST in the Indian Ocean, strong positive correlations could be found all year round. The records were not de-trended, so long-term trends within the record are considered in this correlation. The normalized composite record shows positive correlations with SST over the study area, the northern Indian Ocean and around Indonesia all year (Fig. 21). The averaged composite record positively correlated with SST over the same areas, but the correlation was weaker (Fig. 22). When the correlation was limited to the period 1940-1980, the correlation over the Indian Ocean was not detectable anymore (Fig.23). Also, no significant correlations could be identified over the Indian Ocean, when the records were de-trended by removing the one year running median or by removing linear trends (Fig.24).
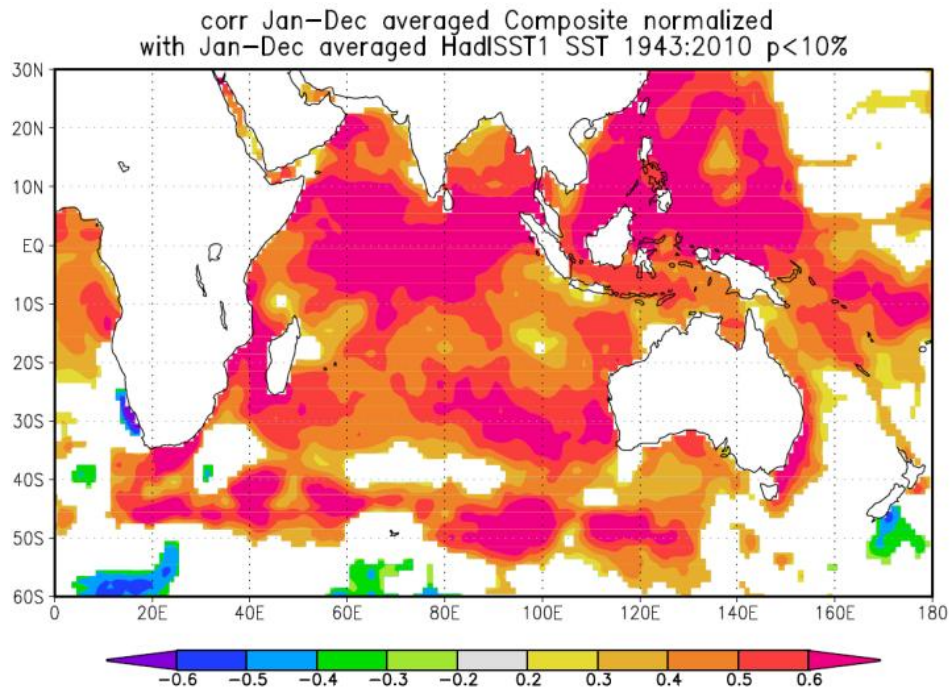
Figure 21: Spatial correlation of the normalized composite record with SST (HadISST) for the period January – December
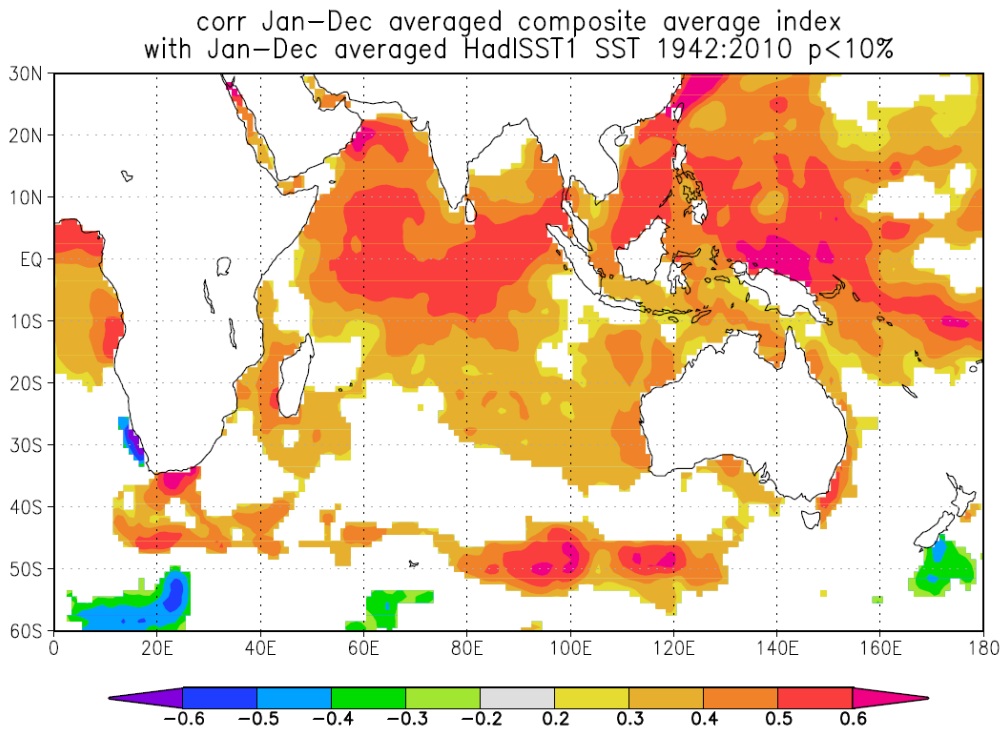
Figure 22: Spatial correlation of the averaged composite record with SST (HadISST) for the period January – December.
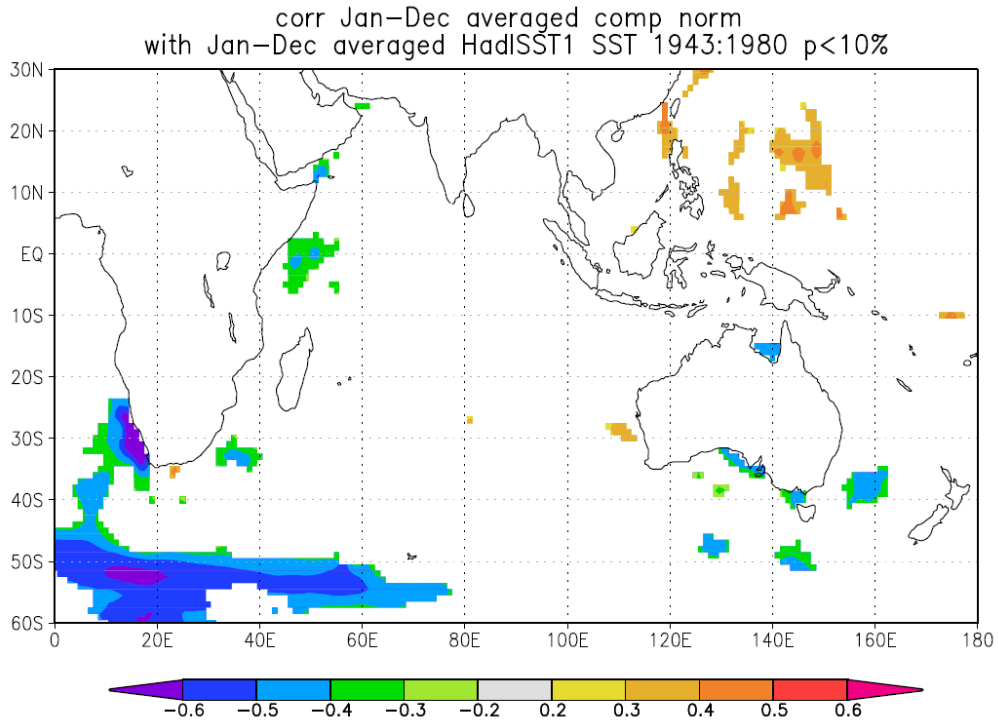
Figure 23: Spatial correlation of G/B composite with SST (HadISST) for the period 1940-1980 for the period January - December
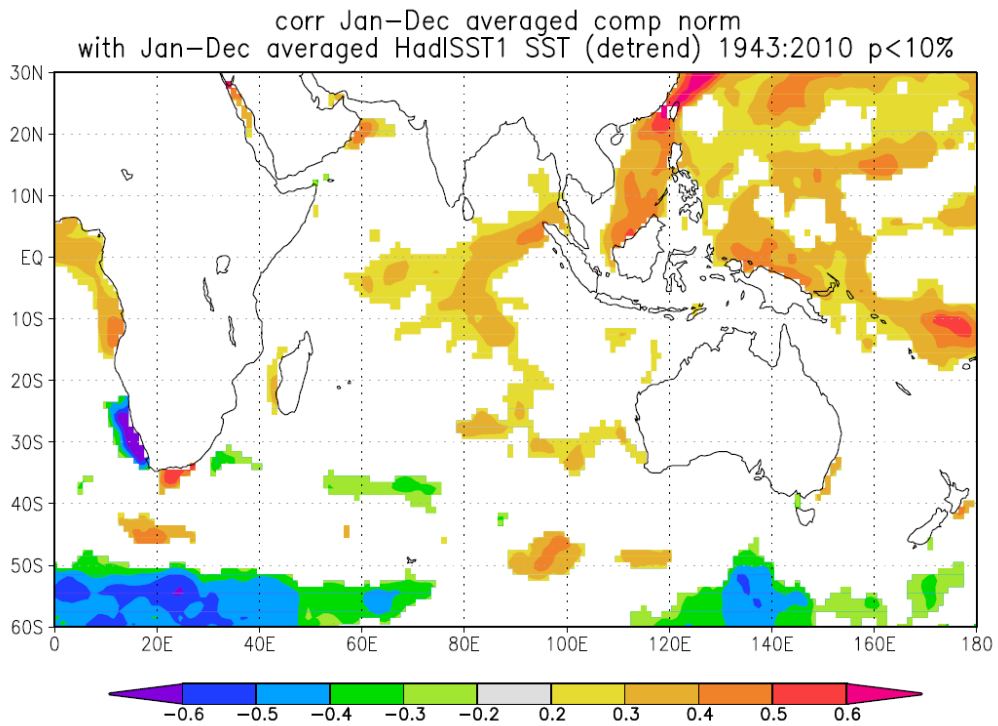
Figure 24: Spatial correlation of de-trended composite record with SST (HadISST) for the period January – December

3.4 Spectral Analysis

To identify oscillations longer than the annual cycle within the records, spectral analysis was performed on the individual G/B records and the de-trended G/B records. The records that had been de-trended by removing the one year running median were selected for spectral analysis. The multi-taper method was chosen for the analysis. The significant frequencies and corresponding periods for all records are shown in table 10. The G/B records of Qui6 and Qui2b share the significant frequency 0.293. When the de-trended records of these two corals were analyzed with spectral analysis, it became apparent that they have two significant frequencies in common: 0.281 and 0.434. The G/B record Qui4.1m also carries a signal with the frequency 0.434. A signal with the frequency 0.352 recurs in the records of Qui2b and Qui4.1m. The frequencies identified in the individual G/B records average around a recurrence period of approximately 3 years. This is similar to the recurrence period of the IOD.

	G/B			De-trended G/B		
	Frequency [1/year]	Period [year]	Significance level	Frequency [1/year]	Period [year]	Significance level
Qui4	0.258	3.9	99%	0.352	2.8	90%
	0.328	3.0	95%	0.434	2.3	99%
Qui2b	0.293	3.4	90%	0.281	3.6	99%
	0.352	2.8	99%	0.434	2.3	99%
Qui6	0.293	3.4	95%	0.281	3.6	99%
				0.434	2.3	99%
Qui7				0.188	5.3	99%
				0.363	2.8	99%

Table 10: Significant frequencies of signals in the individual G/B records detected by spectral analysis.

3.5 Correlation of G/B with ENSO

Spectral analysis indicated no ENSO frequency in the coral records with the exception of Qui7 (f=0.188). Nevertheless, we investigated possible connections to ENSO using the two G/B composite records and the de-trended composite records (one and two year running median subtracted), which were correlated with the climate indices Niño3, Niño3.4 and Niño4. The data were averaged over one, three, six and twelve months for comparison.

Both composite records did not show any correlation with any of the indices. If the composite records were de-trended by removing the one year and two year running median, no correlations with ENSO became apparent in agreement with spectral analysis. Extreme events visible in the composite G/B records, as well as the four individual coral G/B records were compared to historical El Niño events. In general, peaks in the G/B records did not line up with historical El Niño events. Peaks in the composite records occurring in 1964, 1966 and 1977 were the only years that could be correlated with historical El Niño events, while additional peaks in the record did not occur simultaneously with historical El Niño events.

3.6 Correlation of G/B with IOD indices

Spectral analysis indicated that frequencies similar that of the IOD were recorded in the G/B records of the four individual cores (Table 10). To further investigate the influence of the IOD on the luminescence signal recorded by the corals, the G/B composite records were compared to two IOD indices, one index was based on HadISST SST reconstructions, while the other was based on ERSST. The data of the records were averaged over one, three, six and twelve months for the correlations. No significant correlations of the two composite records with either DMI (IOD) index could be identified. However, if the composite records were de-trended by removing the one year and two year running median correlations with the DMI (IOD) indices became apparent. When the one year running median was removed from the composite record based on normalized data, the record showed significant correlations with both DMI (IOD) indices. The correlations were centered around the southern hemisphere winter (Table 11), while the mature phase of the IOD is September - November.

DMI (IOD) HadISST				
1 year RM	12 months	April - March	p=0.0378	r=0.254
DMI (IOD) ERSST				
1 year RM	3 months	June - August	p=0.0243	r=0.275
1 year RM	6 months	May-October	p=0.0408	r=0.251
1 year RM	12 months	April-March	p=0.0250	r=0.274
1 year RM	12 months	May-April	p=0.0085	r=0.321

Table 11: Correlations of the de-trended composite record based on normalized data with DMI (IOD) indices. Significant correlations only occurred when the one year running median was removed.

3.7 Correlations of G/B with PDO indices

The two composite G/B records were compared to PDO indices, to investigate the influence of the PDO on the G/B of the corals. The records were compared to two PDO indices, one of them was based on the SST reconstruction of HadISST, the other on the one of ERSST. No significant correlation could be identified between the composite records and PDO indices. However, if long-term trends were removed by subtracting the one year and two year running median, negative correlations of the normalized composite record with both PDO indices became apparent. The correlations were centered around the second half of the calendar year (Table 12). The composite records were filtered for 120 consecutive months by a first order low pass loess filter, to emphasize long-term trends and reduce the influence of inter-annual oscillations as the PDO is a multi-decadal climate oscillation and its influence can be expected to be recorded in long-term trends. Correlating this time series with PDO indices did not reveal a significant correlation. However, when linear trends were subtracted from this time series, a spatial correlation with SST resembling an inverted PDO SST spatial pattern could be identified (Fig 25).
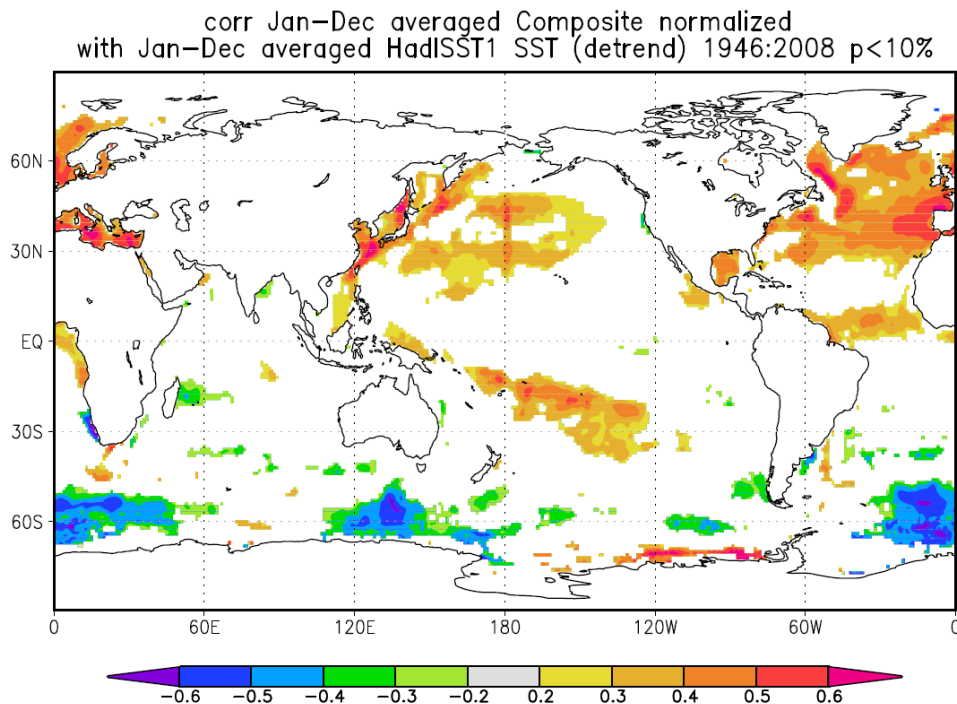
Figure 25: Correlation of the filtered and de-trended composite record with SST (HadISST)

PDO (HadISST)				
2 year RM	3 months	September - November	p=0.0477	r=-0.248
1 year RM	6 months	August – January	p=0.0491	r=-0.245
1 year RM	6 months	September – February	p=0.0232	r=-0.281
PDO (ERSST)				
2 year RM	1 month	September	p=0.0488	r=-0.242
2 year RM	3 months	September – November	p=0.0483	r=-0.244
1 year RM	6 months	August - January	p=0.0459	r=-0.245
1 year RM	6 months	September – February	p=0.0429	r=-0.248
2 year RM	12 months	February - January	p=0.0436	r=-0.251

Table 12: Correlations of the de-trended composite record based on normalized data with PDO indices

As correlations with Qui6 and Qui7 as well as Qui4 and Qui2b were strong when you remove the one year running median, two composites based on Qui6 and Qui7 as well as Qui4 and Qui2b were constructed (Table 3). These two composite records were also filtered for 120 consecutive months by applying a first order low pass loess filter and linear trends were removed. While the composite based on Qui4 and Qui2b showed a similar result to the original composite, the composite of Qui6 and Qui7 showed a strong negative spatial correlation with the PDO SST pattern (Fig. 26).
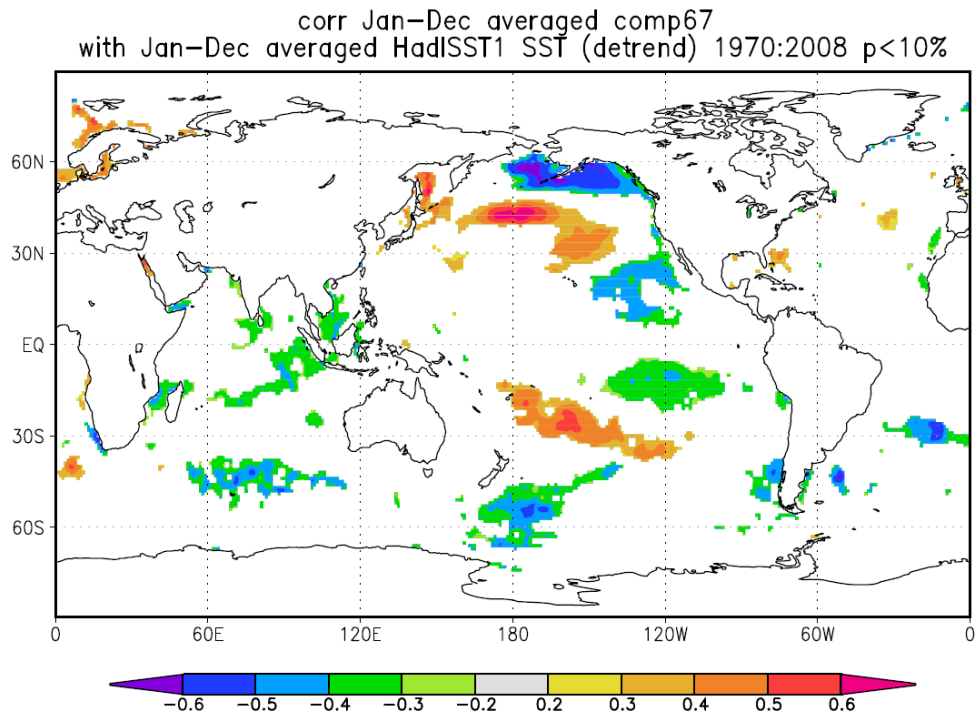
Figure 26: Correlation of the filtered and de-trended composite record based on Qui6 and Qui7 with SST (HadISST)

3.8 Correlation of G/B with the AMO

To assess the influence of the Atlantic Ocean as a climate driver in northern Mozambique, the G/B records of the composite record and the de-trended (1 year running median removed) composite record were correlated with AMO indices. Both records were also de-trended by removing linear trends that could be observed in the records.

The composite record positively correlated with the AMO index for all periods when the records were averaged over 12 months (Table 13). This correlation became even stronger, when the record was de-trended by removing linear trends (Table 13). The correlations between the composite and the de-trended composite were also significant when the data was averaged over shorter time periods.

Correlation	period	Composite		Composite (de-trended)	
		p	r	p	r
Composite – AMO (HadISST)	Jan – Dec	0.010	0.314	<0.001	0.487
Composite – AMO (HadISST)	Feb – Jan	0.009	0.319	<0.001	0.491
Composite – AMO (HadISST)	Mar – Feb	0.009	0.315	<0.001	0.483
Composite – AMO (HadISST)	Apr – Mar	0.010	0.312	<0.001	0.480
Composite – AMO (HadISST)	May – Apr	0.012	0.306	<0.001	0.473
Composite – AMO (HadISST)	Jun – May	0.011	0.309	<0.001	0.474
Composite – AMO (HadISST)	Jul – Jun	0.013	0.303	<0.001	0.468
Composite – AMO (HadISST)	Aug - Jul	0.015	0.295	<0.001	0.466
Composite – AMO (HadISST)	Sep – Aug	0.012	0.304	<0.001	0.475
Composite – AMO (HadISST)	Oct - Sep	0.012	0.303	<0.001	0.476
Composite – AMO (HadISST)	Nov - Oct	0.013	0.303	<0.001	0.475
Composite – AMO (HadISST)	Dec - Nov	0.011	0.310	<0.001	0.484

Table 13: Correlation of the composite record and the composite record that had been de-trended by removing linear trends with the AMO index based on HadISST averaged over one year.

To assess the correlation of the G/B composite record with the AMO further, the composite record and the composite record that had been de-trended by removing linear trends have been correlated with SST all over the globe. A strong positive correlation in the northeast Atlantic Ocean was observed that was apparent all year round. This correlation was even stronger when the composite record was de-trended by removing linear trends first (Fig 27).

To compare long-term oscillations in the composite record to the ones typical for the AMO and PDO, the filtered G/B composite was plotted with filtered AMO and PDO indices (Fig.28). Depressions in the G/B composite record in the early 1960s and late 1980s co-occur with peaks in the PDO index. A small depression in the G/B composite record in the early 1970s coincides with a depression in the AMO index.
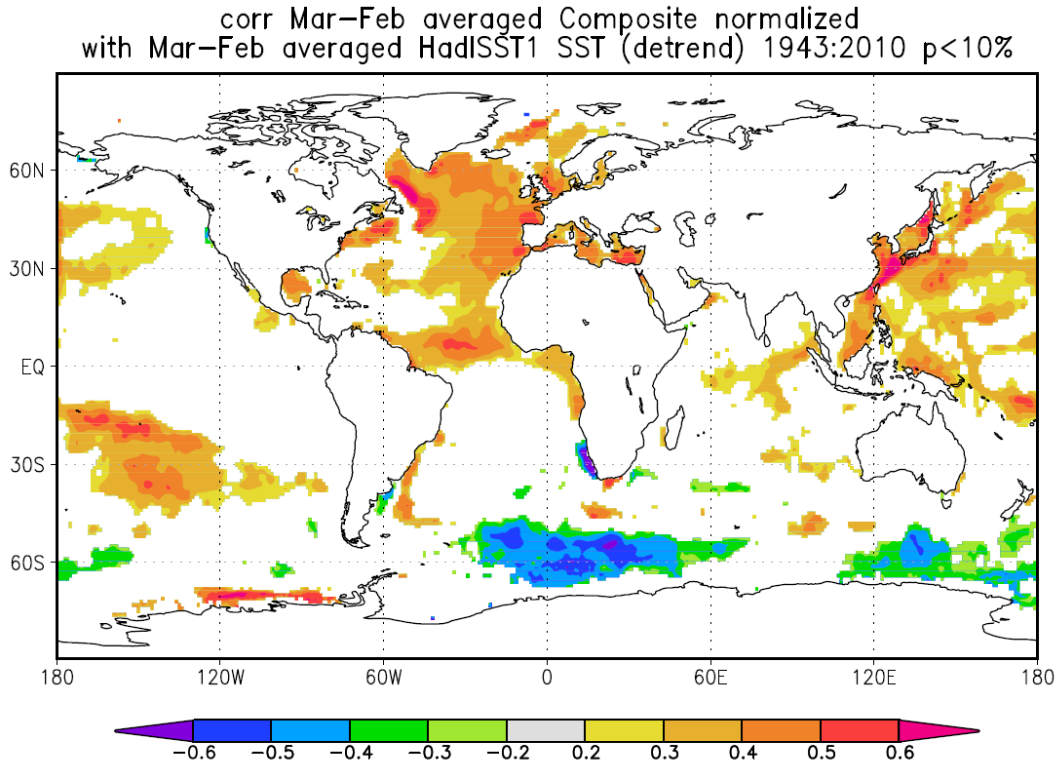
Figure 27: Spatial correlation of the composite record after linear trends had been removed with SST.
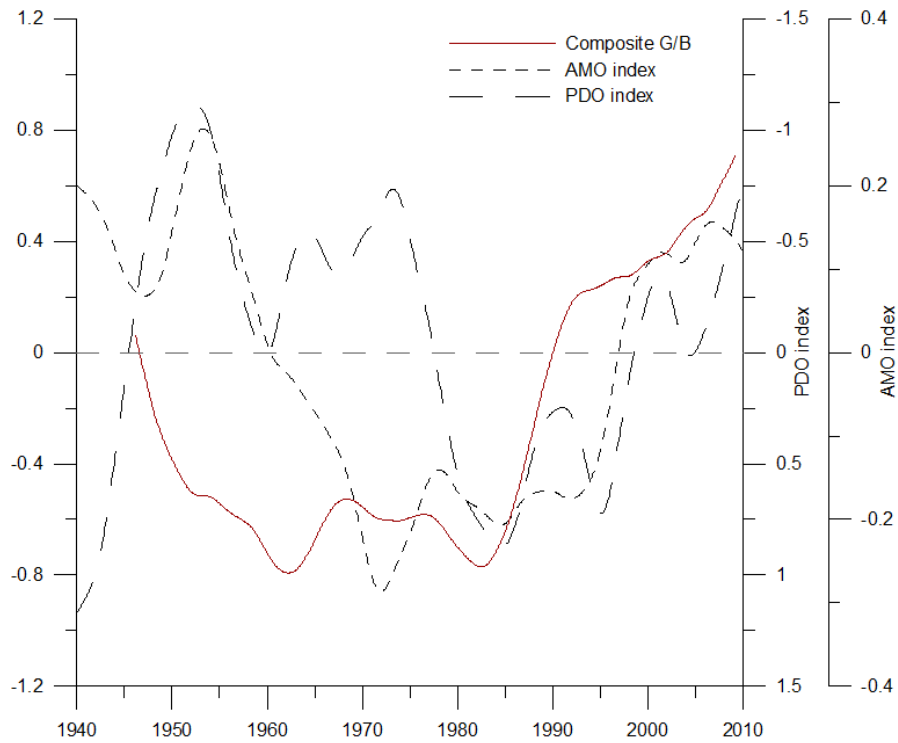
Figure 28: The composite G/B record and the climate indices of the AMO and PDO, both based on HadISST, filtered over 120 months.

3.9 Geochemistry

The growth rates for each individual year for each individual core are displayed in table 14. Core Qui4 showed the lowest growth rate ranging from 1.2 – 2.2 cm/yr averaging at 1.36 cm/yr. Qui2b and Qui7 exhibited similar average growth rates with 1.93 and 1.95 cm/yr respectively. The variability in growth rate was higher for Qui2b, where it was ranging from 1.5 cm/yr to 2.7 cm/yr while Qui7's growth rate varied between 1.7 and 2.5 cm/yr. Qui6 had the highest average growth rate of all four cores with 2.26 cm/year. Growth rates varied between 1.8 and 3.0 cm/yr.

	Qui2b	Qui4	Qui6	Qui7
2010/2011	1.6 cm/yr		2.6 cm/yr	1.9 cm/yr
2009/2010	1.8 cm/yr	1.3 cm/yr	2.2 cm/yr	1.8 cm/yr
2008/2009	2.1 cm/yr	1.6 cm/yr	2.1 cm/yr	2.0 cm/yr
2007/2008	2.1 cm/yr	1.3 cm/yr	2.6 cm/yr	1.7 cm/yr
2006/2007	2.1 cm/yr	1.2 cm/yr	2.0 cm/yr	1.8 cm/yr
2005/2006	2.7 cm/yr	1.3 cm/yr	2.5 cm/yr	1.8 cm/yr
2004/2005	2.3 cm/yr	1.9 cm/yr	2.2 cm/yr	1.9 cm/yr
2003/2004	1.9 cm/yr	1.6 cm/yr	2.2 cm/yr	1.8 cm/yr
2002/2003	1.7 cm/yr	1.2 cm/yr	3.0 cm/yr	1.9 cm/yr
2001/2002	1.8 cm/yr	1.7 cm/yr	1.9 cm/yr	1.9 cm/yr
2000/2001	1.5 cm/yr	1.3 cm/yr	1.8 cm/yr	2.1 cm/yr
1999/2000	2.1 cm/yr	1.5 cm/yr	2.2 cm/yr	2.1 cm/yr
1998/1999	1.6 cm/yr	1.8 cm/yr	1.9 cm/yr	1.8 cm/yr
1997/1998	1.9 cm/yr	1.3 cm/yr		2.5 cm/yr
1996/1997	1.5 cm/yr	1.5 cm/yr		2.2 cm/yr
1995/1996		1.5 cm/yr		
1994/1995		1.5 cm/yr		
1993/1994		2.2 cm/yr		
1992/1993		1.4 cm/yr		
1991/1992		1.2 cm/yr		
average	**1.93 cm/yr**	**1.36 cm/yr**	**2.26 cm/yr**	**1.95 cm/yr**

Table 14: Growth rate per year for the four selected corals according to the age model based on Sr/Ca and Ba/Ca data. One year was defined from September-August.

3.9.1 Correlations between cores

The annual averages (September – August) of the geochemical proxies of the four cores were correlated with each other to investigate how reproducible the signals recorded by the corals are. The data up to September 2010 was chosen for correlation. The carbonate secreted in 2011 still partly contained the tissue layer, which may have influenced the reliability of the proxy data. Annual averages (September – August) of the proxy data were compared in order to remove the seasonality effect on the correlation.

Proxy data	Correlation	Time period	N	P	R	R^2
Ba/Ca	Qui4 – Qui7	1997 - 2010	13	0.028	0.584	0.341
Sr/Ca	Qui4 – Qui7	1997 - 2010	13	0.024	0.598	0.357
Mg/Ca	Qui4 – Qui2b	1997 - 2010	13	0.048	0.535	0.287
Y/Ca	Qui2b – Qui7	1997 - 2010	13	0.008	0.679	0.461
U/Ca	Qui6 – Qui7	1999 - 2010	11	0.011	0.704	0.496
La/Ca	Qui4 – Qui6	1999 - 2010	11	0.009	0.715	0.511

Table 15: Significant correlations of geochemical data averaged annually

When comparing the G/B records to each other, particularly strong relationships between Qui6 and Qui7 as well as Qui2b and Qui4 were identified. These results could not be confirmed by the geochemistry data. When Ba/Ca data were compared, the only significant correlation occurred between Qui4 and Qui7. The same cores were significantly correlated when comparing Sr/Ca data. When correlating Mg/Ca data, the cores Qui4 and Qui2b significantly correlated. Qui2b and Qui7 showed a significant correlation when comparing their Y/Ca data. When U/Ca data of the cores were compared, Qui6 and Qui7 significantly correlated and Qui4 and Qui6 significantly correlated when comparing La/Ca data. No significant correlations were found when comparing Pb/Ca and Mn/Ca data.

3.9.2   Ba/Ca and Y/Ca

The properties of the G/B records for the time period 1996 – 2010 are given as a comparison for the geochemical data (Table 16). While the records averaged at similar values, the amplitudes varied between 0.08 (Qui7) and 0.25 (Qui4).

Coral core	Time period	Average	Standard Deviation	Maximum	Minimum	Max - Min
Qui2b	1996 – 2010	0.86	0.03	0.96	0.74	0.22
Qui4	1996 – 2010	0.85	0.03	1.00	0.74	0.25
Qui6	1996 – 2010	0.86	0.03	0.93	0.81	0.12
Qui7	1996 – 2010	0.84	0.02	0.88	0.80	0.08

Table 16: Properties of the four G/B records

The Ba/Ca records of the four corals are shown in figure 29. A peak that was common to all cores can be seen in 2001 (Fig.29), which coincides with the occurrence of tropical cyclone Dera. Additionally, Ba/Ca records of cores Qui4, Qui2b and Qui7 peaked in 1998, 2003 and 2007 (Fig.29). 1998 was characterized by an El Niño and positive IOD event, while in 2007 a positive IOD event occurred. In 2003, tropical cyclone Atang came close to the study site. In 1997, a peak in the Ba/Ca record of Qui4 and Qui2b could be observed (Fig.29). In the same year, tropical cyclone Lisette passed through close to the sampling site. Cores Qui6, Qui4 and Qui7 displayed a decreasing trend from 1997 – 2008, while no trend could be observed in Qui2b. Qui2b Ba/Ca record had the highest average of all cores (5.31) followed by Qui4 (4.68), Qui7 (4.23) and Qui6 (4.09) (Table 17). The standard deviations of cores Qui2b and Qui6 were similar with 0.59 and 0.55 respectively. Contrastingly, the standard deviations of Qui4 and Qui7 were significantly higher with 0.90 and 0.81 respectively (Table 17).This implies that within the error range of one standard deviation, the baselines of the cores overlap. Core Qui4 had the lowest growth rate (1.36 cm/year, table 14) but the highest variability in its Ba/Ca record (table 17).

Contrastingly, Core Qui6 had the highest growth rate (2.26 cm/year, table 14) and the lowest variability in its Ba/Ca record (table 17). There were no significant correlations between the Ba/Ca records of the corals and rainfall.
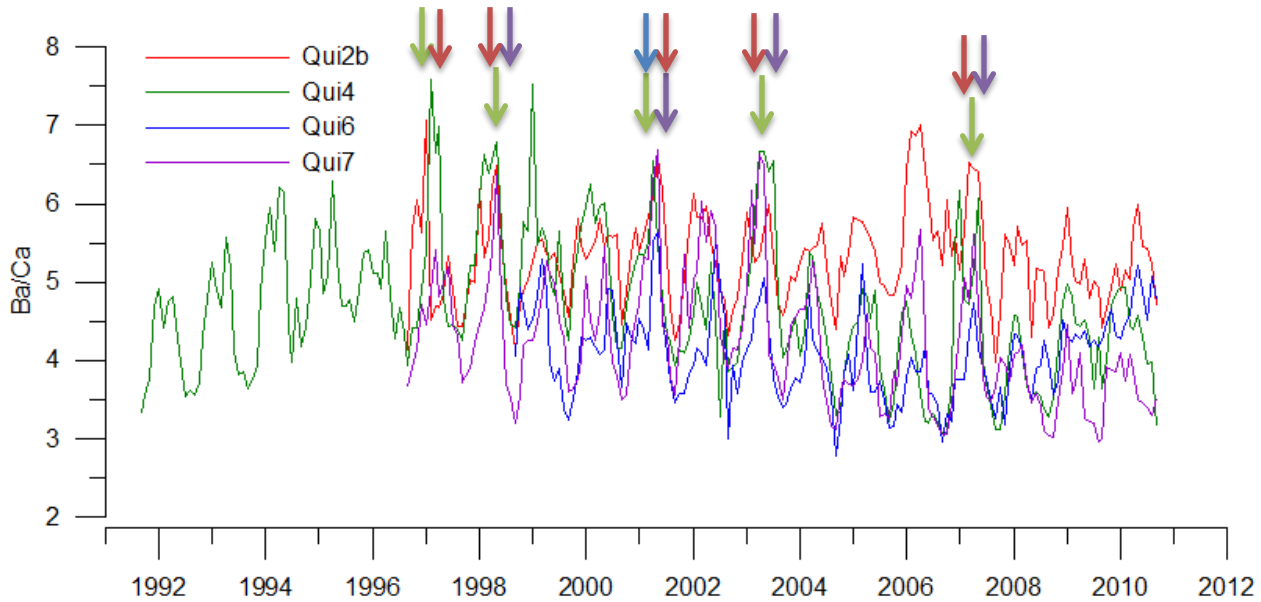
Figure 29: Ba/Ca of the four coral cores.

Coral core	Time period	Average	Standard Deviation	Maximum	Minimum	Max - Min
Qui2b	1996 – 2010	5.31	0.59	7.06	3.98	3.08
Qui4	1991 – 2010	4.68	0.90	7.59	3.06	4.53
Qui6	1998 – 2010	4.09	0.55	5.63	2.78	2.85
Qui7	1996 – 2010	4.23	0.81	6.69	2.95	3.73

Table 17: Ba/Ca record properties of the four cores.

The Y/Ca records of the four Quirimbas corals are depicted in figure 30. Cores Qui2b, Qui6 and Qui7 averaged at approximately 0.032, while Qui4 was significantly lower (0.026) (table 18). With the error range of one standard deviation, the Y/Ca baselines of Qui2b, Qui6 and Qui7 overlap. Additionally, positive excursions could clearly be recognized in Qui2b, Qui6 and Qui7, whereas positive anomalies were less extreme in Qui4 (Fig. 30). Qui2b and Qui7 display common positive anomalies in 2001 and 2005, which correlate with the occurrences of tropical cyclone Dera and tropical storm TS02R. Qui6 showed an excursion to more positive values in 1998, a year that was characterized by a positive IOD and El Niño event (Fig. 30). No long-term trends were visible in the Y/Ca records. There was no significant correlation between any of the four Y/Ca records and rainfall.
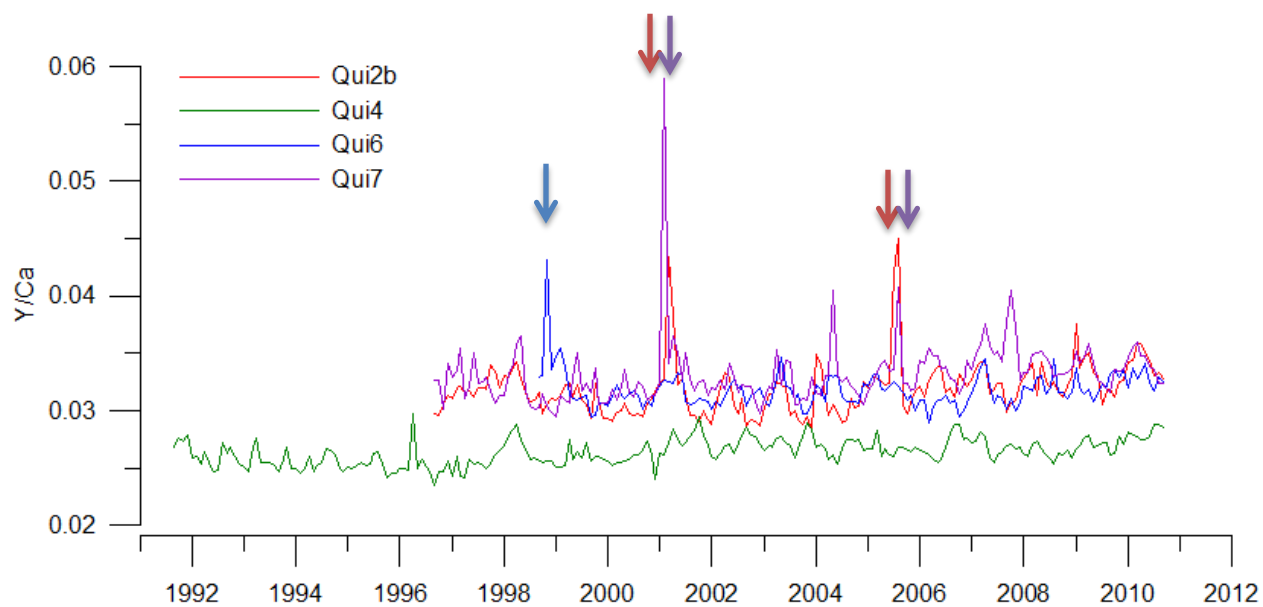
Figure 30: Y/Ca records of the four corals.

Coral core	Time period	Average	Standard Deviation	Maximum	Minimum	Max - Min
Qui2b	1996 – 2010	0.032	0.002	0.045	0.028	0.017
Qui4	1991 – 2010	0.026	0.001	0.030	0.026	0.006
Qui6	1998 – 2010	0.032	0.002	0.043	0.028	0.015
Qui7	1996 – 2010	0.033	0.003	0.059	0.029	0.030

Table 18: Y/Ca record properties of the four cores

3.9.3 Sr/Ca and U/Ca
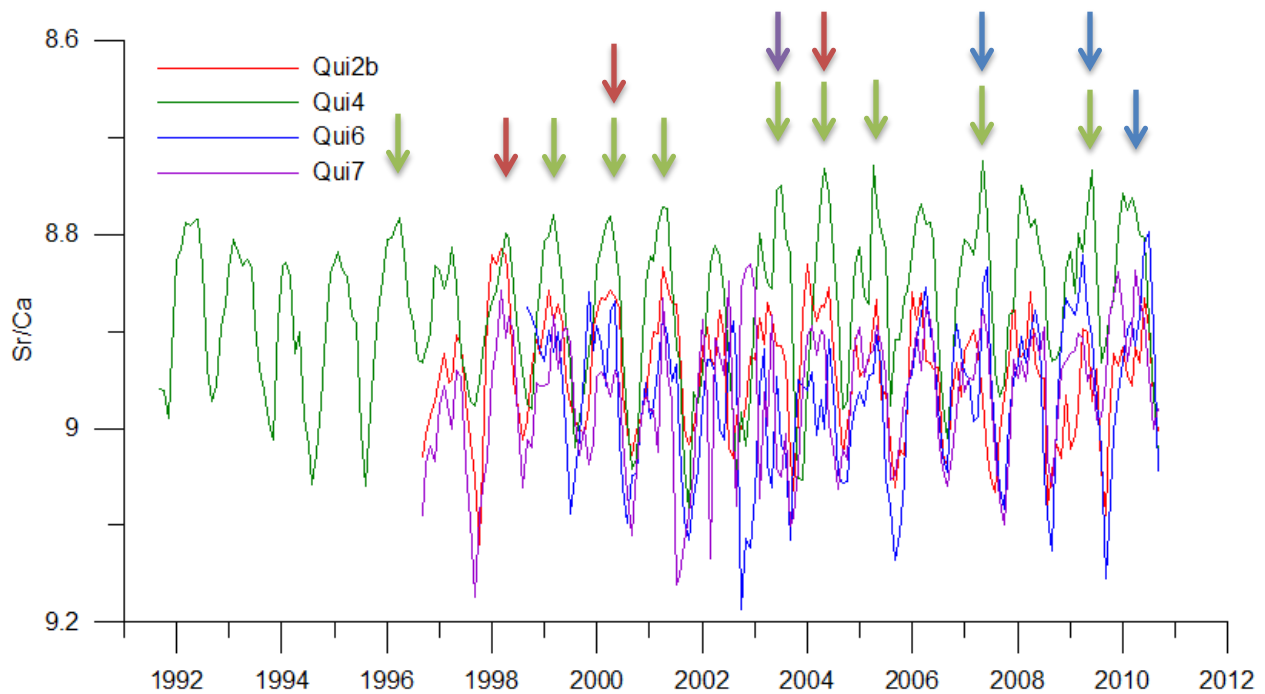
Figure 31: Sr/Ca records of the four coral cores.

The Sr/Ca records of the four cores are depicted in figure 31. While cores Qui 2b, Qui6 and Qui7 were centered on a similar average (table 19), Qui4's Sr/Ca is lower (table 19). However, they did overlap within the error range of one standard deviation. The variability in the data was highest for Qui2b, while being similar for the other three corals (table 19). Excursions to lower values were observed in Qui4 for the years of 1996, 1999 – 2001, 2003 – 2005, 2007 and 2009 (Fig.31). Qui2b displayed relatively low values in 1998, 2001 and 2004, while Qui7's Sr/Ca record was relatively low in 2003 (Fig.31). Core Qui6 had its most negative values centered in its most recent years including 2007, 2009 and 2010 (Fig.31). No long-term trends could be observed in the Sr/Ca data. The Sr/Ca record of core Qui7 positively correlated with SST (Qui7 – ERSST: n=14, p=0.011, r=0.652, r2=0.452; Qui7 – HadISST: n=14, p=0.031, r=0.577, r2=0.333). No significant correlation could be identified between the other corals' Sr/Ca records and SST.

Coral core	Time period	Average	Standard Deviation	Maximum	Minimum	Max - Min
Qui2b	1996 – 2010	8.95	0.07	9.35	8.81	0.53
Qui4	1991 – 2010	8.88	0.08	9.08	8.72	0.36
Qui6	1998 – 2010	8.97	0.08	9.19	8.80	0.39
Qui7	1996 – 2010	8.97	0.07	9.17	8.83	0.35

Table 19: Sr/Ca properties of the four cores
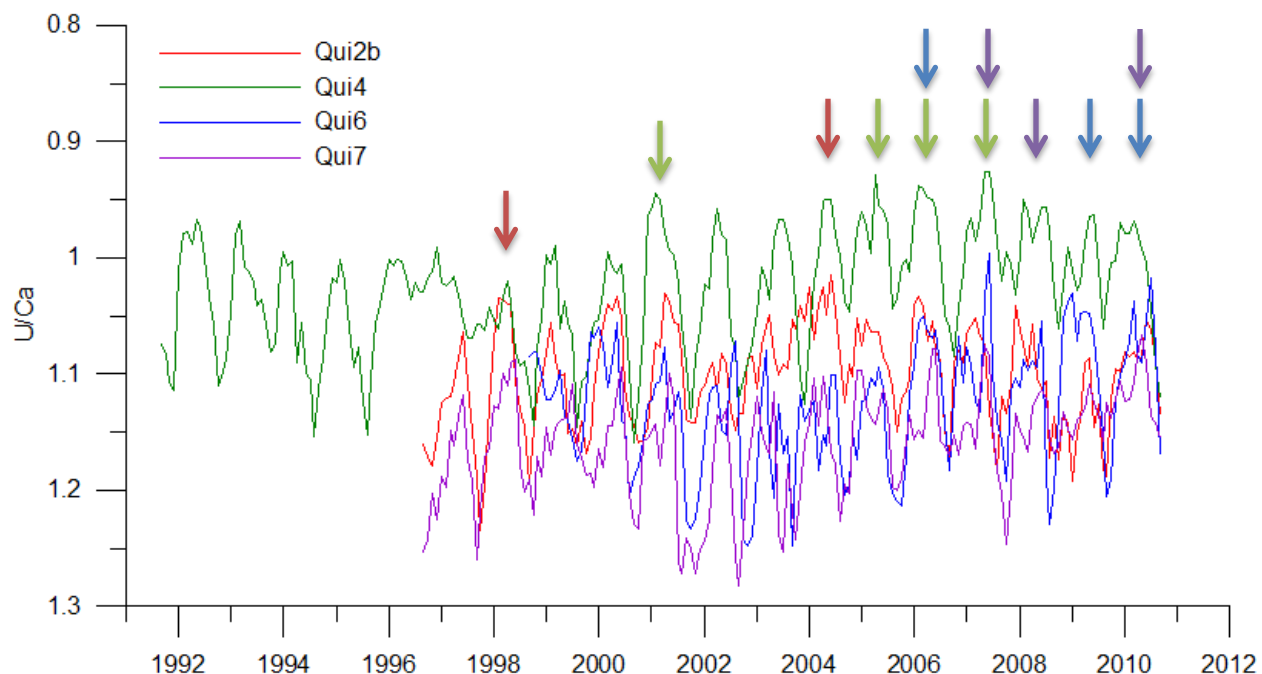
Figure 32: U/Ca profiles of the four cores.

The U/Ca records of the four cores are depicted in Figure 32. Similarly to the Sr/Ca records, the U/Ca records of Qui2b, Qui6 and Qui7 were centered on a similar average while the average of Qui4's U/Ca record was significantly lower (table 20). Relatively low values as recorded by Qui4 occured in 2001 and 2005 – 2007 (Fig.32). In the U/Ca record of Qui2b, 1998 and 2004 were relatively low, while Qui6 recorded low U/Ca in 2007, 2009 and 2010 (Fig.32). Qui7 showed relatively low U/Ca ratios in 2007, 2008 and 2010 (Fig.32). No long-term trends could be observed any of the four U/Ca records and no significant correlation could be established between any of the four U/Ca records and SST.

Coral core	Time period	Average	Standard Deviation	Maximum	Minimum	Max - Min
Qui2b	1996 – 2010	1.10	0.05	1.26	1.00	0.26
Qui4	1991 – 2010	1.02	0.05	1.16	0.93	0.23
Qui6	1998 – 2010	1.12	0.05	1.25	1.00	0.25
Qui7	1996 – 2010	1.16	0.05	1.28	1.06	0.22

Table 20: U/Ca properties of the four cores

3.10 Correlation of G/B with cyclones

The G/B records of the two composite records were correlated with cyclone data available at the KNMI climate explorer (http://climexp.knmi.nl/). The records were compared to tracks of tropical storms and cyclones as well as maximum wind speeds. The KNMI data was available on a 5x5° grid.
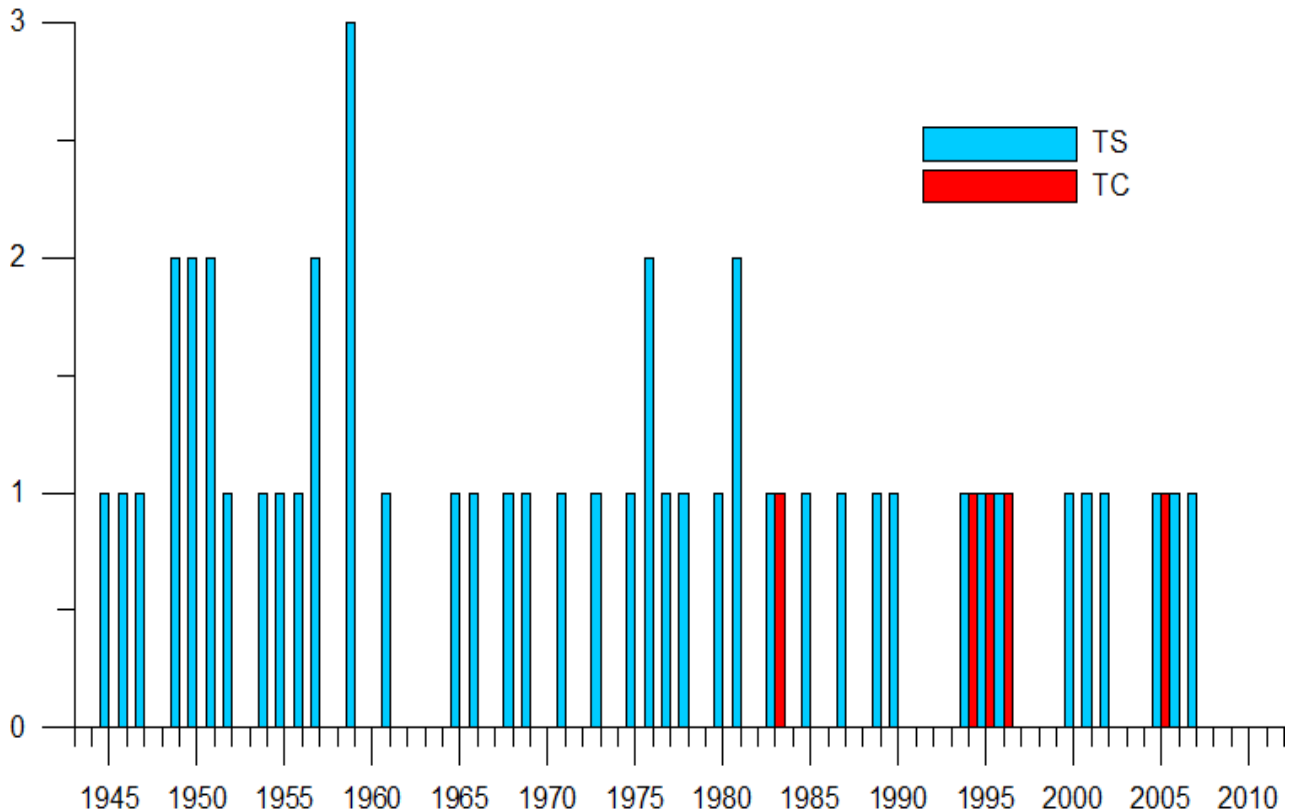
Figure 33: Number of tropical storms and tropical cyclones that occurred close to the study area. These storms occurred in the area 10-11S, 40-41E. Tropical storms (windstrengths 7-11 Bf) are depicted in blue while tropical cyclones (windspeeds >11 Bf) are shown in red.

The composite record constructed of normalized data showed a positive correlation over the western Indian Ocean when compared to tropical cyclone tracks for the period November to May (Fig. 31). Also it correlated with maximum wind speeds over the western Indian Ocean, including the study area for the period November-June (Fig. 34). The other composite record, constructed by averaging all four records, correlated with cyclone tracks and maximum wind speed over the Indian Ocean from November – June (Fig. 34 & 35).
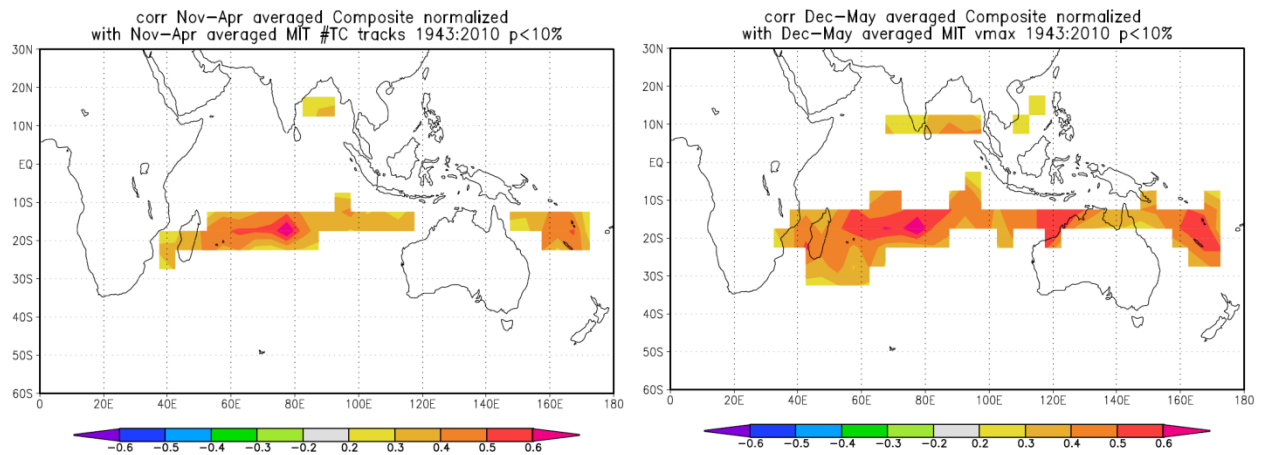
Figure 34: Spatial correlation of the composite record based on normalized data with tropical cyclone tracks (left) and maximum wind speed (right).
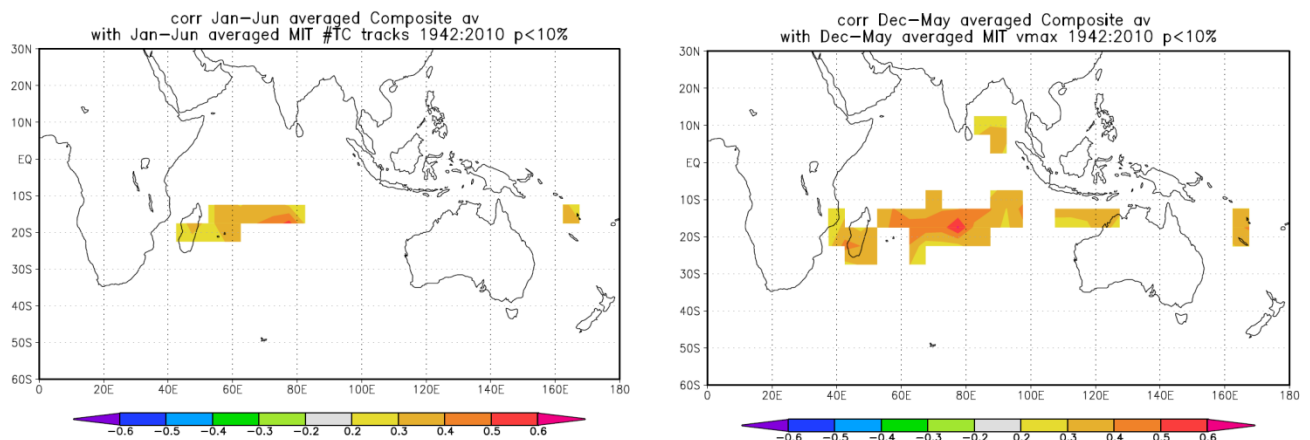
Figure 35: Spatial correlation of the composite record based on averaged data with tropical cyclone tracks (left) and maximum wind speed (right).

In general, peaks in the Ba/Ca, Y/Ca and G/B record match up with cyclones that came close to the study area (Fig. 36). In March 1994, tropical cyclone Nadia hit the northern coast of Mozambique. Its signal could be recognized in the G/B record. In March 1997, tropical cyclone Lisette travelled across northern Mozambique and its signal was registered in the Ba/Ca record. Tropical cyclone Dera reached the coast of northern Mozambique in March 2001 and its signal could be found in all three records. In November 2002, tropical cyclone Atang reached the coastline of southern Tanzania. Its signal was registered in the Ba/Ca record. Tropical storm 02R arrived at the coast of northern Mozambique in November 2004 and its signal could be traced in the G/B and Y/Ca record.
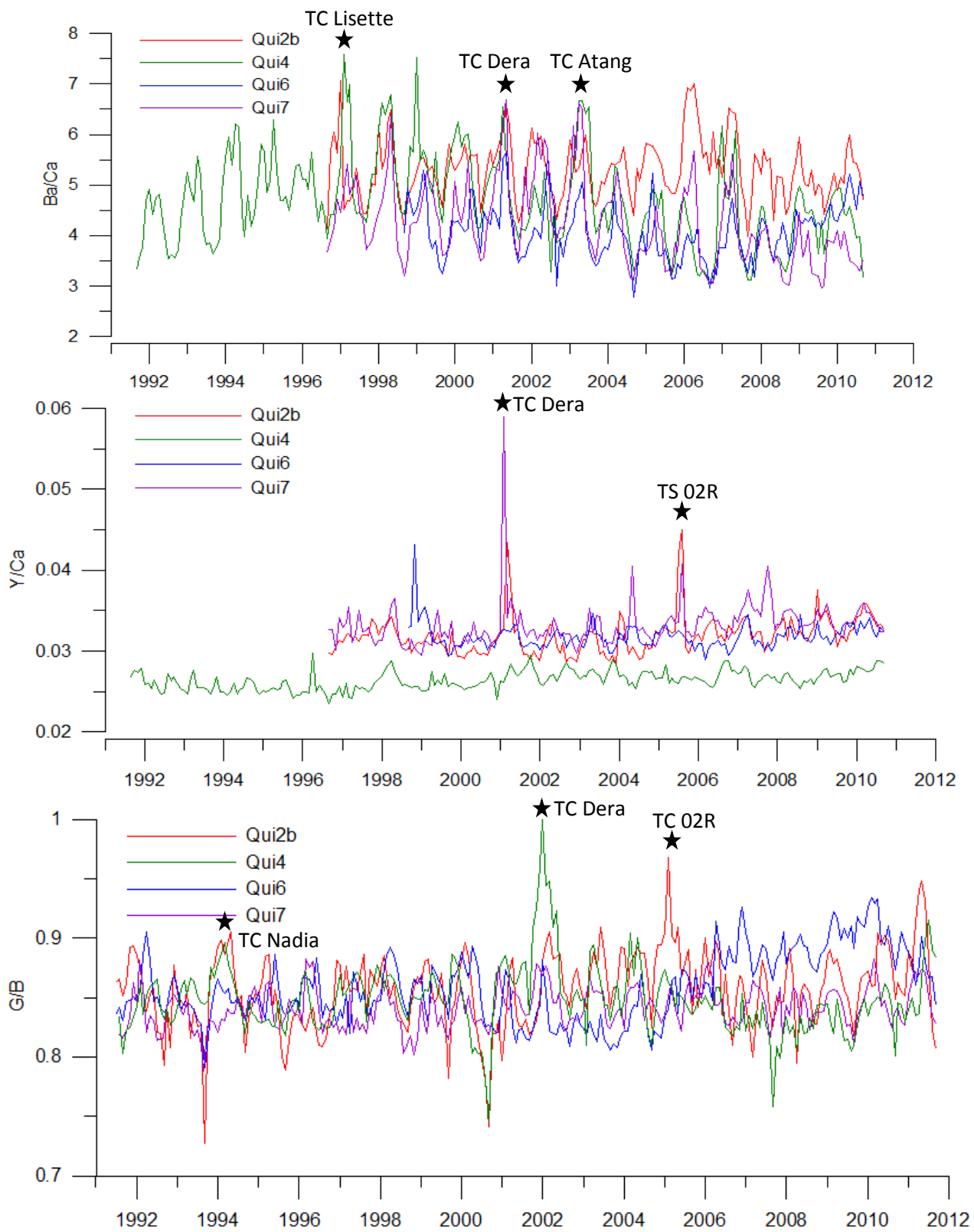
Figure 36: Peaks in the Ba/Ca, Y/Ca and luminescence record match up with cyclones that came close to the study area.

The peaks in the G/B records have been shown to line up with tropical cyclones that came close to the study area. The number of peaks in a given 5-year and 10-year period are shown in Table 21. No significant trends can be observed in the number of anomalously high peaks can be observed for the period 1968-2011.

Period	# G/B peaks	# G/B peaks	# TS peaks	# TS peaks	# TC peaks	# TC peaks
1968-1973	2	4	4	9	0	0
1973-1978	2		5		0	
1978-1983	2	5	4	6	1	1
1983-1988	3		2		0	
1988-1993	3	4	2	5	0	3
1993-1998	1		3		3	
1998-2003	3	7	3	6	0	0
2003-2008	4		3		1	
2008-2011	1	1	0	0	0	0

Table 21: Number of positive G/B anomalies in the composite record when removing the 1 year running median. Anomalies are given per 5 year and 10-year periods. For comparison, number of tropical storms (TS) and tropical cyclones (TC) passing through the area 10-12S/40-42E are shown (data from KNMI climate explorer: http://climexp.knmi.nl)

The G/B records of the two composite records and the MIT tropical cyclone and tropical storm record close to the study site are shown in Figures 37 and 38. Distinct peaks in the G/B records did not always line up with the most intense cyclones that have been reconstructed to have occurred in the close vicinity of the study site.

When a cyclone passes through, large amounts of freshwater and sediments are flushed into the bay. These are stress factors affecting the coral and should be registered as decrease in growth rate in the year the cyclone passes through. In this study, extension rates were calculated for all corals for the period 1998-2010. Relatively low extension rates occurred in the season of 1998/1999, except for Qui4 (Table 22). In this season, no cyclone affected came close to the study area, however, in December 1999, tropical cyclone Astrid passed through. Assuming an uncertainty of ±1 year in the age model, the two signals overlap. In the season 2000/2001, all corals except Qui7 displayed relatively low extension rates, which correlated with tropical cyclone Dera that passed through in March 2001 (Table 22). In the season of 2002/2003, the corals from site 2 and 3 showed significantly reduced growth rates. This can be correlated with tropical cyclone Atang, which came close to the area in November 2002 (Table 22). Another season characterized by relatively low extension rates was the season of 2006/2007 (Table 22). In November 2006, tropical cyclone Anita passed through.

	Qui2b	Qui4	Qui6	Qui7	Tropical Cyclone
2010/2011	1.6 cm/yr		2.6 cm/yr	1.9 cm/yr	
2009/2010	1.8 cm/yr	1.3 cm/yr	2.2 cm/yr	1.8 cm/yr	
2008/2009	2.1 cm/yr	1.6 cm/yr	2.1 cm/yr	2.0 cm/yr	
2007/2008	2.1 cm/yr	1.3 cm/yr	2.6 cm/yr	1.7 cm/yr	
2006/2007	2.1 cm/yr	1.2 cm/yr	2.0 cm/yr	1.8 cm/yr	**Anita**
2005/2006	2.7 cm/yr	1.3 cm/yr	2.5 cm/yr	1.8 cm/yr	
2004/2005	2.3 cm/yr	1.9 cm/yr	2.2 cm/yr	1.9 cm/yr	
2003/2004	1.9 cm/yr	1.6 cm/yr	2.2 cm/yr	1.8 cm/yr	
2002/2003	1.7 cm/yr	1.2 cm/yr	3.0 cm/yr	1.9 cm/yr	**Atang**
2001/2002	1.8 cm/yr	1.7 cm/yr	1.9 cm/yr	1.9 cm/yr	
2000/2001	1.5 cm/yr	1.3 cm/yr	1.8 cm/yr	2.1 cm/yr	**Dera**
1999/2000	2.1 cm/yr	1.5 cm/yr	2.2 cm/yr	2.1 cm/yr	**Astrid**
1998/1999	1.6 cm/yr	1.8 cm/yr	1.9 cm/yr	1.8 cm/yr	
1997/1998	1.9 cm/yr	1.3 cm/yr		2.5 cm/yr	
1996/1997	1.5 cm/yr	1.5 cm/yr		2.2 cm/yr	
1995/1996		1.5 cm/yr			
1994/1995		1.5 cm/yr			
1993/1994		2.2 cm/yr			
1992/1993		1.4 cm/yr			
1991/1992		1.2 cm/yr			
average	**1.93 cm/yr**	**1.36 cm/yr**	**2.26 cm/yr**	**1.95 cm/yr**	

Table 22: Reduced growth rates common to most cores correlate with the occurrence of tropical cyclones
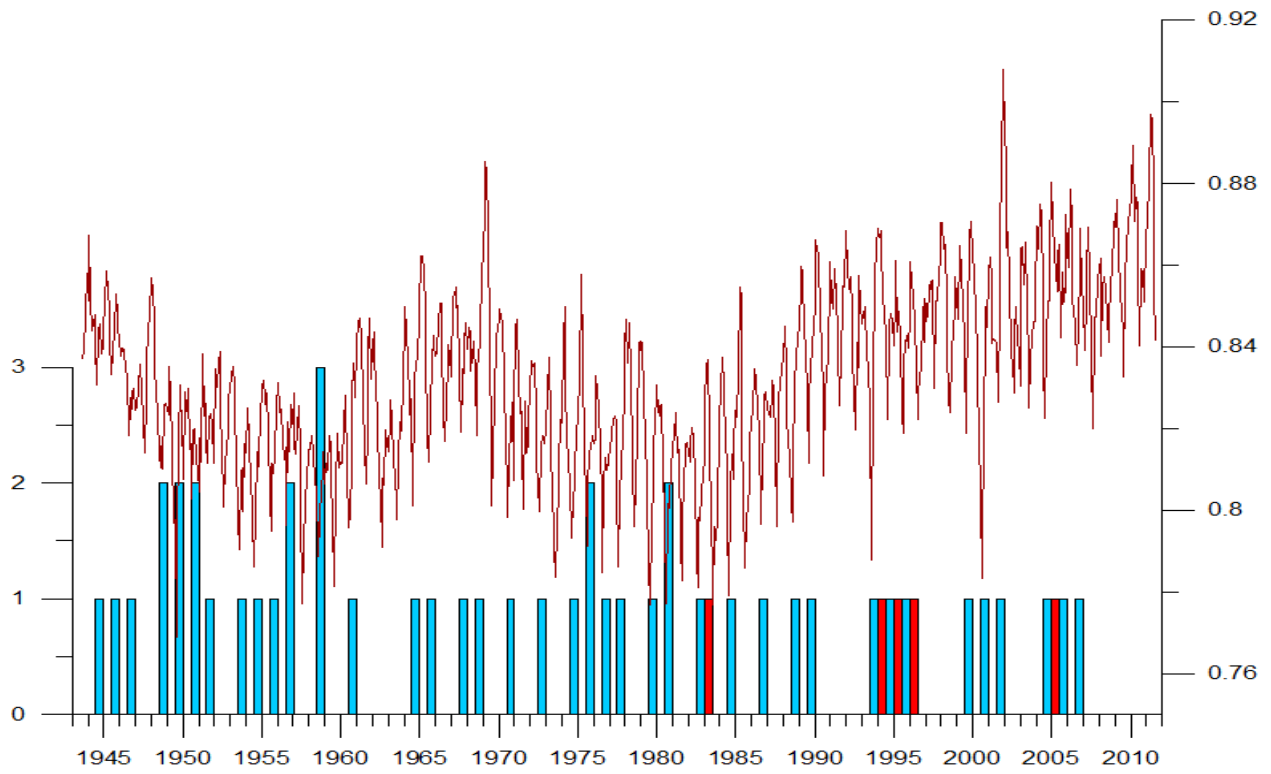
Figure 37: Number of tropical storms (blue) and cyclones (red) over the study area. The annually averaged G/B of the composite record based on the four cores' average is depicted in dark red.
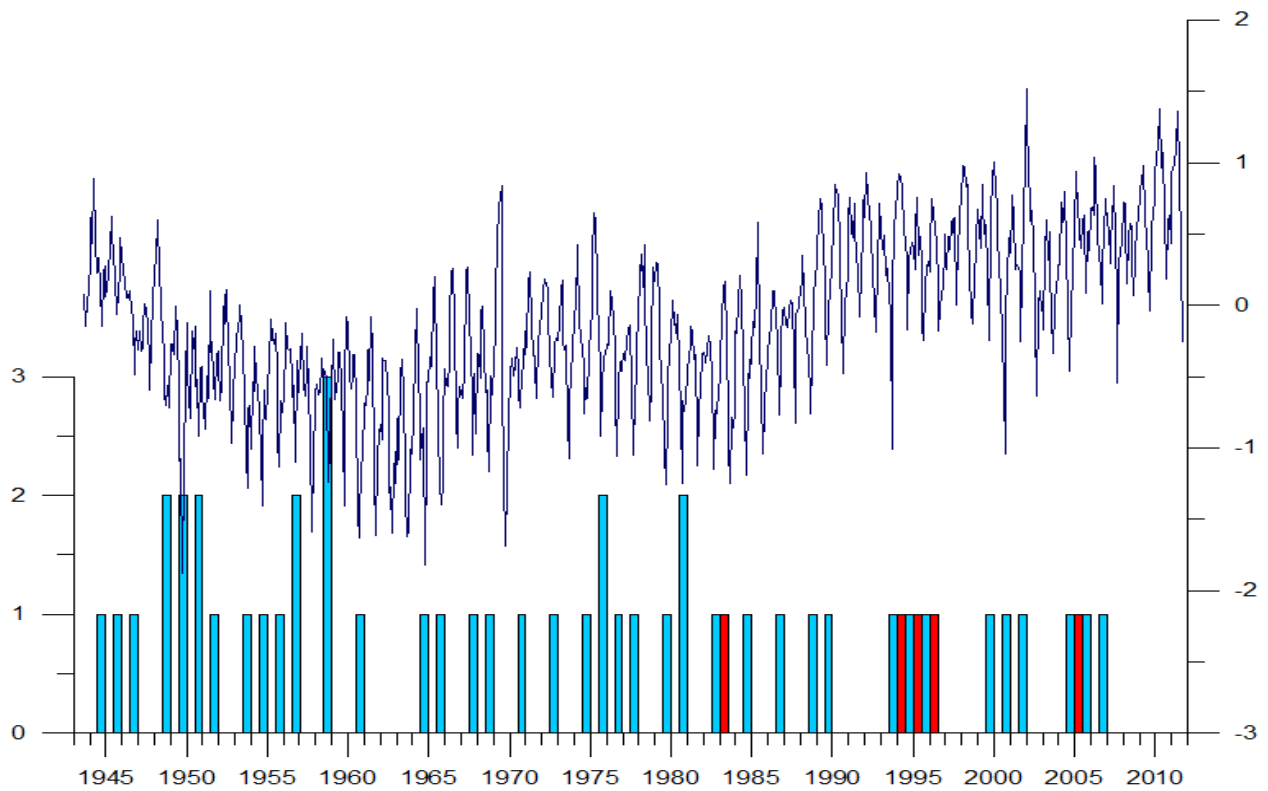
Figure 38: Number of tropical storms (blue) and cyclones (red) over the study area. The annually averaged G/B of the composite record based on the normalized data is depicted in dark blue.

4. Discussion

Coral cores offer valuable insights into local and large scale climate controlling factors and allow us to extend climate records beyond instrumental records (e.g. Cole et al., 2000; Grove et al., 2012a; Hetzinger et al., 2008; McCulloch et al, 2003; Prouty et al., 2010). This makes them a vital tool to assess natural and anthropogenic climate change. Tropical SST are influenced by monsoonal systems, tropical cyclones as well as large scale climate oscillations, such as ENSO or the AMO. Therefore, by reconstructing coral based SST, it is possible to assess long-term climate variability. In addition to oceanic parameters, such as SST, riverine sediment input into coastal systems could be traced by interpreting the Ba/Ca records of coral cores (Fleitmann et al., 2007; McCulloch et al., 2003; Prouty et al., 2010). More recently, coral luminescence has been shown to be a proxy of past rainfall variability and river runoff (Grove et al., 2010; Lough, 2011a). Comparing coral based reconstructed rainfall records has offered new insights into the effects of climate oscillations such as ENSO or the PDO on rainfall patterns (Grove et al., 2012b; Lough 2011a). As not much is known about the influence of these large scale climate oscillations on eastern African rainfall patterns, this study uses the coral luminescence – rainfall relationship to investigate the factors modulating rainfall in northern Mozambique.

Lough (2004) showed that the strength of the coral - climate relationship varies amongst different corals and sometimes even with time. Therefore it is important to assess more than one coral core from a single site, to confirm that the signal interpreted is common to all coral cores. For this reason, here we investigated four corals from a single bay in northern Mozambique. The annual averages of their luminescence G/B records were all significantly correlated with the exception of one relationship, indicating that they were all influenced by the same regional factors. To reduce local variability and the influence of vital effects, a coral composite was constructed. The composite record presented here, based on several significantly related coral cores, increased correlations with instrumental data and provided a more reliable reconstruction of past environmental conditions (Pfeiffer et al., 2009).

The coral cores used in this study often showed dark stains and green discolorations when exposed to UV light (section 3.1). These dark stains and green discolorations were removed when the coral slabs were submerged in bleach. However, occasionally they remained. This indicates that the stains were either not organic material or organic material that could not be removed by bleach. Sayani et al. (2011) determined that secondary aragonite, which can significantly alter the geochemical composition of the aragonitic skeleton, can precipitate within 30 years. The green discolorations picked up by spectral luminescence scanning were probably related to diagenisis that affected the older parts of the skeleton. However, the dark stains also affect younger parts of the skeleton and are therefore not related to diagenisis. Probably, the dark stains were caused by the incorporation of organic material into the skeletal structure that cannot be removed by bleach alone.

4.1 Relationship of coral luminescence with rainfall

Coral luminescence is a proxy for past rainfall variability (Lough 2011a). Lough (2011a) correlated luminescence data of corals from the Great Barrier Reef with instrumental rainfall data of northeastern Australia, confirming the relationship between the two parameters. Here we used Grove et al.'s (2010) method of spectral luminescence scanning to obtain a coral luminescence record. This method provides a density independent luminescence record which is a more quantified proxy record of past river runoff. A significant correlation between rainfall and luminescence could be established. However, not all correlations of rainfall data with G/B records were significant. When long-term trends were removed from the G/B records to focus on inter-annual variability, the correlation with rainfall became stronger. Almost all corals showed a significant correlation with rainfall. This infers that the relationship established by Lough (2011a) is valid in this study and that G/B is a proxy for rainfall in northern Mozambique. The fact that not all correlations of G/B and rainfall were significant can be explained by two reasons. 1) Reliable rainfall data for eastern Africa is scarce (Dewar and Wallace) and becomes less accurate when going back in time (Schneider et al., 2011). Further, the gridded datasets that were used in this study fail to capture local variability as they average over large areas(Schneider et al., 2011) and the weather stations are located at least 65 km away from the study site. This implies that the rainfall datasets used for comparison have a large error range and probably fail to capture the local rainfall signal that is recorded by the corals (Fig. 39). 2) Coral luminescence is only an indirect proxy of past rainfall variability. The luminescent intensities are caused by variable amounts of soil-derived humic acids incorporated into the skeleton (Grove et al., 2010). The amount of humic acids carried into the bay by rivers is typically related to the amount of rainfall, but can also be influenced by changes in hydrology, forest cover and land use (Grove et al., 2012b, Maina et al., 2012). The uncertainties in the luminescence record can typically be resolved by modeling the influencing parameters (Maina et al., 2012), which makes it possible to reconstruct local rainfall variability.

4.1.1 Relationship of coral luminescence with SST

Sea Surface Temperatures in the Indian Ocean are modulated by large scale climate oscillations including ENSO, IOD and PDO (Yamagata et al., 2004; Mantua and Hare, 2002; McPhaden et al., 2006). In turn, SST have been shown to modulate rainfall of the hinterland. Warmer SST are believed to allow more evaporation, which causes precipitation to increase. Therefore, warming SST in the Indian Ocean should cause an increasing trend in rainfall over eastern Africa. However, Funk et al. (2008) modeled results suggest that recent warming of the central Indian Ocean has reduced rainfall over eastern Africa, including northern Mozambique. The G/B luminescence, which is a proxy for past rainfall variability, positively correlates with SST over almost the entire Indian Ocean, suggesting that warmer SST caused increased precipitation over northern Mozambique, opposing Funk et al.'s (2008) findings. When long-term trends of the G/B records were removed, the relationship disappeared. This infers that the correlation was cause by long-term trends common to both datasets and not inter-annual variability. In the past 30 years, SST in the central Indian Ocean continued to increase as part of the global warming trend. An increasing trend in the G/B is observed for the same time period, which probably caused the correlation. When the two datasets were correlated averaging over the time period prior to 1980, no positive correlation could be identified in the Indian Ocean, indicating that the recent warming trend

caused the positive correlation. At this stage, however, we cannot rule out the possibility that land use change caused the increasing trend observed in the G/B since the 1980s.
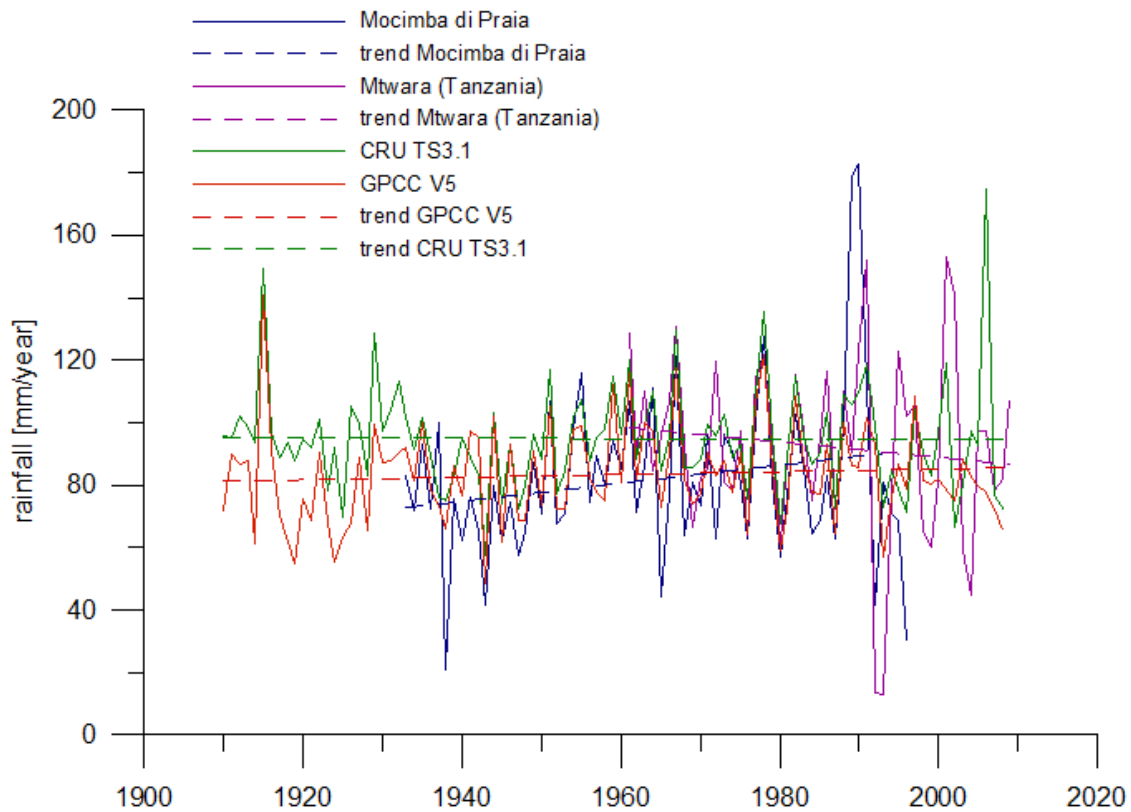
Figure 39: Annual rainfall of the four datasets used in this study. Trends in the datasets are indicated by broken lines.

The increasing trend in the G/B from 1980 onwards indicates that rainfall over the study area has continuously increased over the past 30 years. However, only Mocimba di Praia recorded an increase in annual rainfall since 1933 (Fig. 39). The two gridded datasets do not show any trend in rainfall over the past 100 years, while Mtwara station (Tanzania) recorded a decrease in annual rainfall since 1961. Reliable rainfall data for eastern Africa is scarce (Dewar and Wallis, 1999) and there are only two weather stations recording rainfall data in a 100 km radius of the study site. The gridded datasets average rainfall data over large areas and fail to capture local variability (Schneider et al., 2011). This is likely influencing the relationship of luminescence records with rainfall and could explain why the recent increasing trend observed in the G/B is not captured by the rainfall datasets. Also, it cannot be excluded that the recent increasing trend in the G/B was inflated by land use changes.

4.2 Relationship of coral luminescence with climate oscillations

The climate in northern Mozambique has been shown to be controlled by several large scale climate oscillations including ENSO, IOD and PDO (Deser et al., 2004; Indeje et al., 2000; Yamagata et al., 2004). We investigated the effects of large scale climate oscillation on east African rainfall by analyzing oscillations in coral luminescence records. As long-term trends can obscure relationships, the de-trended records were also compared to climate indices.

Spectral analysis picks up signals related to large scale climate oscillations archived in coral records. It revealed underlying signals with a frequency typical of the IOD. The only coral that recorded an ENSO-like frequency signal was Qui7. This suggests that the IOD modulates runoff in northern Mozambique, while ENSO only plays a minor role. Due to the shortness of the records, the multi-decadal signals of the AMO and PDO could not be picked up by spectral analysis.

Although ENSO supposedly modulates rainfall over northern Mozambique (Indeje et al., 2000), no correlation of the luminescence record with ENSO indices could be identified, suggesting that ENSO only has little to no influence on river runoff in northern Mozambique. This was also confirmed by spectral analysis results as only one significant oscillatory frequency typical for ENSO in the luminescence records was observed for a single record. Lough (2011a) investigated the relationship of coral luminescence intensities from the Great Barrier Reef with ENSO. Although eastern Australian rainfall has clearly been shown to be modulated by ENSO, Lough (2011a) could only identify mixed agreements between reconstructed rainfall and reconstructed ENSO extremes. This shows that the relationship between ENSO and reconstructed rainfall is not as straightforward as initially suggested and could explain why no correlation between could be identified here. Power et al. (1999) showed that the correlation of rainfall with ENSO over Australia was modulated the IPO, the inter-decadal component of the PDO. Similarly, an interplay with another climate oscillation could obscure the relationship of reconstructed rainfall with ENSO in northern Mozambique. When comparing coral based SST reconstructions from all over the Indian Ocean to ENSO reconstructions, strong correlations have been identified (Cole et al., 2000; Mitsuguchi et al., 2008). To further investigate the influence of ENSO on climate in northern Mozambique, Sr/Ca records should be compared to ENSO reconstructions.

Positive correlations of the de-trended luminescence record with IOD indices confirmed the influence of the IOD on runoff in northern Mozambique. The influence of the IOD on rainfall in northern Mozambique was further confirmed by spectral analysis that detected frequencies typical for the IOD in all cores. However, the relationship could not be detected by spatial correlation of the G/B record with SST. This indicates that the IOD may modulate rainfall in northern Mozambique, but the relationship is not strong enough to be detected by the spatial correlation of G/B with SST. This could be due to an interplay of the IOD with ENSO. In the Indian Ocean, ENSO and the IOD have been shown to modulate each other (Meyers et al., 2006), which is why it is difficult to separate the effects of ENSO and IOD when interpreting SST patterns in the Indian Ocean. Also, Abram et al. (2008) identified long-term variability in the recurrence frequency of the IOD, which so far have not been included into the reconstructed IOD indices that could account for uncertainties in the correlations. The relationship between the luminescence data and the IOD could also be obscured by the effects of extreme events, such as cyclones. The impact of cyclones on the luminescence data will be discussed later in more detail.

The PDO modulates the climate in eastern Africa at longer frequencies than the IOD or ENSO (Mantua and Hare, 2002). Negative correlations of the luminescence with PDO indices data were centered around the beginning of the rainy season. The results indicate that during a positive (negative) PDO phase, runoff is decreased (increased) in northern Mozambique. This opposes the findings of Deser et al. (2004), who suggested that Pacific Interdecadal Variability positively correlates with rainfall over southeastern Africa. The opposing results could be due to local effects. Deser et al. (2004) used a large scale climate model to assess pacific inter-decadal variability, while this study uses a localized proxy to reconstruct climatic conditions. The impacts of the PDO on rainfall in northern Mozambique were investigated by a coral record spanning 70 years, while the recurrence period of the PDO is 50-70 years. In order to assess the influence of the PDO on east African climate in more detail, a coral record extending over several cycles of the PDO should be investigated. However, the G/B data of this study clearly indicates that during a positive (negative) PDO phase, rainfall over northern Mozambique is reduced (increased).

Cole et al. (2000) studied a coral record spanning almost 200 years sampled close to the central part of the Kenyan coastline. Next to a strong relationship with ENSO, they also found a recurring oscillatory frequency of 8-14 years, which they attributed to the influence of the Pacific Ocean. When comparing the $\delta^{18}O$ record of the Kenyan coral to the G/B composite records, distinct similarities become apparent. Both records show a decreasing trend from 1940 until approximately 1960, which is followed by an increasing trend and a decreasing trend that dips in approximately 1985. From 1985 onwards, both records reveal an increasing trend. The $\delta^{18}O$ record of the Kenyan coral is believed to primarily reflect changes in SST, while the G/B composite record has been shown reflect changes in rainfall. Rainfall is driven by SST, which is why both corals display the same decadal oscillation. The correlation of the two records indicates that climate along the east African coast is forced by the tropical Pacific (Cole et al., 2000). During a phase of elevated SST along the east African coastline, rainfall is increased.

Grove et al. (2012a) showed that luminescence signals recorded in corals from eastern Madagascar were linked to the PDO. However, the correlation in the 20th century only became apparent after removing the anthropogenic influence on hinterland erosion. They removed the anthropogenic fraction by interpreting the Mn/Ca of their coral records, which are closely linked to slash-and-burn deforestation. In order to investigate the links to anthropogenic influence in northern Mozambique, it would be useful to analyze full geochemical profiles of all four corals and create models to examine the influence of changes in hydrology, forest cover and land use (Maina et al., 2012). Then the anthropogenic fraction of the G/B signal could be removed and the records properly compared to Grove et al.'s (2012a) results.
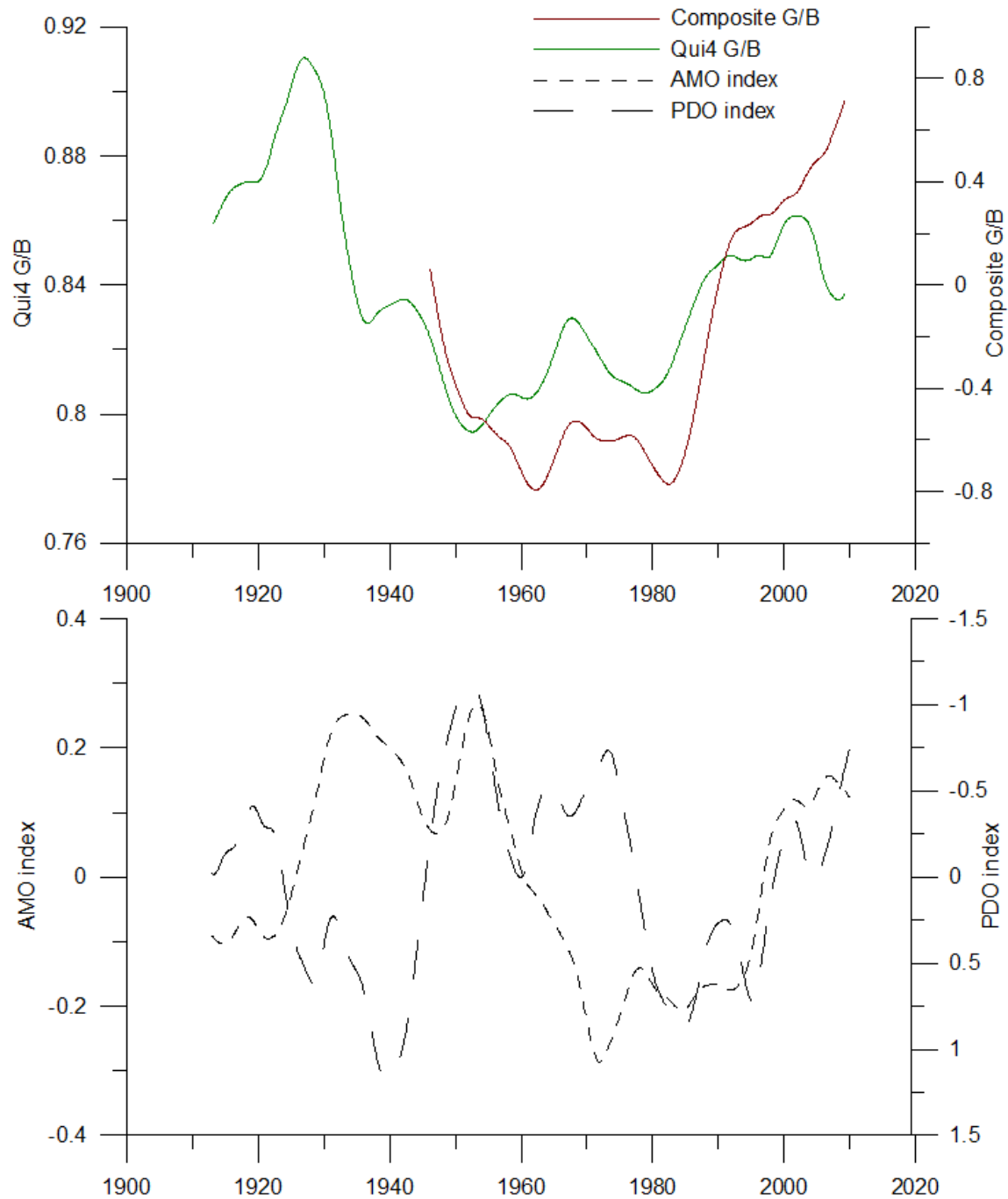
Figure 40: The longest G/B record and the composite record are shown in the top panel. The climate indices of the AMO and PDO, both based on HadISST, are displayed in the lower panel. The data has been filtered over 120 months.

The AMO modulates the climate of Atlantic-bordering regions including the Sahel region (Knight et al., 2006). Its signal has been identified in Caribbean corals, but so far, no teleconnections of the AMO reaching beyond the Atlantic Ocean have been identified (Hetzinger et al., 2008). The G/B composite record revealed strong correlations with AMO indices all year round, suggesting that the AMO influences rainfall in Mozambique. This was further strengthened by the similarities of the spatial patterns that are visible when the G/B records and the AMO indices are correlated with SST. The multi-decadal frequency of the AMO could not be picked up by spectral analysis, which is due to the shortness of the records. The composite records only spans the past 70 years, which is not long enough to fully assess the impact of the AMO on the climate in Mozambique. However, the correlations indicate clearly that probably there is a connection between the AMO and the G/B record of the Mozambique corals. The G/B composite record indicates that during a positive (negative) phase of the AMO, rainfall over northern Mozambique is increased (decreased). Knight et al. (2006) showed that a warm AMO phase is associated with increased rainfall in the Sahel region due to the displacement of the ITCZ relative to its climatological position. This displacement could extent to eastern Africa and cause the signals observed in the corals. No correlation of northern Mozambique rainfall with AMO indices could be found. However, this could be due to inaccuracies in the rainfall data.

When the luminescence data was compared to the AMO and PDO index, depressions in the G/B data could be matched with peaks/depressions in the PDO/AMO index for the period 1960 – 1985 (Fig. 28). The increasing trend in the luminescence data from 1985 onwards is probably related to the recent warming trend. This is why the correlation of the indices and the luminescence data decouples at this point. When the correlation is extended by comparing the longest record to AMO and PDO indices, similarities with both indices can be identified (Fig. 40). Not all peaks and troughs correlate perfectly with troughs and peaks in either the AMO or the PDO index, which is probably due to an interplay of the two climate oscillations. Large scale climate oscillations, such as the IOD and ENSO or the PDO and ENSO, have been shown to modulate each other (Meyers et al., 2006; Power et al., 1999). The AMO and PDO have both been shown to influence rainfall in northern Mozambique, which is why it is probable that they also influence each other. Multiple regression analyses are planned to further investigate this relationship.

4.3 Coral geochemsitry

Sr/Ca and U/Ca are traditional proxies for reconstructing SST (Corrège, 2006). A positive correlation between the annual averages of SST and the Sr/Ca record of Qui7 could be established, confirming that the two are significantly related. However, three of the four cores did not correlate with SST. This can probably be attributed to vital effects, stress factors or the datasets used for comparison (Cardinal et al., 2001; Marshall et al., 2002). Stress factors, such as freshwater pulses or very high SST have been shown to cause a breakdown in the Sr/Ca – SST relationship (Marshall et al., 2002). Similarly, differences in growth rate have been shown to alter the Sr/Ca – SST relationship (Cardinal et al., 2001). Cardinal et al. (2001) showed that U/Ca is not only controlled by SST, which explains why no correlation between SST and U/Ca could be identified in this study. The SST fields were computed by averaging over large areas and likely fail to capture local conditions and local variability within the bay, which were recorded by the corals. No long-term trends could be identified in the Sr/Ca and U/Ca records, while in

the same period, there was an increasing trend in SST over the western Indian Ocean (Funk et al., 2008). However, the records only span the last 15 years, which is too short to properly assess any long-term trends. Extreme events were identified in the geochemical records, but no event was captured by all corals, suggesting that the registered anomalies were localized and did not extend over the entire bay. Extreme events in the records could not be correlated with historical ENSO or IOD events.

Ba/Ca and Y/Ca are related to the amount of sediment that is carried into the bay by rivers (Fleitmann et al., 2007; McCulloch et al., 2003). Three of the four Ba/Ca records display a slightly decreasing trend from 1997 onwards suggesting that sediment input into the bay may have decreased in that period. However, due to the shortness of the records it is not possible to assess the significance of the observed trends. Extreme events that were identified in the records could be correlated with IOD and ENSO events, as well as tropical cyclones. No correlation with rainfall could be established. Ba/Ca and Y/Ca are only an indirect measure of rainfall, as they are controlled by sediment input into the bay. This is traditionally proportional to rainfall. However land-use changes can also affect the amount of sediment flushed into the bay (McCulloch et al., 2003). Additionally, extreme events could obscure the relationship (Prouty et al., 2010). Also, the rainfall records may not capture the local signal that is recorded by the corals as the weather stations are relatively far away and the gridded datasets average over large areas.

The correlation of the geochemical data of the four cores revealed that some cores were significantly related. When the G/B records were correlated with each other, almost all relationships were significant. The fact that not all cores are significantly correlated when comparing geochemical records is probably due to the shortness of the records (n=13) and the robustness of the method. The method of comparing annual averages that was chosen for the correlation requires a very strong connection between the two correlated records for the correlation to be significant. The significance of the correlation could be obscured by vital effects. When visually assessing peaks in the Ba/Ca and Y/Ca records, it was clear that cores shared similarities in extreme events.

There are significant differences in the average growth rates determined from the geochemical records of the four cores. While two of the corals grow at similar rates, one coral grows significantly faster and one significantly slower. The difference in growth rate could also be the reason why the correlation between Qui6 and Qui4 was not significant, as the cores with the highest and slowest growth rate were compared to each other. The differences in growth rate could be due to several factors. It could be related to the age of the coral. The youngest coral has the fastest growth rate, while the two corals of similar age have similar growth rates and the oldest coral grows the slowest. Only the top 30 cm were sampled to determine growth rates. As growth rates decrease as the coral grows older (Lough and Cooper, 2011), the age difference could explain the differences in extension rate. Also, coral biology could influence the growth rate. Species differences or different zooxanthellae clades living in symbiosis with the coral could also affect the growth rate. However, preliminary results indicate that all corals shared a symbiotic relationship with the same zooxanthellae clade, suggesting that in this case the differences in growth rates were not caused by different zooxanthellae. The corals were sampled at similar depths, but local environmental conditions related to turbidity of the water column, which in

turn affects the availability of light, or differences in nutrient availability could also influence the growth rate (Lough and Cooper, 2011).

The differences in growth rate have to be taken into consideration when interpreting geochemical data. Corals pick up the building blocks of their skeleton from the water column. Typically, trace elements are incorporated into the crystal lattice instead of the calcium ion (Fallon et al., 2002). As a coral grows more slowly, less aragonite has to be secreted. This implies that when assembling the skeleton forming ions from the water column, the amount of trace elements relative to the amount of calcium ions will be reduced in a slow growing coral relative to a fast growing coral. Consequently, the baseline of a trace element – Calcium ratio will be lower in slower growing corals. This phenomenon can be observed when looking at Y/Ca, Sr/Ca and U/Ca baselines. Here, the baseline for Qui4 was significantly lower than the baselines of the other three records. However, this phenomenon could not be observed for the Ba/Ca records of the four corals.

4.4 Relationship of corals with tropical cyclones

The cyclone data used in this study was provided by the MIT tropical meteorology group. They integrate data on tropical cyclone paths and intensities from multiple cyclone forecast and tracking centers including the National Ocean and Atmospheric Administration (NOAA), Japan Meteorological Agency, United Kingdom Meteorological Office and Australian Bureau of Meteorology.

The G/B records of this study were compared to maximum wind speed as well as past cyclone tracks recorded by the MIT tropical meteorological group. The maximum resolution of the data was 5°x5°. Cyclones that affect eastern Africa typically develop over the central Indian Ocean, from where they move west towards the coast of eastern Africa and Madagascar. The spatial correlation of the composite records with maximum wind speed revealed a significant correlation over the Central and Western Indian Ocean, extending over the study area. The correlation with historical cyclone tracks is weaker, however, it still clearly indicated the connection between the G/B records cyclones. Positive anomalies in individual G/B records and the geochemistry data could be correlated with historical cyclone activity for the past 20 years close to the study area making the relationship between the coral data and cyclones more evident. When the luminescence data was compared to the cyclone record of the study site for the period 1940-2010, positive anomalies in the G/B record did not always co-occur with the cyclone data provided by the MIT tropical meteorology group. The data only captured cyclones that passed through in the close vicinity of the study area, which can explain the discrepancies between the MIT cyclone record and G/B composite. Cyclones that pass through further away can still have a huge effect on the watershed of the river and thereby on the amount of humic acids that are transported to the corals. Additionally, cyclone tracking in this part of the world is very difficult as reliable tracking stations are scarce. Different sources provide varying information on the strengths and the exact path of a cyclone. Information also become less accurate when going back in time. This could account for some of the variability in the data when correlating peaks with precise cyclone tracks. In addition, when comparing specific cyclone tracks to peaks within the data, it becomes apparent that cyclones that pass relatively far north or south of the study area can have a huge influence on the corals. This may be related to the Rovuma River plume. The river has a huge catchment area, and if a cyclone affects parts of that catchment, not necessarily close to the study site, large amounts of humic acids will

be carried by the plume due to increased erosion in the cyclone affected part. This signal is then recorded by the corals, despite the fact that the cyclone did not pass through in close proximity to the study site.

Large amounts of freshwater and sediments are flushed into the bay as a cyclone passes through the region. It has been shown that corals can stop calcifying when under stress (Lough and Cooper, 2011). Thus, a cyclone passing over the site directly may not be recorded as intensely as a cyclone that passes by a little further apart, as the corals in the bay stop calcifying or reduce their calcification rates due to the stress caused by high turbidity and low salinity. As corals reduce their calcification rates, there will be no or only little record of the cyclone passing through incorporated into the skeletal structure. If this is the case, years with cyclones passing through should be characterized by relatively low extension rates. In this study, extension rates were calculated for all corals for the period 1998-2010. Years with low extension rates common to most cores could be correlated with cyclones passing by in the vicinity of the study site. This correlation suggests that there is a link between the two components. In order to investigate this further, it would be useful to determine annual growth rates spanning the entire length of all four cores. These could then be compared to historical cyclone tracks to confirm the relationship and could potentially offer more insights into the recurrence frequency of cyclones affecting northern Mozambique and a potential change in their recurrence frequency. Reduced growth rates during the occurrence of a cyclone also explain why the cyclone signal is more apparent in some corals than in others. The corals that were affected most heavily by the cyclone probably reduced their growth rates significantly or even stopped calcifying and therefore did not record the cyclone signal, while the corals that continued growing incorporated the cyclone signal into their skeleton. The local effects on the individual corals were reduced by constructing the composite record and comparing this record to historical cyclone tracks.

The occurrence of strong tropical cyclones has been shown to increase as SST continue to increase (Webster et al., 2005). Webster et al. (2005) determined that the number of tropical cyclones in the southern Indian Ocean occurring in the period 1990-2004 increased by approximately 220% compared to the period 1975-1989, which can be linked to the 0.5°C temperature increase in the southern Indian Ocean in the same time period. Also, the intensity of the strongest tropical cyclones has likely increased over the southern Indian Ocean (Elsner et al., 2008). It has been shown that peaks in the geochemistry as well as the G/B records of the cores of this study correlate with cyclones. In addition, a positive correlation of tropical cyclone tracks over the Indian Ocean and the composite G/B records could be established. Consequently, analyzing the intensity and recurrence frequency of the G/B peaks should allow estimating if tropical cyclones have become more frequent or stronger. The number of anomalous events does not reveal a significant trend over the past 70 years. This suggests that in contrast to the results proposed by climate models, cyclones affecting eastern Africa at this location have not become more frequent or stronger over the past 70 years. However, the period of 70 years may in fact be too short to identify significant trends, as no data spanning the time period preceding the Industrial Revolution and thereby the onset of anthropogenic climate change is available for comparison. Corals pick up a localized signal, which makes them not ideal tracers of cyclone activity. The signal that is picked up by the coral is a combination of the effects of the cyclone's intensity and the

distance of its pathway to the corals. A strong cyclone that passes by relatively far away can cause the same signal as a weak cyclone passing directly over the study site. Additionally, the path followed by cyclones does not stay the same. Only slight changes in the paths can cause changes in the signal picked up by the corals. Interpreting this signal could lead to inferring trends that do not exist. Consequently, reconstructed cyclone activity based on coral records should always be interpreted with larger scale meteorological data to confirm that the observed trends are not a local artifact.

Kilbourne et al. (2011) tried to reconstruct tropical cyclone activity by investigating the $\delta^{18}O$ of coral skeletons. They hypothesize that due to the intense rainfall accompanying a cyclone, SSS and thereby the isotopic composition will be significantly altered and the event will be recorded in the coral skeleton. However, due to large uncertainties in the data they were unable to distinguish between the isotopic signal caused by normal rainfall and rainfall associated with tropical cyclones. This study focuses on proxies that are related to hinterland erosion, which is a more direct approach to model the effects of cyclones and positive correlations could be identified. However, it is important to keep in mind that there is no clear border between the signals caused by cyclones and by relatively heavy rainfalls. Relatively strong rains not associated with a tropical cyclone could cause a similar signal in the coral record. This could be the reason why some of the peaks in the G/B records and geochemistry do not match up with cyclones.

4.5 Climate in Mozambique

This study showed that rainfall over northern Mozambique is modulated remotely from the Pacific and Atlantic Ocean. Analyzing these patterns carefully could offer new insights into future rainfall variability. Knowledge of future rainfall variability is vital for the country's agricultural sector and Mozambique's mission to increase agricultural production to fight malnutrition (FAO, 2010). At the moment, 8.3 million people (38%) are undernourished (FAO, 2011) and population growth is high with 2.1% averaged over the whole country and 4% in rural areas, like the north of Mozambique. In order to promote food security and economic growth, the Mozambican government supports the intensification and expansion of agriculture (FAO, 2010). A larger agricultural sector is even more vulnerable to extreme rainfall events, making information on future rainfall variability a crucial managing tool. As rainfall data in Mozambique is scarce (Dewar and Wallace, 1999), the information on past runoff variability that is archived in corals is an important tool to assess past rainfall variability and thereby make predictions for future rainfall trends. Based on this information, the impacts of variable rainfall could be mitigated by agricultural development. This could ensure food security in Mozambique, potentially reduce malnutrition and make the agricultural sector a reliable producer of export goods (Funk et al., 2008).

This study was the first to confirm the influence of large scale climate oscillations on northern Mozambican climate. To properly assess the influence of these climate oscillations on Mozambican climate and to identify local differences, it is important to extend this study by analyzing coral cores from other sites along the Mozambican coastline. Also, it would be useful to determine full geochemical profiles for all cores and analyze models linking the local watershed and the Rovuma watershed to the corals to assess the impacts of changes in hydrology, forest cover, land use and population change on the proxy data (Grove et al., 2012b; Maina et al., 2012). Deforestation and/or increased erosion of the

hinterland increase the amount of humic acids that are transported into the bay and could be interpreted as a false increasing trend in runoff (Grove et al., 2012b). As the Mozambican government has started to promote the expansion and intensification of agriculture, it is likely that land use changes have had an effect on the G/B records. Therefore, it is important to deconvolve the signals before making final conclusions.

In addition to the effects of an increased sediment load due to increased hinterland erosion, corals in Baia de Tunge will be affected by the mining practices in and around the bay. The Mozambican government plans to establish the Rovuma-Palma National Park, which would protect the corals in Baia de Tunge (Guerreiro, 2011). However, the petroleum mining company Anadarko is building a large production plant for processing liquefied natural gas at the southern shore of Baia de Tunge (Boman, 2012). Dredging activities and shipping traffic are likely to have a huge influence on the coral communities within the bay. Parts of the coral reefs will be destroyed by the dredging, while the rest has to cope with elevated pollutant concentrations in the water and increased turbidity. Increased concentrations of suspended particulate matter (SPM) have been shown to have different effects on coral growth (Lough and Cooper, 2011). Up to a certain threshold, SPM is an additional food source and provides energy to increase growth rates. However, if concentrations are higher that the optimal threshold, growth rates have been reported to decline (Tomascik and Sander, 1985). Sediment loads due to dredging operations have been shown to reach levels higher than 50 mg/cm2/d, which is catastrophic for coral growth. Corals close to dredging sites have been reported to have decreased growth rates, reduced skeletal density, reduced calcification rates or increased mortality (Bak, 1978). Nutrients and pollutants released into the bay by ships will also have an effect on the corals living in the bay. Increased levels of nutrients have been shown to increase growth rates initially, but once a certain threshold has been exceeded, growth rates, calcification rates and photosynthesis have been shown to be reduced (Lough and Cooper, 2011). Increased levels of pollutants in the water column cause coral growth rates to decrease (Scott, 1990). As the corals are located in the close vicinity of the mining and processing sites, an oil spill poses a serious threat to coral communities within and close to the bay. An oil spill in Panama caused coral cover and species diversity to decrease (Guzmann et al., 1991). The surviving corals had significantly reduced growth rates after the oil spill (Guzmann et al., 1991). As mining and processing practices in and around the bay pick up, the corals' growth rates will most likely decrease. Overall mortality is likely to increase and the worsened conditions will make it more difficult for new coral reefs to develop.

5. Conclusions

As corals grow, they archive environmental and climatic information of their surroundings. Coral based palaeo-climatic reconstructions link SST and rainfall proxies to large-scale climate oscillations and cyclones. This study investigated rainfall signals recorded in four corals from Baia de Tunge, northern Mozambique. The annual averages of their luminescence G/B records were all significantly correlated with the exception of one relationship. As all cores were likely influenced by the same regional factor, a coral composite record could be constructed to reduce local variability.

The luminescence data was shown to be a proxy of past rainfall variability. It revealed that rainfall in northern Mozambique was modulated by the PDO and AMO at multi-decadal timescales. The coral luminescence record indicated that during a positive phase of the PDO, rainfall was decreased over northern Mozambique, while a positive phase of the AMO typically caused an increase in rainfall over the region. On inter-decadal timescales, the IOD probably influenced rainfall over northern Mozambique, while the influence of ENSO on east African rainfall could not be confirmed. During a positive phase of the IOD, rainfall close to the study site was suggested to increase.

In addition to large-scale climate oscillations, tropical cyclones were found to have a significant effect on the corals. Spatial correlations of the luminescence record with maximum wind speed and cyclone tracks revealed strong correlations over the central and western Indian Ocean. Peaks in the geochemical and luminescence records could be aligned with tropical cyclones passing through close to the study area. Annual growth rates also displayed a link to tropical cyclones. As peaks in the luminescence record could be correlated with tropical cyclones, analyzing the number of peaks occurring within the G/B record could provide an indication of possible frequency changes of cyclones that reach the coast close to the study site. No significant trend in the number of extreme events could be observed indicating, that in contrast to what other studies suggest, cyclones have not become more frequent at this site over the past 70 years. However, corals are not ideal to infer the regional occurrence of tropical cyclones as they record a localized signal and are thereby unable to capture variations in cyclones' pathways and intensities.

An increasing trend was observed in the G/B record for the past 30 years, positively correlating with increasing SST in the Indian Ocean for the same time period. This infers that as Indian Ocean SST has increased in response to anthropogenic pressure, rainfall over northern Mozambique increased. However, this trend could not be confirmed by rainfall data. Models assessing changes in hydrology, forest cover and land use over the past 30 years and their impact on the luminescence data need to be developed to confirm that the observed increasing trend in the luminescence record is caused by an increase in rainfall and not an inflation of the record due to land use changes.

The variability in the data also confirmed that even at a local scale it is important to analyze several cores to get a clear record of past climate variability. Climate controlling factors could only be identified after removing local variability by constructing a composite record. Therefore, reconstructed climate signals can only be regarded reliable when the signal is shared by several corals.

This study offered vital new insights into the factors that influence climatic variability in eastern Africa. As historical climate data in eastern Africa are scarce, the results of this study can potentially extend existing records and help defining future rainfall variability. Information on future rainfall variability are a useful managing tool when developing agricultural strategies. Currently, the Mozambican government is intensifying and expanding its agricultural practices to fight malnourishment. The conclusions of this study provide vital information to minimize the effects of future rainfall variability on the agricultural sector and improve food security in Mozambique.

6. Outlook

This study was the first to assess coral samples from Mozambique. A lot of new insights into past climatic conditions and factors influencing climate could be gained from these coral cores. However, some questions could not be resolved yet, which was mostly due to the lack of comparable data. In Mozambique, historic climate data are scarce and mostly incomplete. It was not possible to compare the luminescence data to local rainfall data, as the closet weather station is situated 66 km away from the study site. Additionally, only broad current data was available. No data regarding the currents within the bay was available. This hampered the proper assessment of the influence of the Rovuma plume on the corals. Also, no discharge data for either the Rovuma River or the local rivers was available. As the luminescence within the corals is caused by humic acids that are flushed into the bay by rivers, it would have been useful to be able to compare the records to discharge data.

This project placed 2 temperature loggers within the bay, attached to two of the studied corals. They will be collected after one year. The data recorded by the loggers should provide more insights into local conditions within the bay. Additionally, a top-core of the two corals, the loggers were attached to will be taken in order to calibrate the data recorded in the coral with instrumental data. Next to temperature loggers, a water sampling system was established. Water samples will be taken every two weeks for one year. This should improve the understanding of processes within the bay and allow for a calibration of the corals with the collected data. This in turn could provide more reliable estimates of past environmental conditions within the bay.

It would also be useful to extend the geochemical profiles over the entire length of the cores. Most studies regarding corals in eastern Africa focus on Ba/Ca or δ^{18}O records. For comparison, it would be useful to create similar profiles. Models assessing changes in hydrology, forest cover or land use over the past 100 years would be a valuable addition to this study. With their help, it would be possible to quantify and remove the effects of anthropogenic land use change from the luminescence data and thereby create a more precise rainfall record.

This study can be considered a valuable addition to coral palaeo-climatic research. It was possible to determine drivers of Mozambican climate and identify teleconnections of large-scale, multi-decadal climate oscillations in eastern Africa that so far have only been suggested to exist. Extending this study with the data that is currently collected by the two temperature loggers and water samples will hopefully offer even more insights into what factors control east African climate and help to find answers to questions that until now had to remain open.

References

Abram N. J., Gagan M.K., Cole J.E., Hantoro W.S. and Mudelsee M. (2008): Recent intensification of tropical climate variability in the Indian Ocean. Nature Geoscience, Vol. 1, pp 849-853

Anadarko Petroleum Corporation (2012b): Operations in Mozambique. www.anadarko.com/Operations/Pages/LNGmozambique.aspx (Last accessed 21.03.2012)

Anadarko Petroleum Corporation (2012a): Anadarko announces another major appraisal success offshore Mozambique (January 12th, 2012). http://www.anadarko.com/SiteCollectionDocuments/PDF/News%20Releases/Lagosta-2%201-17-12.pdf (last accessed 21.03.2012)

Bak R.P.M. (1978): Lethal and sub-lethal effects of dredging on coral reefs. Marine Pollution Bulletin, Vol. 9, pp 14-16

Boman K. (2012): Anadarko: Mozambique Could Become World's Third Largest LNG Exporter. Rigzone.com, Inc. http://www.rigzone.com/news/article.asp?a_id=118108 (last accessed 21.6.2012)

Bunce M., Brown K. and Rosendo S. (2010): Policy misfits, climate change and cross-scale vulnerability in coastal Africa: how development projects undermine resilience. Environmental Science and Policy, Vol. 13, pp. 485-497

Cardinal D., Hamelin B., Bard E. and Pätzhold J. (2001): SrrCa, UrCa and $\delta18O$ records in recent massive corals from Bermuda: relationships with sea surface temperature. Chemical Geology, Vol. 176, pp 213–233

Cole J.E., Dunbar R.B, McClanahan T.R. and Muthiga N.A. (2000): Tropical Pacific Forcing of Decadal SST Variability in the Western Indian Ocean over the Past Two Centuries. Science, Vol. 287, pp 617-619

Correge T. (2006): Sea surface temperature and salinity reconstruction from coral geochemical tracers. Paleogeography, Paleoclimatology, Paleoecology, Vol. 232, pp 408-428

Couto A.E.L., Oorvest U., Andre E., Guissamulo A., Gervasio, H.F., Wilson J., van der Walt J., Hoguane A. M., Woie R., Oberholzer M., Cruz L., Quilambo C., Costa N and Miguelez J.R. (2008): Deepwater Exploration, Drilling in the Rovuma Offshore Area 1, Volume II, Part A: Environmental Impact Study. Published by Anadarko

Deser C., Phillips A.S. and Alexander M.A. (2010): Twentieth century tropical sea surface temperature trends revisited. Geophysical Research Letters, Vol. 37, L10701, doi: 10.1029/2010GL043321

Dewar R.E. and Wallis J.R. (1999): Geographical Patterning of Interannual Rainfall Variability in the Tropics and Near Tropics: An L-Moments Approach. Journal of Climate, Vol. 12, pp 3457-3466

Elsner J.B., Kossin J.P. and Jagger T.H. (2008): The increasing intensity of the strongest tropical cyclones. Nature, Vol. 455, pp 92-95

Fallon S., White J.C. and McCulloch M.C. (2002): Porites Corals as recorders of mining and environmental impacts: Misima Island, Papua New Guinea. Geochimica et Chosmochimica Acta, Vol. 66, pp 45-62

Food and Agriculture Organization of the United Nations (FAO) (2010): FAO/WFP Crop and Food Security Assessment Mission to Mozambique. Special Report. Food and Agricultural Organization of the United Nations, Rome.

Food and Agriculture Organization of the Unitred Nations (FAO): (2011): Mozambique. Monitoring progress towards hunger reduction targets of the World Food Summit (WFS) and the Millenium Development Goals (MDG). Food and Agricultural Organization of the United Nations, Statistic Division.

Fleitmann D., Dunbar R.B., McCulloch M., Mudelsee M., Vuille M., McClanahan T.R., Cole J.E. and Eggins S. (2007): East African soil erosion recorded in a 300 year old coral colony from Kenya. Geophysical Research Letters, Vol. 34, L04401, doi: 10.1029/2006GL028525

Funk C., Dettinger M.D., Michaelsen J.C., Verdin J.P., Brown M.E., Barlow M. and Hoell A. (2008): Warming of the Indian Ocean threatens eastern and southern African food security but could be mitigated by agricultural development. PNAS, Vol. 105, pp 11081-11086

Grove C.A., Nagtegaal R., Zinke J., Scheufen T., Koster B., Kasper S., McChulloch M.T., van den Berg G. and Brummer G.-J. A. (2010): River runoff reconstructions from novel spectral luminescence scanning of massive coral skeletons. Coral Reefs, Vol. 29, pp 579-591

Grove C.A., Zinke J., Peeters F., Park W., Scheufen T., Kasper S., Randriamanantsoa B., McCulloch M. and Brummer G.-J. A. (2012a): Madagascar corals reveal Pacific multidecadal modulation of rainfall since 1708. Clim. Past Discuss., Vol. 8, pp 787-817, doi:10.5194/cpd-8-787-2012

Grove C.A., Scheufen T., Zinke J., Maina J., Epping E., Boer W., Randriamanantsoa B. and Brummer G.-J. A. (2012b): Spatial linkages between coral proxies of terrestrial runoff across a large embayment in Madagascar. Biogeosciences Discuss., Vol. 9, pp 3099-3144, doi:10.5194/bgd-9-3099-2012

Guan B. and Nigam S. (2008): Analysis of Atlantic SST Variability Factoring Interbasin Links and the Secular Trend: Clarified Structure of the Atlantic Multidecadal Oscillation. Journal of Climate, Vol., 22, pp 4228-4240

Guerreiro J., Chircop A., Grilo C., Ribeiro R., Viras A. and van der Elst R. (2010): Establishing a transboundary network of marine protected areas: Diplomatic and management options for the east African context. Marine Policy, Vol. 34, pp 896-910.

Guerreiro J., Chircop A., Dzidzornu D., Grilo C., Ribeiro R., van der Elst R. and Viras A. (2011): The role of international environmental instruments in enhancing transboundary marine protected areas: An approach in Eastern Africa. Marine Policy, Vol. 35, pp 95-104.

Guzman H.M., Jackson J.B.C. and Weil E. (1991): Short-term ecological consequences of a major oil spill on Panamanian subtidal reef corals. Coral Reefs, Vol. 10, pp 1–12

Hetzinger S., Pfeiffer M., Dullo W.C., Keenlyside N., Latif M. and Zinke J. (2008): Carribean coral tracks Atlantic Multidecadal Oscillation and past hurricane activity. Geology, Vol. 36, pp 11-14

Indeje M., Semazzi F.H.M. and Ogallo L.J. (2000): ENSO signals in East African Rainfall Signals. International Journal of Climatology, Vol. 20, pp 19-46.

Kilbourne K.H., Moyer R.P., Quinn T.M. and Grottoli A.G. (2011): Testing coral-based tropical cyclone reconstructions: An example from Puerto Rico. Palaeogeography, Palaeoclimatology, Palaeoecology, Vol. 307, pp 90-97

Knight J.R., Folland C.K. and Scaife A.A. (2006): Climate impacts of the Atlantic Multidecadal Oscillation. Geophysical Research Letters, Vol. 33, L17706, doi: 10.1029/2006GL026242

Lough J.M., Barnes D.J. and McAllister F.A. (2002): Luminescent lines in corals from the Great Barrier Reef provide spatial and temporal records of reefs affected by land runoff. Coral Reefs, Vol.21 pp 333-343

Lough J.M. (2004): A strategy to improve the contribution of coral data to high-resolution paleoclimatology. Paleogeography, Paleoclimatology, Paleoecology, Vol. 204, pp 115-143

Lough J.M. (2011a): Great Barrier Reef coral luminescence reveals rainfall variability over northeastern Australia since the 17th century. Palaeoceanography, Vol. 26, PA 2201, doi: 10.1029/2010PA002050

Lough J.M. (2011b): Measured coral luminescence as a freshwater proxy: comparison with visual indices and a potential age artifact. Coral Reefs, Vol. 30, pp 169-182

Lough J.M. and Cooper T.F. (2011): New insights from coral growth band studies in an era of rapid environmental change. Earth-Science Reviews, Vol 108, pp 170-184

Maina J., Moel de H., Vermaat J.E., Bruggenmann J.H., Guillaume M.M.M., Grove C.A., Madin J.S., Mertz-Kraus R. and Zinke J. (Linking coral river runoff proxies with climate variability, hydrology and land-use in Madagascar catchments. Marine Pollution Bulletin, http://dx.doi.org/10.1016/j.marpolbul.2012.06.027

Mantua N.J. and Hare S.R. (2002): The Pacific Decadal Oscillation. Journal of Oceanography, Vol. 58, pp 35-44

Marshall J.F. and McCulloch M.T. (2002): An assessment of the Sr/Ca ratio in shallow water hermatypic corals as a proxy for sea surface temperature. Geochimica et Cosmochimica Acta, Vol. 66, pp 3263–3280

McConnaughey T. (1989): ^{13}C and ^{18}O isotopic disequilibrium in biological carbonates: I. Patterns. Geochimica et Cosmochimica acta, Vol. 53, pp 151-162

McCulloch M., Fallon S., Wyndham T., Hendy E., Lough J. and Barnes D. (2003): Coral record of increased sediment flux to the inner Great Barrier Reef since European settlement. Nature, Vol. 42, pp 727-730.

McPhaden M.J., Zebiak S.E. and Glantz M.H. (2006): ENSO as an Integrated Concept in Earth Science. Science, Vol. 314, pp 1740-1745

Meyers G., McIntosh P., Pigot L. and Pook M. (2007): The Years of El Niño, La Niña, and Interactions with the Tropical Indian Ocean. Journal of Climate, Vol. 20, pp 2872-2880

Mitsuguchi T., Dang P.X., Kitagawa H., Uchida T and Shibata Y. (2008): Coral Sr/Ca and Mg/Ca records in Con Dao Island off the Megong Delta> Assessment of their potential for monitoring ENSO and East Asian monsoon. Global and Planetary Change, Vol. 63, pp 341-352

Motta H., Pereira A.M., Gonçalves M., Ridgway T. and Schleyer M.H. (2002). Coral reef monitoring in Mozambique. II: 2000 report. MICOA/CORDIO/ORI/WWF. Maputo, Mozambique Coral Reef management Programme. 31 pp.

Nagtegaal R., Grove C.A., Kasper S., Zinke J., Boer W. and Brummer G.J.A. (2012): Spectral luminescence and geochemistry of coral aragonite: Effects of whole core treatment. Chemical Geology, Vol. 318-319 pp 6-15

Newmann M., Compo G.P. and Alexander M.A. (2003): ENSO-forced Variability of the Pacific Decadal Oscillation. Journal of Climate, Vol. 16, pp 3853-3857

Obura D.O. (2009): Coral Reefs bleach to resist stress. Marine Pollution Bulletin, Vol. 58, pp 206-212

Pfeiffer M., Dullo W.C., Zinke J. and Garbe-Schönberg (2009): Three monthly coral Sr/Ca records from the Chagos Archipelago covering the period 1950-1995 A.D.: reproducibility and implications for quantitative reconstructions of sea surface temperature variations. International Journal of Earth Sciences, Vol. 98, pp 53-66

Power S., Casey T., Folland C., Colman A. and Mehta V. (1999): Inter-decadal modulation of the impact of ENSO in Australia. Climate Dynamics, Vol. 15, pp 319-324

Prouty N.G., Field M.E., Stock J.D., Jupiter S.D. and McCulloch M. (2010): Coral Ba/Ca records of sediment input to the fringing reef of the southshore of Moloka'i, Hawai'I over the last several decades. Marine Pollution Bulletin, Vol. 60, pp 1822-1835.

Ramana M.V., Krishnan P., Muraleedharan Nair S. and Kunhikrishnan P.K. (2004): Experimental observations of air–sea parameters and fluxes associated with anomalous event in the Indian Ocean during 1997-1998 El Niño period. Atmospheric Research, Vol. 70, pp 21-32.

Ren L., Linsley B.K., Wellington G.M., Schrag D.P. and Hoegh-Guldenberg O. (2002): Deconvolving the $\delta^{18}O$ seawater component from subseasonal coral $\delta^{18}O$ and Sr/Ca at Rarotonga in the southwestern subtropical Pacific for the period 1726 to 1997. Geochimica et Cosmochimica Acta, Vol. 67, pp 1609-1621.

Rodrigues, M.J., Motta, H., Pereira, M., Gonçalves, M., Carvalho, M. & Schleyer, M. 1999. Monitoring Programme and 1999 report, MICOA-ORI- IIP, Maputo, 64 p.

Rovuma Consultancy (2012): Introduction to the Rovuma River Basin. http://ruvumariver.org/introduction.html (last accessed 21.03.2012)

Sayani H.R., Cobb K.M., Cohen A.L., Crawford Elliott W., Nurhati I.S., Dunbar R.B., Rose K.A. and Zaunbrecher L.K. (2011): Effects of diagenesis on paleoclimate reconstructions from modern and young fossil corals. Geochimica et Cosmochimica Acta, Vol. 75, pp 6361 – 6373

Schlesinger M.E. and Ramakytty N. (1994): An oscillation in the global climate system of period 65-70 years. Nature, Vol. 367, pp 723-726

Schneider U., Becker A., Meyer-Christoffer A., Ziese M. and Rudolf B. (2011): Global Precipitation Analysis of the GPCC. Global Precipitation Climatology Centre (GPCC), Deutscher Wetterdienst, Offenbach a. M., Germany

Scott P.J.B. (1990): Chronic pollution recorded in coral skeletons in Hong Kong. Journal of Experimental Marine Biology and Ecology, Vol. 139, pp 51-64

Sinclair D.J. and McCulloch M.T. (2004): Corals record low mobile barium concentrations in the Burdekin River during the 1974 flood: evidence for limited Ba supply to rivers? Paleogeography, Paleoclimatology, Paleoecology, Vol. 214, pp 155-174

Spencer T., Telenki K.A., Bradshaw C. and Spalding M.D. (2000): Coral Bleaching in the Southern Seychelles During the 1997-1998 Indian Ocean Warm Event. Marine Pollution Bulletin, Vol. 40, pp 569-586.

Taylor R.B, Barnes D.J. and Lough J.M.(1995): On the inclusion of trace materials into massive coral skeletons. 1. Materials occurring in the environment in short pulses. Journal of Experimental Marine Biology and Ecology, Vol. 185, pp 255-278.

Tomascik T. and Sander F. (1985): Effects of eutrophication on reef-building corals. 1. Growth rate of the reef-building coral Montastrea annularis. Marine Biology, Vol 87, pp 143-155

Tzipermann E., Cane M.A., Zebiak S.E., Xue Y. and Blumenthal B. (1998): Locking of El Nino's Peak Time to the End of the Calendar Year in the Delayed Oscillator Picture of ENSO. Journal of Climate, Vol. 11, pp 2191-2199

University of East Anglia Climate Research Unit [Jones P. and Harris I] (2008): CRU Time Series (TS) high resolution gridded datasets. NCAS British Atmospheric Data Center. http://badc.nerc.ac.uk/view/badc.nerc.ac.uk__ATOM__dataent_1256223773328276 (last accessed 23.04.2012)

Webster P.J., Holland G.J., Curry J.A and Chang H.-R. (2005): Changes in Tropical Cyclone Number, Duration and Intensity in a warming Environment. Science, Vol. 309, pp 1844-1846

WIOMSA (2011): Migrant fishers and fishing in the Western Indian Ocean: Socio-economic dynamics and implications for management. Final Report of Commissioned Research Project MASMA/CR/2008/02.

Yamagata T., Behera S.K., Luo J.-J., Masson S., Jury M.R. and Rao S.A. (2004): Coupled Ocean-Atmosphere Variability in the Tropical Indian Ocean. Geophysical Monograph, Vol. 147, pp 189-211

Appendix

A.1 Correlation with rainfall

Correlation	n	p	r	r2
Qui6 - Mocimba di Praia	30	0.37	0.17	0.0288
Qui6 - Mtwara	43	0.956	0.00872	0.00076
Qui6 - CRU	42	0.437	0.123	0.0152
Qui6 - GPCC	42	0.517	0.103	0.106
Qui2b - Mocimba di Praia	56	0.652	0.0616	0.00379
Qui2b - Mtwara	49	0.587	0.0796	0.00633
Qui2b - CRU	68	0.365	0.112	0.025
Qui2b - GPCC	68	0.371	0.11	0.0121
Qui7 - Mocimba di Praia	40	0.976	0.00681	0.0000463
Qui7 - Mtwara	49	0.352	0.136	0.0185
Qui7 - CRU	52	0.524	0.0904	0.00818
Qui7 - GPCC	52	0.258	0.16	0.0255
Qui4 - Mocimba di Praia	64	0.75	0.0405	0.00164
Qui4 - Mtwara	49	0.984	0.00296	0.00000873
Qui4 - CRU	99	0.969	0.00401	0.0000161
Qui4 - GPCC	98	0.049	0.2	0.0399

Table A1: Correlation of annual averages of individual cores with rainfall

The annual averages of the G/B records of the four cores were correlated with two annually averaged rainfall station data and two annually averaged re-analysis field rainfall datasets (Table A1). The only correlation that was found to be significant was Qui4 – GPCC. When the one year and two year moving median were removed to de-trend the record, correlations of Qui6, Qui2b and Qui4 with rainfall became apparent (Tables A2&A3). The two composite records also showed a significant correlation with rainfall, once a one or two year running median was removed (Tables A4-A7).

Correlation	n	p	r	r2
Qui6 - Mocimba di Praia	29	0.547	0.117	0.0136
Qui6 - Mtwara	42	0.012	0.383	0.147
Qui6 - CRU	41	0.09	0.268	0.072
Qui6 - GPCC	40	0.009	0.407	0.165
Qui2b - Mocimba di Praia	39	0.267	0.182	0.0332
Qui2b - Mtwara	49	0.019	0.334	0.111
Qui2b - CRU	51	0.545	0.0868	0.00753
Qui2b - GPCC	50	0.152	0.206	0.0423
Qui7 - Mocimba di Praia	55	0.657	0.0612	0.00374
Qui7 - Mtwara	49	0.065	0.265	0.0703
Qui7 - CRU	67	0.32	0.123	0.0152
Qui7 - GPCC	66	0.113	0.197	0.0388
Qui4 - Mocimba di Praia	64	0.249	0.146	0.0214
Qui4 - Mtwara	49	0.126	0.221	0.049
Qui4 - CRU	98	0.523	0.0639	0.00409
Qui4 - GPCC	97	0.024	0.228	0.0522

Table A2: Correlation of annual averages of the four G/B records after removing the one year running median with annually averaged rainfall

Correlation	n	p	r	r2
Qui6 - Mocimba di Praia	29	0.324	0.19	0.036
Qui6 - Mtwara	42	0.004	0.423	0.186
Qui6 - CRU	41	0.017	0.37	0.137
Qui6 - GPCC	40	0.003	0.456	0.208
Qui2b - Mocimba di Praia	39	0.148	0.236	0.0556
Qui2b - Mtwara	49	0.016	0.343	0.118
Qui2b - CRU	51	0.174	0.193	0.0373
Qui2b - GPCC	50	0.009	0.368	0.136
Qui7 - Mocimba di Praia	55	0.786	0.0374	0.0014
Qui7 - Mtwara	49	0.749	0.0469	0.0022
Qui7 - CRU	67	0.827	0.0273	0.000743
Qui7 - GPCC	66	0.493	0.0859	0.00738
Qui4 - Mocimba di Praia	64	0.494	0.0871	0.00759
Qui4 - Mtwara	49	0.264	0.163	0.0265
Qui4 - CRU	98	0.595	0.0544	0.00295
Qui4 - GPCC	97	0.073	0.183	0.0335

Table A3: Correlation of annual averages of the four G/B records after removing the two year running median with annually averaged rainfall

Correlation	n	p	r	r2
Composite (normalized) - Mo. Di Praia	54	0.838	0.0286	0.00816
Composite (normalized) - Mtwara	49	0.811	0.035	0.00123
Composite (normalized) - CRU	66	0.722	0.0446	0.001999
Composite (normalized) - GPCC	66	0.156	0.177	0.00312

Table A4: Correlation of annual averages of the composite record constructed by normalizing the data prior to averaging all cores with rainfall

Correlation	n	p	r	r2
Composite (averaged) - Mo. Di Praia	54	0.791	0.0369	0.00136
Composite (averaged - Mtwara	49	0.551	0.0872	0.00761
Composite (averaged - CRU	66	0.702	0.048	0.0023
Composite (averaged - GPCC	66	0.166	0.173	0.0298

Table A5: Correlation of annual averages of the composite record constructed averaging all cores with rainfall

Correlation	n	p	r	r2
Composite (1RM) - Mo. Di Praia	55	0.66	0.0606	0.00367
Composite (1RM) - Mtwara	49	0.003	0.411	0.169
Composite (1RM) -CRU	67	0.333	0.12	0.0144
Composite (1RM) - GPCC	67	0.248	0.145	0.0209

Table A6: Correlation of annual averages of the composite record with the one year running median removed with rainfall

Correlation	n	p	r	r2
Composite (2RM) - Mo. Di Praia	55	0.8	0.0349	0.00122
Composite (2RM) - Mtwara	49	0.03	0.31	0.0961
Composite (2RM) - CRU	67	0.482	0.0874	0.00764
Composite (2RM) - GPCC	67	0.414	0.101	0.0103

Table A7: Correlation of annual averages of the composite record with the two year running median removed with rainfall

A.2 Correlation of individual G/B with ENSO indices

The G/B records of the four corals and the de-trended G/B records (one year running median subtracted) were correlated with the climate indices Niño3, Niño3.4 and Niño4 to investigate the influence of ENSO on the corals. The data were averaged over one, three, six and twelve months for comparison.

No correlation could be found between the G/B records of the corals and the ENSO indices. If the G/B time series were de-trended by subtracting the one-year running median from the initial time series, correlations with ENSO indices became apparent.

Coral	Niño3			
	1 month	**3 months**	**6 months**	**12 months**
Qui6.1m	Apr (p=0.03, r=0.321)			
Qui7.1m	Apr (p=0.012, r=-0.417)	Apr-Jun (p=0.027, r=-0.374)	Mar-Aug (p=0.036, r=-0.361)	
Qui2b.1m				
Qui4.1m				

	Niño3.4			
	1 month	**3 months**	**6 months**	**12 months**
Qui6.1m				
Qui7.1m	Apr (p=0.006, r=-0.483) Aug (p=0.038, r=0.353)	Apr-Jun (p=0.029, r=-0.404)	Mar-Aug (p=0.032, r=-0.370)	
Qui2b.1m				
Qui4.1m				Sep-Aug (p=0.029, r=0.268) Oct-Sep (p=0.019, r=0.289) Nov-Oct (p=0.037, r=0.258)

	Niño4			
	1 month	**3 months**	**6 months**	**12 months**
Qui6.1m				
Qui7.1m	Apr (p=0.003, r=-0.448)	Apr-Jun (p=0.016, r=-0.370)	Mar-Aug (p=0.031, r=-0.370)	
Qui2b.1m				
Qui4.1m				Aug-Jul (p=0.025, r=0.276) Sep-Aug (p=0.004, r=0.346) Oct-Sep (p=0.004, r=0.347) Nov-Oct(p=0.015, r=0.299)

Table A8: Correlations between the de-trended G/B of the four corals after trend-removal by subtracting the one year running median and ENSO indices Niño3, Niño3.4 and Niño4.

When the G/B data was averaged over one month, Qui6.1m and Qui7.1m significantly correlated with Niño3 in April, Qui7.1m significantly correlated with Niño3.4 in April and August as well as with Niño4 in April (Table A8). When the data was averaged over three months, only Qui7.1m correlated with all three indices for the period April-June (Table A8). Significant correlations between all three indices and Qui7.1m were observed for the six month average ranging from March till August (Table A8). In addition, Qui6.1m significantly correlated with the Niño3.4 index when averaged over six months for the periods April-October and July-December (Table A8). The G/B of Qui2b.1m did not show any significant correlation with either index while the G/B of Qui4.1m only displayed significant correlations with the Niño3.4 and Niño4 index when averaged over 12 months (Table A8).

A.3 Correlation of individual G/B with PDO and IOD indices

The individual and de-trended G/B records were correlated to DMI (IOD) and PDO indices. Both, the PDO as well as DMI (IOD) index were based on two different reconstructions: HadISST and ERSST, thus all G/B records were compared to two DMI (IOD) and two PDO indices. The data of the records were averaged over one, three, six and twelve months for the correlations.

The G/B record of Qui4 showed the strongest correlations with DMI (IOD) index based on ERSST. When averaged over 1 month, correlations were significant for the months of February, March and April (Table A9). When the data was averaged over several months, significant correlations were found for the periods enclosing these three months (Table A9). There were no significant correlations between the G/B record of Qui4 and the DMI (IOD) index based on HadISST. The G/B record of Qui6, data averaged over one month, displayed a significant correlation with the DMI (IOD) index based on HadISST for the month of September (p=0.0486, r=0.296) and the G/B of Qui2b significantly correlated with the same index when averaged over 1 month for the month of April (p=0.030, r=0.259). No significant correlations occur between the G/B of Qui7 and either DMI (IOD) index.

	DMI (IOD) ERSST			
	1 month	**3 months**	**6 months**	**12 months**
Qui4	Feb (p=0.0128, r=-0.300)	Jan-Mar (p=0.0186, r=-0.285)	Dec-May (p=0.007, r=-0.324)	Jun-May (p=0.0424, r=-0.249)
	Mar (p=0.0347, r=-0.257)	Feb-Apr (p=0.0034, r=-0.351)	Jan-Jun (p=0.0059, r=-0.331)	Jul-Jun (p=0.0212, r=-0.281)
	Apr (p=0.0456, r=-0.243)	Mar-May (p=0.0144, r=-0.296)	Feb-Jul (p=0.0175, r=-0.288)	Aug-Jul (p=0.0182, r=-0.288)
				Sep-Aug (p=0.0345, r=-0.257)

Table A9: Correlations of the G/B record of Qui4 with the DMI (IOD) index based on ERSST

	Qui4.1m	**Qui7.1m**	**Qui2b.1m**
IOD (DMI) (HadISST)	Feb (p=0.0368, r=-0.256)	Sep – Aug (p=0.0235, r=-0.388)	
	Jan – Mar (p=0.019, r=-0.286)	Oct – Sep (p=0.0270, r=-0.379)	
	Jan – Jun (p=0.0298, r=-0.268)	Nov – Oct (p=0.0358, r=-0.361)	
		Dec – Nov (p=0.0425, r=-0.350)	
IOD (DMI) (ERSST)	Feb – Apr (p=0.0337, r=-0.259)	July (p=0.0225, r=0.385)	Dec (p=0.030, r=0.261)
	Jan – Jun (p=0.0109, r=-0.311)		Jan – Dec (p=0.0135, r=0.301)
			Feb – Jan (p=0.0450, r=0.244)

Table A10: Significant correlations of the de-trended G/B records with IOD (DMI) indices.

The de-trended G/B records of the four records were also correlated with the DMI indices. The G/B records of Qui4.1m and Qui7.1m show significant correlations with both DMI indices, while Qui2b.1m only correlated significantly with the DMI (IOD) index based on ERSST (Table A10). The G/B record of Qui6.1m did not show any significant correlations with either index.

	Qui4	Qui4.1m	Qui7
1 month	Jan (p=0.042, r=0.248) Mar (p=0.002, r=0.378) Apr (p=0.003, r=0.363) May (p=0.027, r=0.270) Jun (p=0.017, r=0.291)	Mar (p=0.003, r=0.352) Apr (p=0.049, r=0.242) Oct (p=0.009, r=-0.381) Nov (p=0.042, r=-0.249)	Jul (p=0.023, r=-0.365) Sep (p=0.009, r=-0.423) Nov (p=0.033, r=-0.357)
3 months	Jan-Mar (p=0.009, r=0.315) Feb-Apr (p=0.003, r=0.359) Mar-May (p=0.004, r=0.349) Apr-Jun (p=0.008, r=0.326) May-Jul (p=0.019, r=0.285)	Jan-Mar (p=0.042, r=0.251) Feb-Apr (p=0.005, r=0.346) Mar-May (p=0.044, r=0.251) Aug-Oct (p=0.033, r=-0.265)	May-Jul (p=0.047, r=-0.333) Jun-Aug (p=0.033, r=-0.355) Jul-Sep (p=0.011, r=-0.420) Aug-Oct (p=0.026, r=-0.376) Sep-Nov (p=0.026, r=-0.370)
6 months	Nov-Apr (p=0.019, r=0.287) Dec-May (p=0.007, r=0.335) Jan-Jun (p=0.004, r=0.349) Feb-Jul (p=0.005, r=0.340) Mar-Aug (p=0.008, r=0.323) Apr-Sep (p=0.039, r=0.255) May-Oct (p=0.032, r=0.266)	Jan-Jun (p=0.014, r=0.305) Feb-Jul (p=0.016, r=0.300) Jun-Nov (p=0.022, r=-0.285) Jul-Dec (p=0.032, r=-0.266) Nov-Apr (p=0.027, r=0.274) Dec-May (p=0.009, r=0.325)	Apr-Sep (p=0.025, r=-0.372) May-Oct (p=0.046, r=-0.340) Jun-Nov (p=0.021, r=-0.390) Jul-Dec (p=0.009, r=-0.437) Aug-Jan (p=0.012, r=-0.421)
12 months	Jan-Dec (p=0.017, r=0.298) Feb-Jan (p=0.027, r=0.277) Mar-Feb (p=0.033, r=0.267) Apr-Mar (p=0.033, r=0.266) May-Apr (p=0.022, r=0.285) Jun-May (p=0.024, r=0.282) Jul-Jun (p=0.020, r=0.291) Aug-Jul (p=0.016, r=0.300) Sep-Aug (p=0.015, r=0.301) Oct-Sep (p=0.020, r=0.288) Nov-Sep (p=0.010, r=0.320) Dec-Nov (p=0.012, r=0.311)		Jan-Dec (p=0.018, r=-0.397) Feb-Jan (p=0.020, r=-0.391) Mar-Feb (p=0.019, r=-0.395) Apr-Mar (p=0.018, r=-0.398) May-Apr (p=0.017, r=-0.401) Jun-May (p=0.017, r=-0.402) Jul-Jun (p=0.015, r=-0.409) Aug-Jul (p=0.017, r=-0.401) Sep-Aug (p=0.039, r=-0.346) Oct-Sep (p=0.027, r=-0.368) Nov-Sep (p=0.043, r=-0.344) Dec-Nov (p=0.033, r=-0.362)

Table A11: Correlations of the G/B records of Qui4, Qui4.1m and Qui7 with the PDO index based on HadISST.

When the G/B records of the four corals were correlated to both PDO indices, strong correlations between the records of Qui4 and Qui7 and both indices became evident for all averaging periods (Table A11&A12). Contrastingly, no significant correlations between the G/B records of corals Qui6 and Qui2b and either PDO index could be identified. When the de-trended G/B records were compared to both PDO indices, strong correlations became evident for Qui4.1m when the data was averaged over one, three and six months, with both indices (Table A11&A12). When the data was averaged over six months, significant correlations between Qui6.1m and both PDO indices for the periods December – May (HadISST: p=0.0278, r=-0.326; ERSST: p=0.0326, r=-0.340) and January – June (HadISST: p=0.0221, r=-0.350; ERSST: p=0.0230, r=-0.353) became apparent. The G/B record of Qui7.1m significantly correlated with both indices when the data was averaged over one month for the month of September (HadISST: p=0.0453, r=-0.341; ERSST: p=0.0318, r=-0.363), while there were no significant correlations between either of the two indices and Qui2b.1m.

	Qui4	Qui4.1m	Qui7
1 month	Jan (p=0.029, r=0.266) Feb (p=0.034, r=0.258) Mar (p=0.001, r=0.423) Apr (p=0.001, r=0.397) May (p=0.013, r=0.302) Jun (p=0.005, r=0.337) Jul (p=0.013, r=0.302)	Mar (p=0.002, r=0.370) Oct (p=0.009. r=-0.319) Nov (p=0.031, r=-0.264)	Jul (p=0.022, r=-0.387) Sep (p=0.011, r=-0.420) Nov (p=0.045, r=-0.264)
3 months	Dec-Feb (p=0.047, r=0.241) Jan-Mar (p=0.005, r=0.337) Feb-Apr (p=0.001, r=0.390) Mar-May (p=0.001, r=0.392) Apr-Jun (p=0.002, r=0.364) May-Jul (p=0.004, r=0.350) Jun-Aug (p=0.008, 0.322) Jul-Sep (p=0.039, r=0.253)	Jan-Mar (p=0.036, r=0.257) Feb-Apr (p=0.004, r=0.343) Mar-May (p=0.030, r=0.266) Aug-Oct (p=0.034, r=-0.260)	Jun-Aug (p=0.039, r=-0.351) Jul-Sep (p=0.010, r=-0.430) Aug-Oct (p=0.023, r=-0.382) Sep-Nov (p=0.031, r=-0.360)
6 months	Nov-Apr (p=0.009, r=0.314) Dec-May (p=0.002, r=0.365) Jan-Jun (p=0.001, r=0.384) Feb-Jul (p=0.001, r=0.386) Mar-Aug (p=0.001, r=0.383) Apr-Sep (p=0.005, r=0.341) May-Oct (p=0.006, r=0.272)	Jan-Jun (p=0.011, r=0.310) Feb-Jul (p=0.013, r=0.305) Mar-Aug (p=0.050, r=0.241) Jun-Nov (p=0.029, r=-0.266) Jul-Dec (p=0.033, r=-0.261) Nov-Apr (p=0.024, r=0.276) Dec-May (p=0.008, r=0.325)	Apr-Sep (p=0.041, r=-0.347) May-Oct (p=0.028, r=-0.373) Jun-Nov (p=0.013, r=-0.417) Jul-Dec (p=0.007, r=-0.448) Aug-Jan (p=0.012, r=-0.419)
12 months	Jan-Dec (p=0.009, r=0.316) Feb-Jan (p=0.014, r=0.298) Mar-Feb (p=0.015, r=0.296) Apr-Mar (p=0.014, r=0.299) May-Apr (p=0.012, r=0.307) Jun-May (p=0.009, r=0.319) Jul-Jun (p=0.007, r=0.332) Aug-Jul (p=0.005, r=0.344) Sep-Aug (p=0.004, r=0.343) Oct-Sep (p=0.005, r=0.340) Nov-Sep (p=0.005, r=0.337) Dec-Nov (p=0.006, r=0.332)		Jan-Dec (p=0.021, r=-0.388) Feb-Jan (p=0.021, r=-0.388) Mar-Feb (p=0.019, r=-0.395) Apr-Mar (p=0.018, r=-0.399) May-Apr (p=0.017, r=-0.402) Jun-May (p=0.034, r=-0.365) Jul-Jun (p=0.033, r=-0.367) Aug-Jul (p=0.043, r=-0.350) Nov-Sep (p=0.049, r=-0.336) Dec-Nov (p=0.037, r=-0.353)

Table A12: Correlations of the G/B records of Qui4, Qui4.1m and Qui7 with the PDO index based on ERSST.

A.4 Spatial correlation of individual G/B records with SST

Spatial correlations of all G/B records with SST were performed using the KNMI climate explorer (http://climexp.knmi.nl/). The HadISST dataset spanning the time period 1870-2011 was selected for the spatial correlation.

The G/B record of Qui 6 positively correlated with SST at the sampling site all year long (Fig. A1). Also positive correlations with SST were found west of Australia for the period May-November and in the northern Indian Ocean for the period June-November (Fig. A1). The G/B record of Qui6.1m positively correlates over the study area in December (Fig. A1). The G/B record of Qui2b shows a positive correlation with SST over the study area and close to the Indonesian Archipelago from December to February (Fig. A2). The de-trended record did not show any significant correlations with SST. The G/B record of the core Qui7 positively correlated with SST over the study area in the months of January – March (Fig. A3). Additionally, positive correlations could be identified over the northern Indian Ocean for the same time period (Fig. A3). The de-trended record of the same core showed negative correlations with SST over the northern and western Indian Ocean in May (Fig. A3). The G/B record of Qui4 can be positively correlated with SST at the study site for the period December - July as well as the northern Indian Ocean and close to Indonesia all year (Fig. A4). The de-trended record of this coral core and SST at the study site correlate positively in May (Fig. A4).
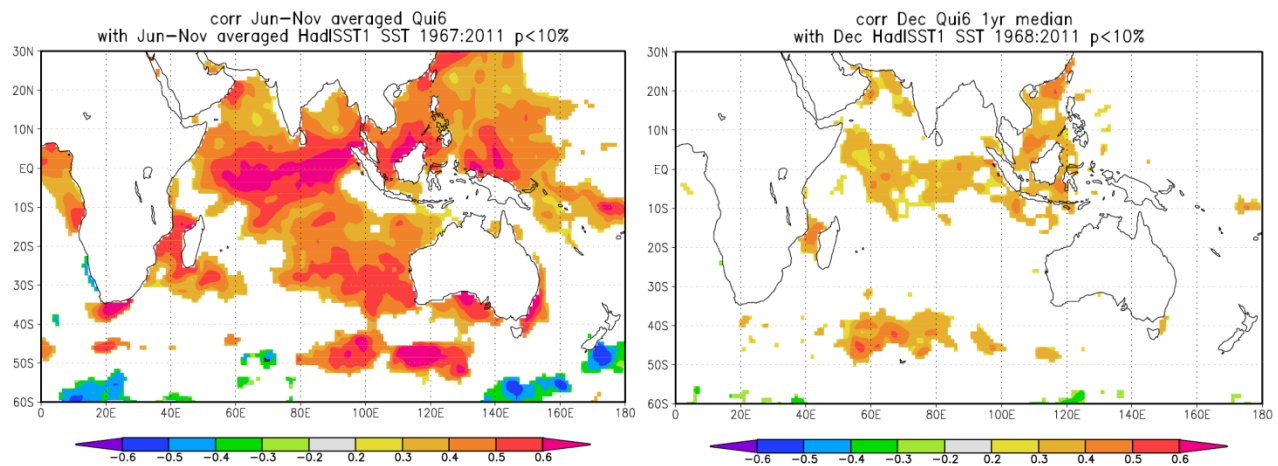
Figure A1: Spatial correlation of Qui6 and Qui6.1m with SST (HadISST). The left figure shows the correlation between Qui6 and SST from June – November. On the right, the spatial correlation of Qui6.1m and SST in December is shown.
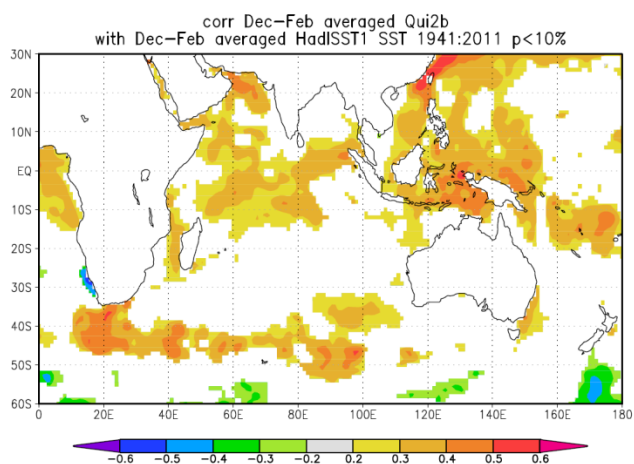
Figure A2: Spatial correlations of Qui2b with SST from December – February.
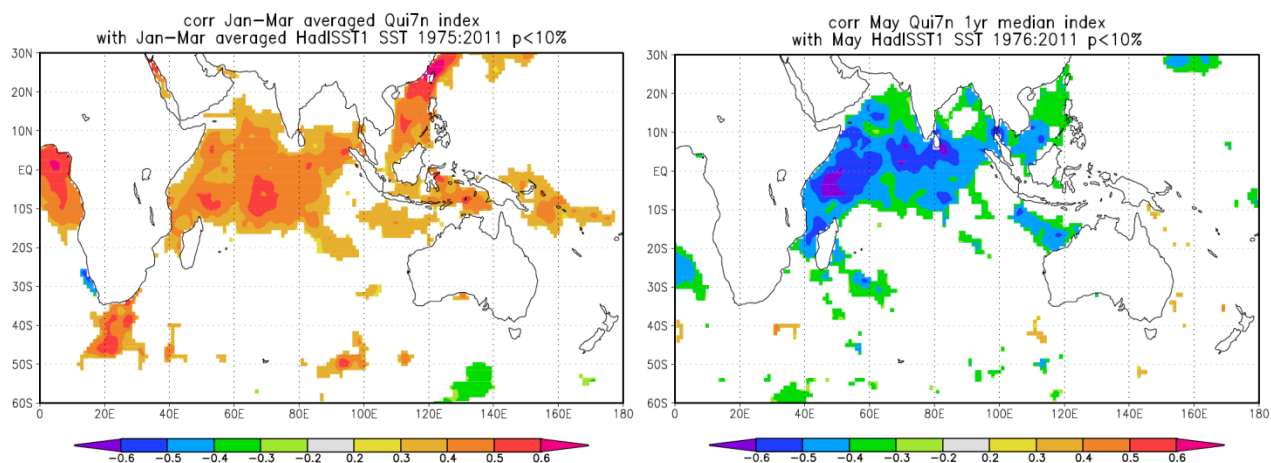
Figure A3: Spatial correlation of Qui7 and Qui7.1m with SST (HadISST). On the left, the correlation of Qui7 and SST from January – March is displayed. The spatial correlation of Qui7.1m and SST in May and is shown.
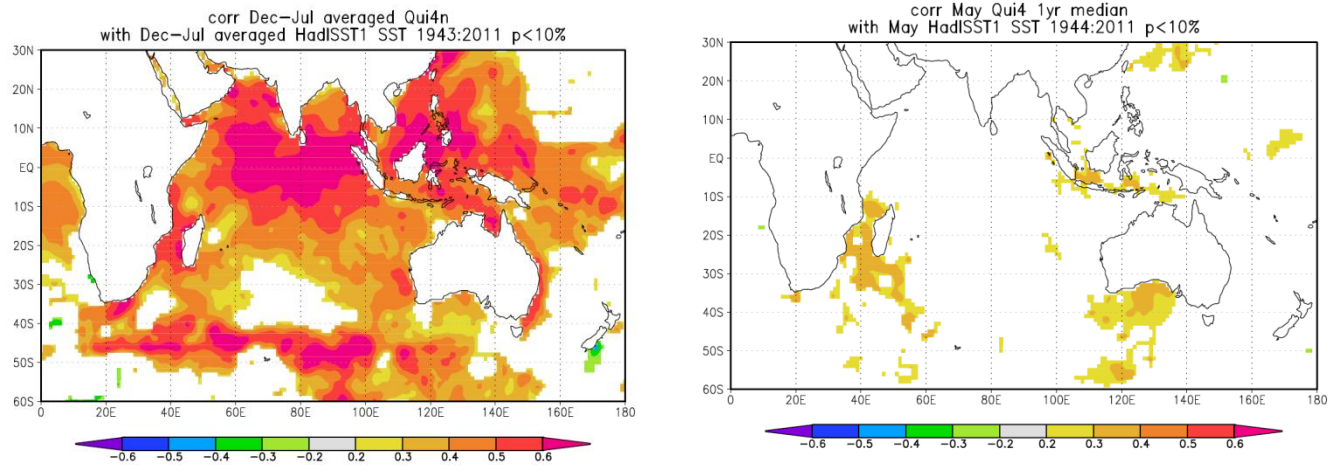
Figure A4: Spatial correlation of Qui4 with SST (HadISST) between December and July (left) and Qui4.1m with SST (HadISST) in May (right).

A.5 Correlation of individual G/B records with cyclones

The G/B records of the four individual corals and the ones where the one year median had been subtracted to remove any long-term trends were correlated with cyclone data available at the KNMI climate explorer (http://climexp.knmi.nl/). The records were compared to tracks of tropical storms and cyclones as well as maximum wind speeds. The KNMI data was available on a 5x5° grid.
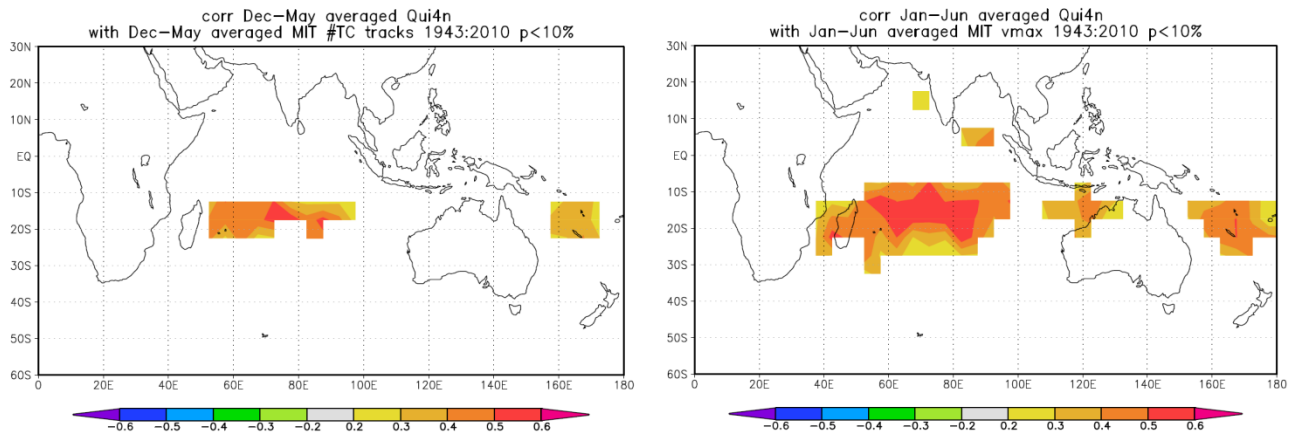
Figure A5: Spatial correlation of Qui4 with tropical cyclone tracks (left) and maximum wind speed (right).
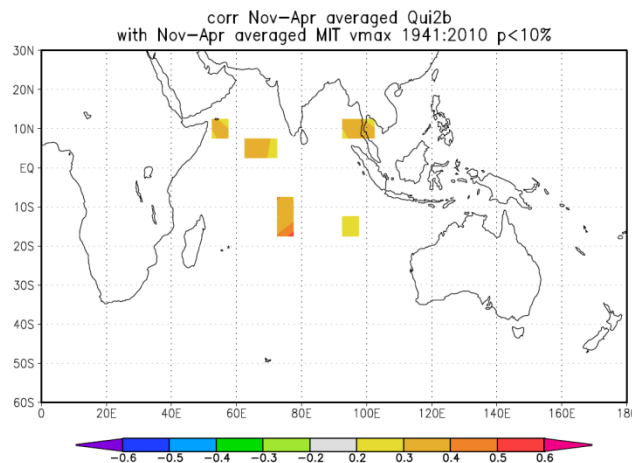
Figure A6: Spatial correlation of Qui2b with maximum wind speed.

Only two of the four G/B records showed significant correlations with cyclone related data in the Indian Ocean. The G/B of Qui2b correlated with maximum wind speed over the central Indian Ocean for the period November-April (Fig. A6). For the period November-May, the G/B of core Qui4 correlated with tropical storm and tropical cyclone tracks over the western Indian Ocean and as well as maximum wind speeds in the period ranging from November-July (Fig. A5). No correlations were found for the de-trended records.

The G/B records of the four cores and the tropical cyclone and tropical storm record close to the study site are shown in Figures A7-A10. Distinct peaks in the G/B records generally do not line up with this historical cyclone record for northern Mozambique.
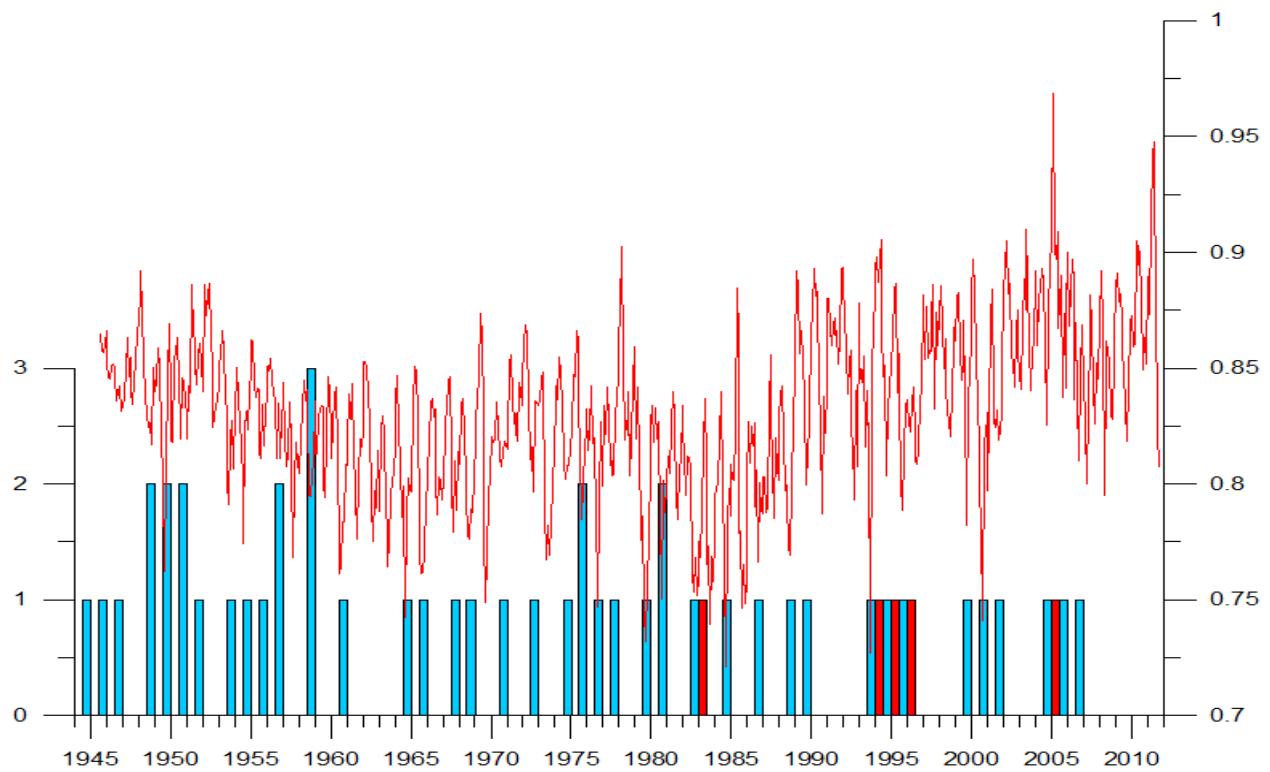
Figure A7: Number of tropical storms (blue) and cyclones (red) over the study area. The annually averaged G/B of Qui2b is depicted in red.
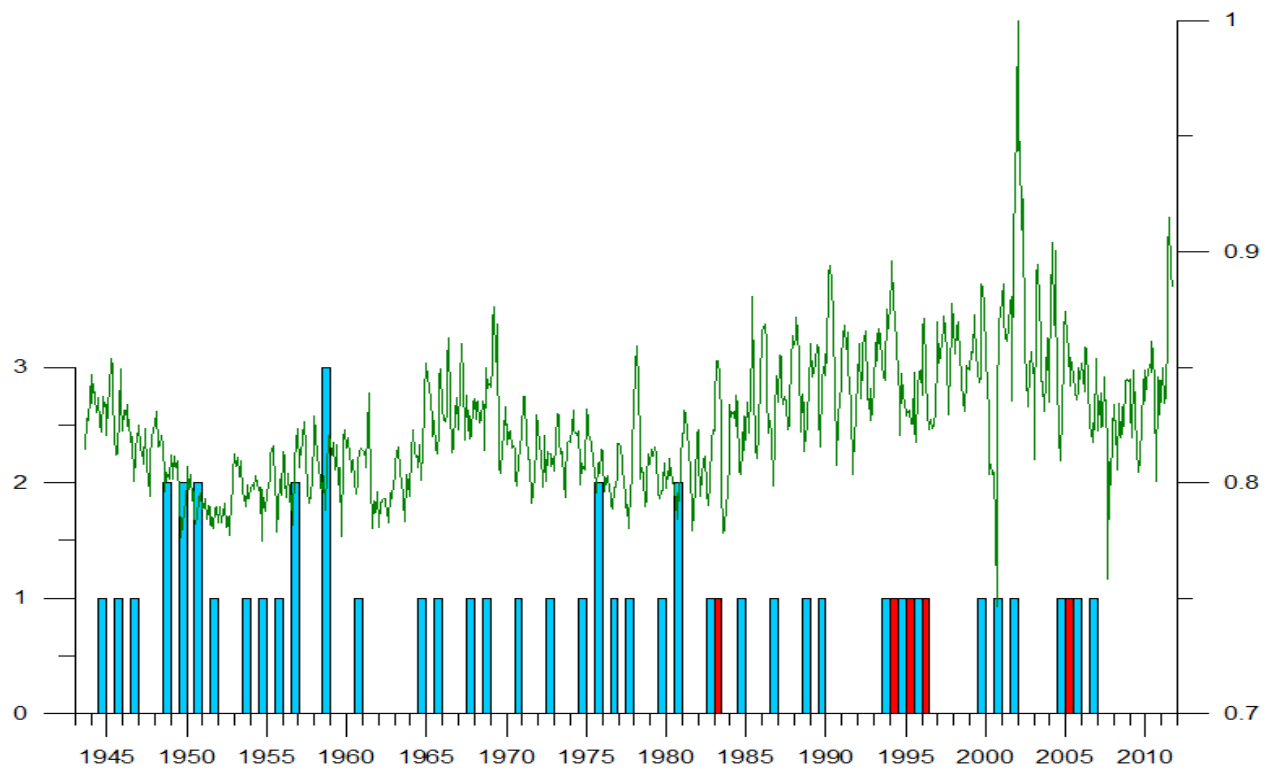
Figure A8: Number of tropical storms (blue) and cyclones (red) over the study area. The annually averaged G/B of Qui4 is depicted in green.
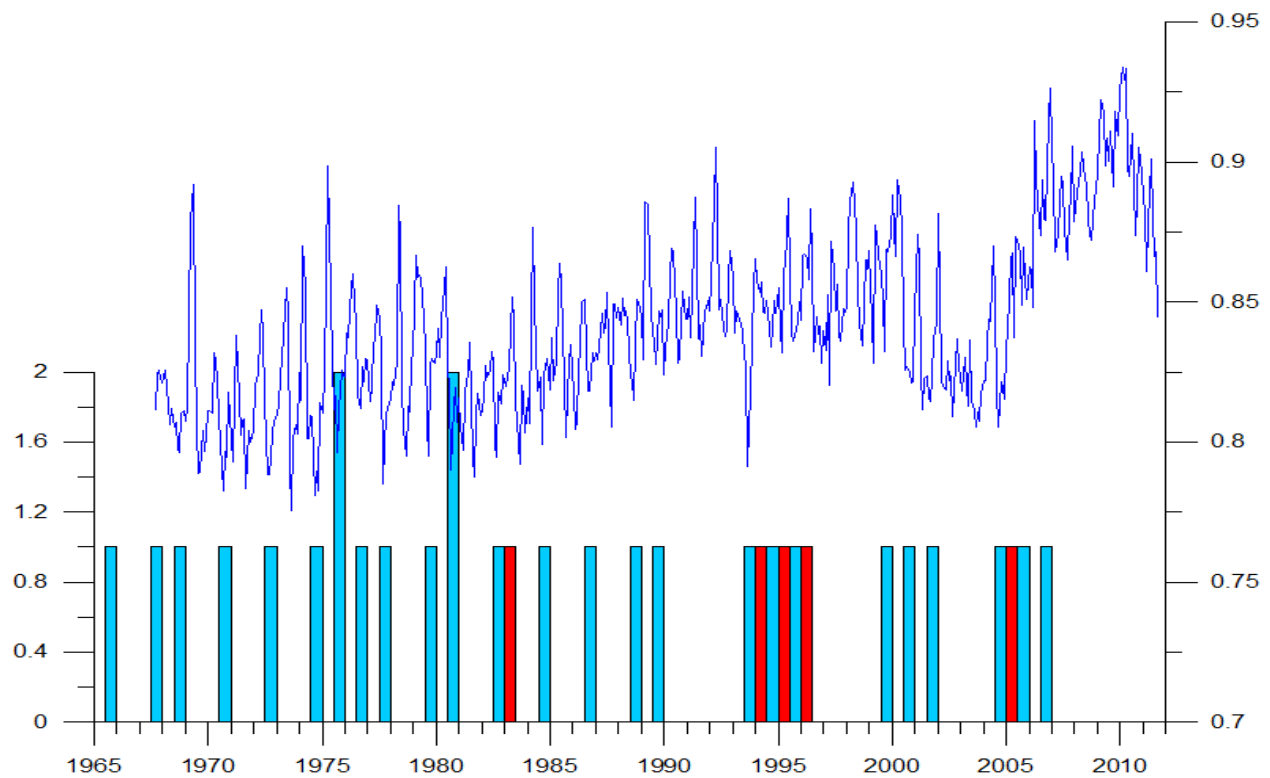
Figure A9: Number of tropical storms (blue) and cyclones (red) over the study area. The annually averaged G/B of Qui6 is depicted in blue.
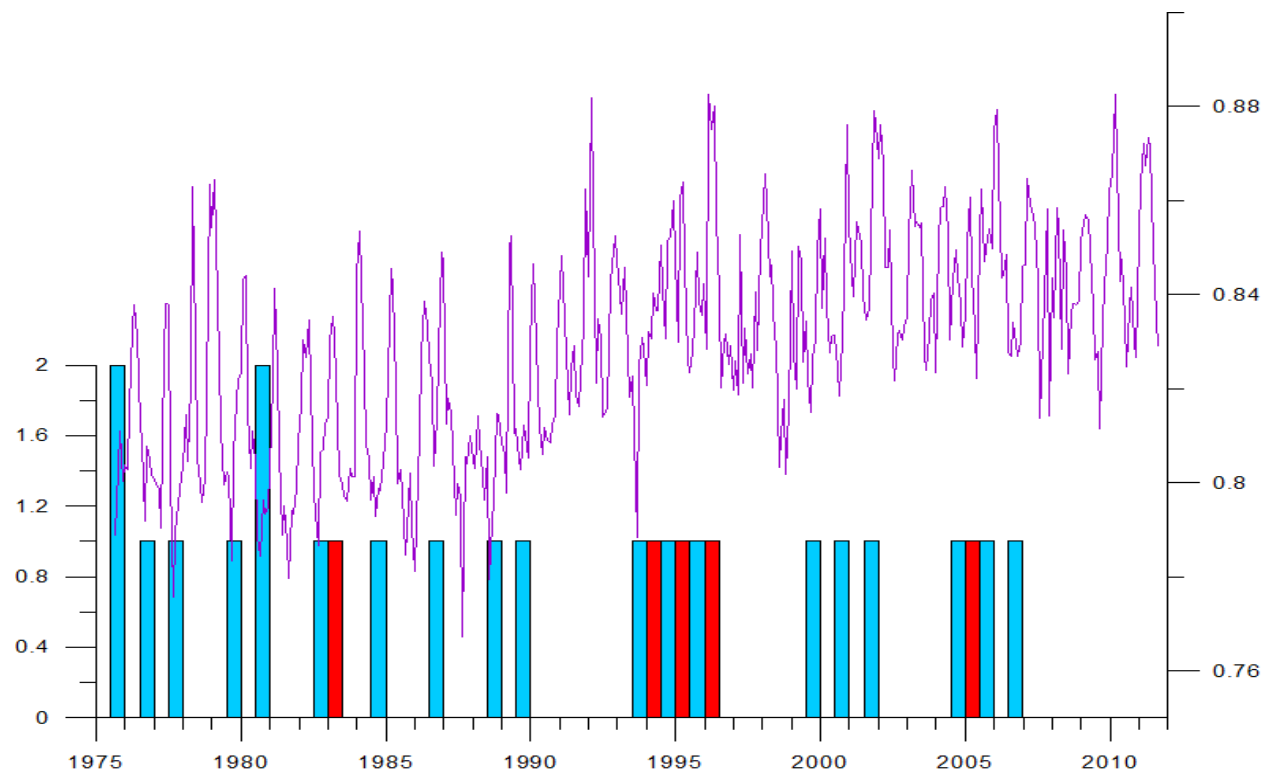
Figure A10: Number of tropical storms (blue) and cyclones (red) over the study area. The annually averaged G/B of Qui7 is depicted in purple.